UFL/COEL-95/021

LABORATORY MOBILE BED MODEL STUDIES ON INLET PART II: EBB TIDAL SHOAL EVOLUTION PROCESS

---

by

Hsiang Wang
Lihwa Lin
and
Xu Wang

1995

Sponsored by

Florida Sea Grant College
Sea Grant Project No. R/C-S-33
Grant No. NA36RG0070

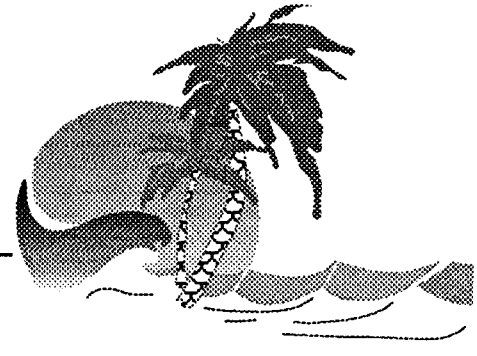

Coastal & Oceanographic Engineering Department
433 Weil Hall • P.O. Box 116590 • Gainesville, Florida 32611-6590

UNIVERSITY OF
FLORIDA

TABLE OF CONTENTS

LIST OF FIGURES

LIST OF TABLES

LABORATORY STUDY ON INLET EBB TIDAL SHOAL EVOLUTION

1. INTRODUCTION

Ebb tidal shoal is a common feature associated with tidal inlets in coastal area. It is created by the combined deposition of littoral material diverted from adjacent beaches together with the alluvial material carried out from the inlet by the tidal current. When inlets are stabilized with training structures, ebb tidal shoals can become more prominent as littoral material is now being diverted further offshore into deeper water. As a consequence, the storage volume also increases. This causes further disruption of the normal longshore sediment transport process and often results in severe downdrift shoreline recession. In Florida, over 85% of the shoreline erosion is considered to be related to inlets, particularly to those with training structures. Since ebb tidal shoal is formed mainly by material diverted from the updrift beach it is a tempting source, and reasonably so, to tap for downdrift beach nourishment. Yet, such practice is not common mainly because the formation of ebb tidal shoal is part of the natural process and disturbing an ebb tidal shoal environment so close to shoreline without knowing clearly its effect is unsettling.

The current knowledge on ebb tidal shoal dynamics is generally poor. There is no known analytical formulation on ebb tidal shoal sedimentary dynamics. Available field information related to inlets is generally limited and may not be suitable, both in temporal and spacial resolutions, for studying ebb tidal shoal evolution which is a process affected by local characteristics of the inlet, currents and waves. This represents a difficult task that requires a large amount of instruments and survey effort for the required spatial resolution and an extended period of deployment for documenting the morphological evolution. This requires a substantial resource commitment over a long time period. For this reason movable-bed hydraulic modeling in the laboratory provides an alternative that could shed insights on the dynamic process on one hand and yield practical information on the other. One of the major advantages of physical modeling is that there is really no prerequisite, even though

helpful, on the knowledge of the specific process to be studied. It can be carried out with reasonable resource at accelerated time scales. It is, however, not without difficulty because the limitations of the physical scale in the laboratory and the still questionable modeling laws that might lead to unrealistic results or erroneous conclusions.

Information on movable-bed tidal shoal and inlet modeling is also scant. In the United States, model studies of this type were mostly carried out by the U.S. Army Engineer Waterways Experiment Station (WES) during the two decades before 1980 (Cain and Kennedy, 1979). All of the WES models were constructed at fairly large prototype to model ratio in the range of 300 to 500 with the vertical to horizontal distortion ratio around five. All WES inlet models use sand as the bed material. The main focus of these model studies was for navigation channel improvement although some of them also addressed the effects on adjacent shorelines due to the proposed improvement measures mostly of jetties structures. The topic of ebb tidal shoal evolution was not addressed in any of them. The issue on model scaling although raised practically in all these studies no serious attempt was made to construct the model based on any proposed modeling laws. Model calibrations were carried out in an ad hoc manner mainly by adjusting current velocities in the vicinity of the navigation channel and by observing scouring-accretion patterns in the nearshore zone. Sill, (1981) and Hayter, (1988) investigated ebb tidal shoal dynamics in laboratory using a small scale movable-bed inlet model with an inlet width of 0.3 m and a wave paddle of 3.1m wide. Their model studies showed that the volume and shape of ebb tidal shoal obtained in the laboratory bore. Certain resemblance to the field measured data. Their models mixed prototype-scale sand and tidal period with laboratory-scale geometry and waves. Owing to the small model scale and, hence, highly distorted model conditions, the question on modeling laws cannot be addressed. Consequently, the morphological time scale on ebb tidal shoal evolution could not be addressed either.

For this reason movable-bed hydraulic modeling in the laboratory provides an alternative that could shed insights on the dynamic process on one hand and yield practical information on the other. One of the major advantages of physical modeling is that there is no prerequisite, even though helpful, on the fundamental knowledge of the process. It can be carried out with reasonable resource at accelerated time scales. To achieve this goal, modeling law is addressed first with the aid of laboratory model experiments. Inlet model testing is then designed and carried out with the following specific objectives:

(1) Investigating ebb tidal shoal evolution process and the corresponding shoreline responses for a natural, unimproved inlet.

(2) Examining the process of ebb tidal shoal evolution and the corresponding shoreline responses for an inlet with jetty structures.

(3) Evaluating the effects on shoreline due to partial material removal from a matured ebb tidal shoal and the regeneration process.

The investigation of modeling law is given in a separate report " Movable-Bed Modeling Law of Beach Profile Response" (Wang, *et al.*, 1995). This report covers the objectives (1) and (2) as listed above. The task on objective (3) is still continuing and will be reported separately.

2. DESIGN OF INLET MODEL EXPERIMENTS

In nature, tidal inlets appear in different shapes and sizes. The processes of morphological changes including ebb tidal shoal evolution in the surroundings of an inlet are very complicated involving numerous mutually interacting factors. In conducting laboratory model experiment the first step is to narrow down the scope with due consideration of the constraints and then determine the values or range of values of experimental parameters based on modeling laws. The main experimental parameters are the inlet geometry, bottom sediment material, magnitude of sediment supply from the inlet and the natural forces. The important natural forces are recognized as that due to ocean waves, tidal currents and water level changes. Ocean wave is clearly a dominant driving force which produces longshore sediment transport known as littoral drift as well as cross-shore sediment transport that is most prominent under storm wave conditions. The tidal current not only acts as a sediment transport agency but also modifies the nearshore hydrodynamic condition by interacting with waves and topography. The water level defines the boundary affected by the dynamic forces. The design of experiment is discussed in this section with due considerations on experimental constraints and modeling laws.

2.1 Basic Considerations and Constraints

The model inlet experiments are to be carried out in the wave basin located in the laboratory of Coastal and Oceanographic Engineering Department, University of Florida. The approximate dimensions of the basin are 28 m $\times$ 28 m $\times$ 1m. The basin is equipped with a snake-type wave-maker, which consists of 88 independent wave paddles of 24 cm in width each. By adjusting the phase of each individual paddle motion it can generate waves of various oblique angles. However, an oblique angle larger than 15^0 is deemed undesirable because of the basin's lateral constraints. Depending upon the water depth which is limited to about 75 cm, wave heights ranging between 1 to 15 cm and wave periods from 0.9 to 1.9 seconds can be produced without difficulty.

To study ebb tidal shoal evolution, the basic model scale, here defined as the horizontal geometrical scale ratio of prototype to model, must be kept large enough such that a reasonable portion if not all of ebb tidal shoal occurred in nature can be duplicated at the expected laboratory scale. This requires preliminary information on the physical size of ebb tidal shoal associated with inlets found in nature.

Nevertheless, inlets in nature vary greatly in size and shape so are ebb tidal shoal volumes. The first task is then to select a test inlet configuration that is comparable to natural conditions. Walton and Adams (1976), and Marino and Mehta (1986) compiled ebb tidal shoal volumetric data for 15 inlets along the east coast of Florida and proposed different empirical relationships between an ebb tidal shoal volume and tidal prism. The results from Marino and Mehta (1986), with the locations of the inlets included in the analysis, are shown in Figs. 1 and 2, respectively. The results showed that ebb tidal shoal volumes decrease from north to south along this stretch of coast. The ebb tidal shoal volumes from the four northernmost inlets appear to be clustered in one group whereas the ebb shoals of the rest 11 inlets located in the mid and south regions exhibit much smaller shoal volumes. It is decided that the experiment should be representative of the latter group for two practical reasons: (1) It includes more than two third of Florida's east coast inlets located in one of the most densely populated coastal regions. (2) The physical dimensions of the test basin and the associated scale effects impose a limit on the actual size of the ebb tidal that can be adequately simulated. The shoal volumes associated with this group of inlets vary from 0.5 to 10 million m^3, which are generally considered as small to modest sizes. The inlet model is then designed based on an idealized inlet configuration that has the general hydraulic characteristics of inlets in the shaded zone of Fig.1 that covers the largest inlet population in the group. Inlets in this group can generally be classified as mixed energy type in which both waves and currents are important forces to cause inlet morphological changes in time scales of engineering interest from days to decades. Among them, Matanzas Inlet is the only natural inlet and the rest are all improved with jetties. At a horizontal geometrical scale in the range of 40 to 80, the basin size in model can accommodate ebb tidal shoal associated

with smaller inlets in the group. And at a horizontal geometrical scale in the range of 100 or so, ebb tidal shoal associated with mid-sized inlets can be properly simulated. Figure 1 which plots tidal prism versus ebb shoal volume also provides a rough guideline on the range of combinations of tidal current strength and the inlet cross-sectional area.

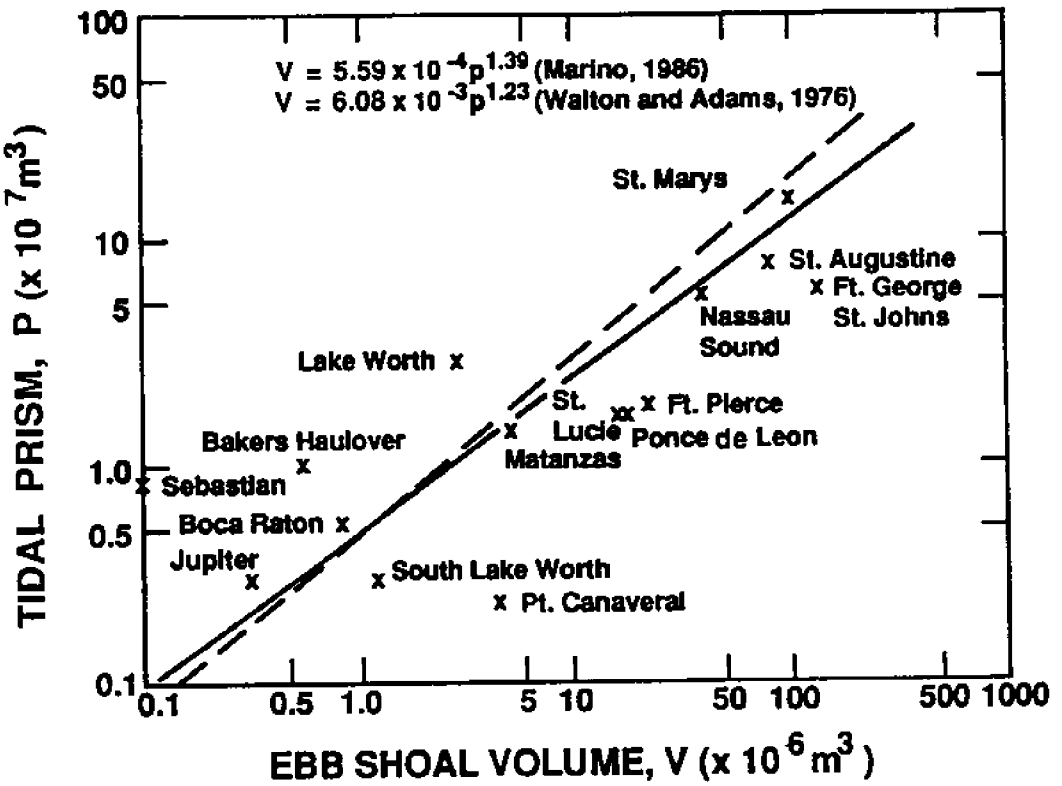

Figure 1: Tidal Prism-Ebb Shoal Volume Relationship for Florida's East Coast Inlets (after Marino, 1986).

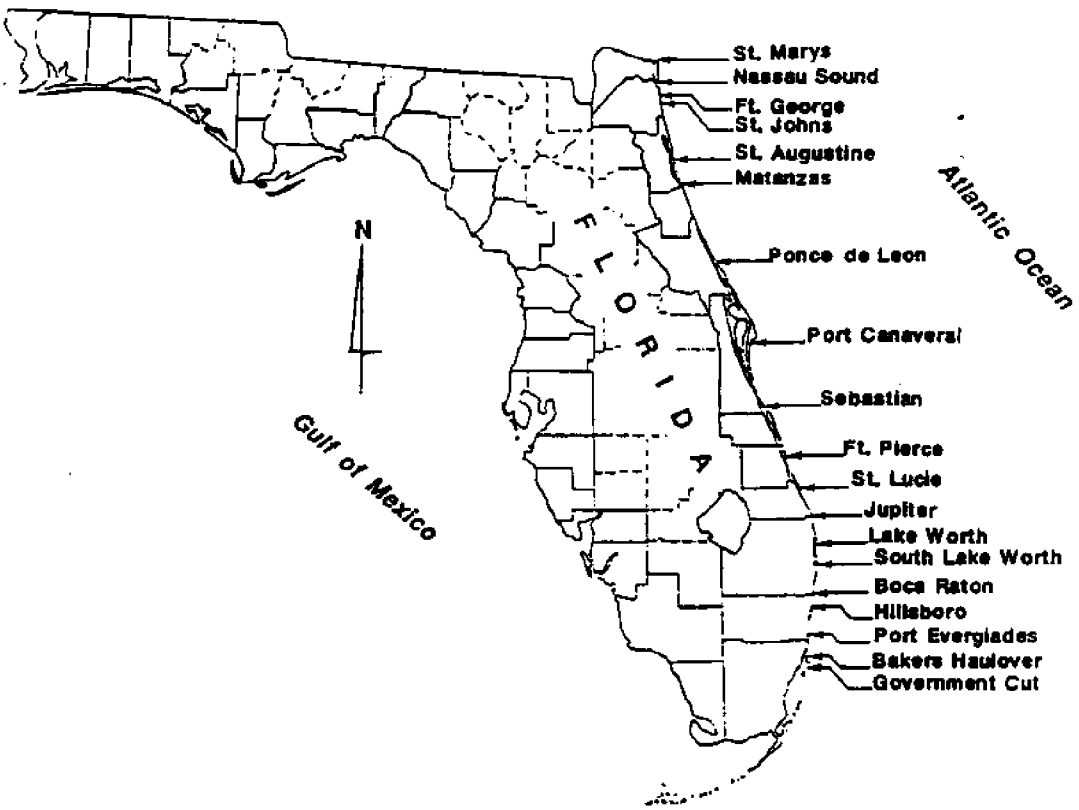

Figure 2: Location Map of Nineteen Inlets along Florida's East Coast.

Selection of experimental wave conditions is a more difficult task. In nature, wave conditions are random in magnitude, period, and direction. In the model experiment, the selection of wave conditions is rather limited owing to the facility and time limitation. In the present study, a simple scheme is devised to select the experimental wave conditions by examining the wave effects on sediment transport and the associated shoreline changes which can be roughly divided into four categories: (1) Waves from dominant weather direction causing beach erosion, (2) Waves from dominant weather direction causing beach accretion, (3) Waves from non-dominant weather direction causing erosion, and (4) Waves from non-dominant weather direction causing accretion. For instance, along the east coast of Florida, the dominant weather direction is from north west whereas the non-dominant

weather direction is from south east. For the mid east Florida's coastal region (Wang, *et al.*, 1993) it is estimated that for about 75% of the time waves are from dominant direction and for the rest 25% of the time waves are either from the non-dominant direction or negligibly small in magnitude. Evidently, sediment transport is dominated by the extreme wave events from either dominant or non-dominant direction. Therefore, it seems adequate to first test the effects of storm waves from the dominant weather direction in the model experiments. Under a storm wave event, suspended sediment transport usually dominates the bed load transport and this mode must be preserved in the experiment.

A major constraint in movable-bed physical modeling is the consideration on the compatibility of flow regime and modes of sediment transport between field and laboratory scales. In nature, the flow is mainly turbulent which needs to be preserved in the laboratory. The modes of sediment transport, on the other hand, could be a combination of suspended-load and bed-load transport, and other subclasses such as sheet-flow transport. In this aspect it is important to preserve the dominant mode of sediment transport in the model. Under storm wave condition the logical choice is the preservation of suspended load transport as observed earlier. In the case of finding flow conditions in the laboratory, Jonsson's(1966) flow regime chart (Fig.3) is used as a guideline. The flow regime consists of three different flow zones and three transition zones. The flow condition is determined by two parameters: a roughness parameter

$$a_m/k_s$$

and Reynolds number

$$R_a = \frac{u_b a_m}{\nu}$$

where a_m and u_b are the amplitudes of the fluid particle displacement and velocity, respectively; ν is the kinematic viscosity, and k_s is the roughness length, generally considered to be on the order of sand size.

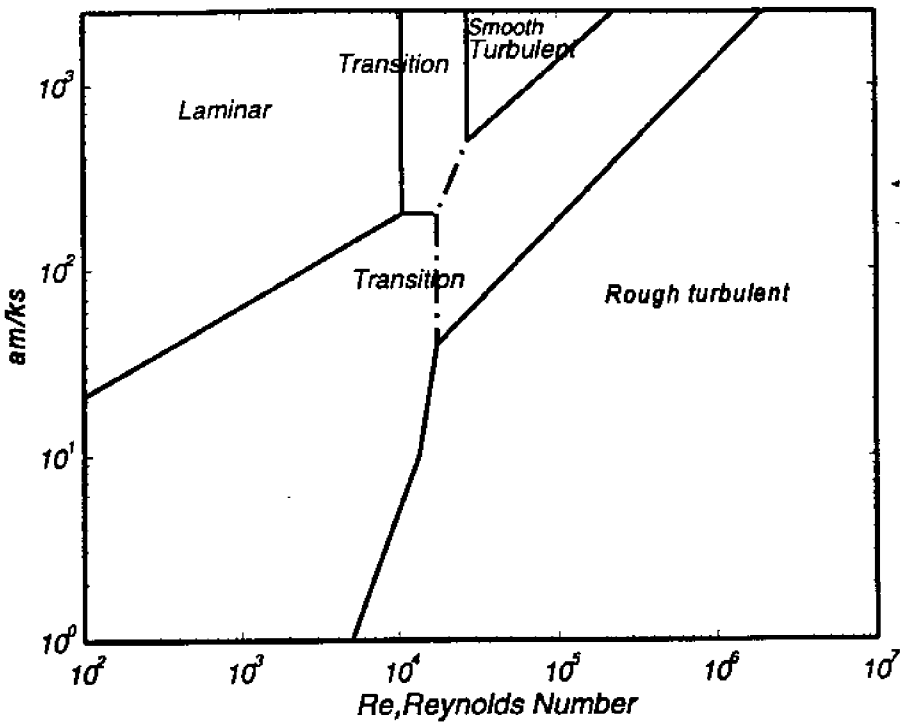

Figure 3: Josson's Flow Regime Chart.

As to determining sediment transport modes, a diagram proposed by Shibayama and Horikawa (1980) is used to classify the sediment transport conditions. The diagram is shown in Fig.4 which consists of the use of two parameters: the relative particle fall velocity

$$u_b/W$$

and the Shields parameter

$$\psi_m = \frac{f_w u_b^2}{2sgd}$$

where W is the particle fall velocity, f_w is the bottom friction coefficient, u_b is the bottom flow velocity, s is the sediment specific gravity, d is the particle size and g is the gravitational constant.

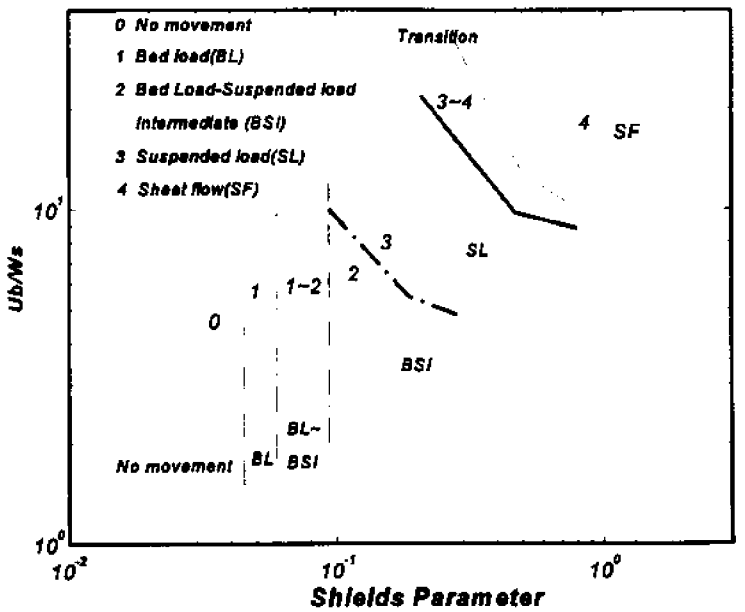

Figure 4: Sediment Transport Modes Diagram After Shibayama and Horikawa (1980).

To achieve turbulent flow and maintain suspended mode of sediment transport in the model while keeping the desirable horizontal scales in the range of 40 to 100, one has certain freedom to select the combinations of bottom material and vertical geometrical scale. Different materials have been proposed and used in movable model experiments but the most common one is still the natural quartz sand for the obvious reason that it closely resembles to, if not the same, the natural beach material and it is easier to obtain at low cost. To use natural sand as bottom material, however, vertical geometrical scale distortion appears to be necessary. The degree of distortion is addressed in the following section in Scaling Laws.

The last constraint in model testing is the consideration of time scale. In prototype, ebb tidal shoal evolution and regeneration are of long-term morphological processes which may take years or decades. In the model, these processes need to be accelerated in a different time scale. Based on Froude number consideration such a time scale in the model can be

shown to be in inverse proportion to the square root of the vertical scale. However, this time scale appears not quite sufficient to describe the ebb shoal process in the model. For instance, even for an undistorted model of vertical scales ranging from 40 to 100, one year prototype time would require nearly two months model run time in a laboratory. The proper accelerated time scale is augmented here by an equivalent storm approach.

Based on laboratory experiment and field observation, it is generally found that both sediment transport rate and the associated bottom topographic changes in nearshore environment are dominated by storm events. An example is shown here in Fig.5 from the results of Sebastian Inlet movable-bed model testing (Wang, *et al.*, 1992). In this example, bottom contour changes were examined in the case for six-day NE storm wave attack (wave height in 1.8 m and wave period in 8 second in prototype equivalents), followed by another eight-day ENE swell condition (0.6 m and 16 second). The model scales used in the testing were N_λ=60, N_δ=41, N_T=9.5, and N_{tm}=6.3. The experimental results indicated that the six-day storm waves produced a prototype sediment transport of 1,700 m^3/day on the downdrift side boundary as opposed to a mere 370 m^3/day in the following eight-day swell period. It is shown in Fig.5 that a marked ebbshoal topographic change (contour increment in 25 cm in prototype equivalent) occurred only during the six-day storm wave event. This trend was also observed for the net sediment loss into the inlet. The commonly accepted sediment transport formulas also support this condition. Therefore, all the present model experiments are conducted under storm wave conditions in order to accelerate the process.

2.2 Modeling Laws

The state of knowledge on nearshore movable-bed modeling is largely a mixture of empiricism and art. Concerning modeling laws on an inlet-beach system, there hardly exists any conceptional guideline. As reviewed earlier, the geometrical scales used in the inlet models were mostly arbitrary. No serious attempt has been made to scale these laboratory results to prototype values. Therefore, the task of scaling presents a new challenge.

(a) topographic change under a 6-day NE storm event (--- erosion, —— accretion).

(b) topographic change under (a) and a 8-day ENE swell condition (contour in 0.6 cm).

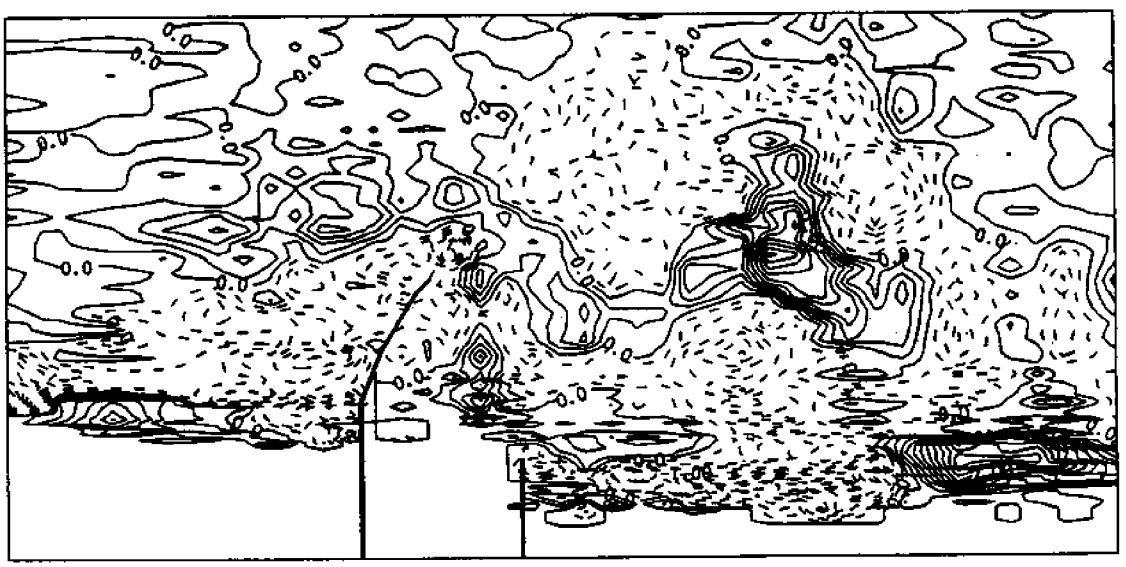

Figure 5: An Example From Sebastian Inlet Physical Model Testing.

Two prerequisites have been discussed in the previous Section that the nearshore flow condition should be turbulent and that the suspended load should be the dominant mode of sediment transport. To fulfill these requirements using natural sand as bottom material, the vertical scale might have to be distorted in the model. Therefore, the modeling law must have a flexibility to accommodate this requirement. In searching for past movable-bed modeling practices, it is found that there has been reasonable success for modeling beach profile responses under storm wave conditions. A summary on beach profile response modeling laws can be found in Hughes (1993). All these modeling laws were based on the assumption that suspended load is the dominant mode and most of them can be applied at distorted scales. Therefore, the prerequisites given above can be satisfied. The present study represents an initial attempt to extend this class of modeling law to an inlet-beach system.

There are two main issues to be addressed. One is to select or modify, if necessary, a modeling law among the existing ones for applications in the present study. The other is more fundamental to see if a beach-response modeling law is actually suitable for inlet-beach system. Of course, it is apparent that beach response under storm condition is mainly wave driven, and it is more or less two dimensional for a straight shoreline whereas in an inlet-beach system the sediment movement is due to the combined forces of waves and currents, and the phenomenon is clearly three dimensional. Considerable effort has been spent on addressing both issues although the second issue can only be examined after model experiments and even then may not be answered for lack of verification.

Concerning the selection of a modeling law among the existing ones, a detailed laboratory model experiment was carried out. The experiment entailed both two-dimensional wave tank and three-dimensional wave basin tests on beach profile responses at different geometrical scales. These test results were the compared with data from a prototype scale experiment performed in German Large Wave Tank (GWK) test (Dette and Uliczka, 1986a,b). The comparison of wave tank test results with GWK data was reported separately (Wang, *et al.*, 1994).

Four different modeling laws, as shown in Table 1, were evaluated based on a series of 2-D wave tank tests carried out at horizontal scales of 20, 30, and 40 with vertical distortions specified by the modeling laws. These four modeling laws were proposed by Le Mehaute (1970), Vellinga (1982), Hughes (1983) and Wang, *et al.* (1990), respectively.

Table 1: Summary of Fall Velocity Distorted Model Laws.

Author	Geometric Distortion	Hydrodynamic Time scale	Morphological time Scale
Le Mehaute(1970)	$N_\delta=(N_w N_\lambda)^{2/3}$	$N_T=\sqrt{N_\delta}$	$N_{tm}=\sqrt{N_\delta}$
Vellinga (1982)	$N_\delta=N_w^{0.44}N_\lambda^{0.78}$	$N_T=\sqrt{N_\delta}$	$N_{tm}=\sqrt{N_\delta}$
Hughes (1983)	$N_\delta=(N_w N_\lambda)^{2/3}$	$N_T=N_\lambda/\sqrt{N_\delta}$	$N_{tm}=N_\lambda/\sqrt{N_\delta}$
Wang, et.al(1990)	$N_\delta=(N_s N_w)^{0.4}N_\lambda^{0.8}$	$N_T=N_\lambda/\sqrt{N_\delta}$	$N_{tm}=\sqrt{N_\delta}$

A parallel sets of experiments with undistorted scales were also conducted. It becomes immediately evident that at undistorted scale extremely fine sand is required in the model. For example, to model a prototype case with median sand grain size of 0.3 mm at a horizontal scale of 40 requires laboratory sand grain size in the order of 0.09 mm. Even finer sand has to be used for scale larger than 40. Table 2 illustrates the scale relationship between prototype and model based on Wang's or Vellinga's criteria. Nevertheless, the actual experiments of the undistorted model were not successful.

Table 2: Model and Prototype Scale Quantities.

Horizontal length scale	$N_\lambda=20$
Vertical length scale	$N_\delta=14.46$
Fluid-motion time scale	$N_T=5.26$
Fall velocity scale	$N_w=1.99$
Morphological time scale	$N_{tm}=3.8$

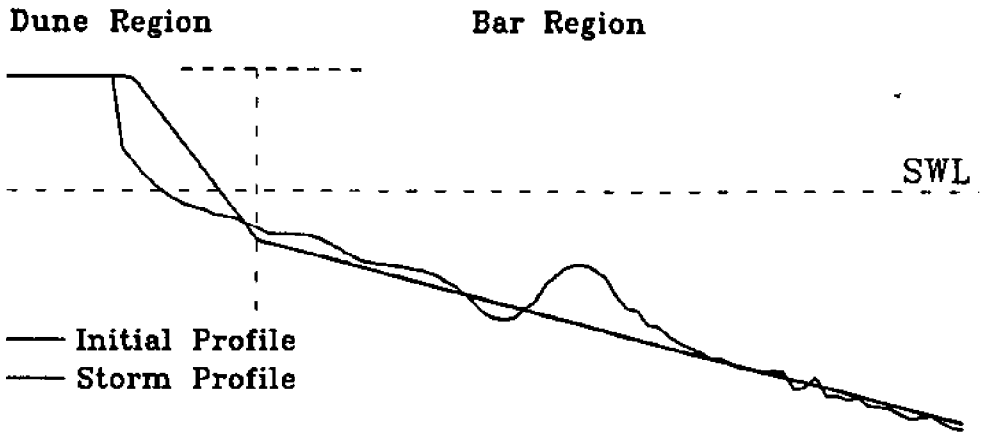

Figure 6: Two Different Beach Profile Regions Scheme.

Since the intent is to extend the beach profile modeling laws to also cover the offshore shoal region, the model evaluation criteria should be extended to include that region. This can be partially accomplished owing to the fact both the GWK tests and the present tests in 2-D wave tank stopped at offshore bar which does not quite include the entire region of ebb tidal shoal. In the present study, the evaluation of modeling laws is carried out in two different beach profile regions: the dune region (shore region) and bar region (offshore region) as shown in Fig.6. Five criteria: (1) dune erosion volume, (2) nearshore profile, (3) bar volume, (4) bar crest location, and (5) bar geometrical location, are selected to evaluate the modeling laws. The results from the 2-D wave tank tests indicated that:

(1) For dune erosion, all four existing modeling laws were reasonably adequate to predict the final erosional volume but over predict the erosion rate before reaching the final experimental stage.

(2) Wang's and Vellinga's modeling laws performed better for nearshore profile.

(3) All the modeling laws predicted the main bar location closer to shoreline than the prototype data.

One probable cause for (3) is that all existing models treated wave height scale the same as the vertical scale. However, in nearshore zone it is known that wave breaking is affected by water depth as well as local beach slope. Thus, waves tend to break earlier at a larger water depth on a more gentle slope than a steeper slope. A general breaking criterion incorporating slope effect can be given as

$$H_b = \gamma(m) h_b$$

where H_b and h_b are wave height and water depth at breaking location, respectively, γ is defined as the breaking index, here expressed as a function of slope, m. In general, the value of γ increases with increasing beach slope. In other words, when the slope becomes exaggerated in a distorted model the wave height scale should also be enhanced accordingly in order to preserve the surf zone width. Therefore, if the wave height is simply scaled according to the vertical geometrical scale the surf zone width in the model when scaled up to prototype will be narrower than that in nature. Hence the breaking bar location from the model prediction will also be closer to shore than that occurs in nature. To rectify this discrepancy, a modified modeling law was proposed with wave height scaling enhancement as follows:

$$N_H = \left(\frac{N_\delta}{N_\lambda}\right) N_\delta$$

where N_δ and N_λ are the vertical and horizontal scale ratios, respectively. The quantity in the parenthesis can also be viewed as breaking index scale (Wang, *et al.*, 1994). Accordingly, some new sets of equations were established for the modified modeling law as shown in Table 3.

This modified modeling law was found to adequately scale both nearshore and offshore regions in the 2-D wave tank tests. This new modeling law was also tested in the 3-D wave basin for a 2-D beach at a horizontal scale of 20. Four sets of experiments were carried out, three under normal incident wave conditions and one under oblique waves of 15^0 angle. The test conditions are summarized in Table 4.

Table 3: Modified Modeling Law.

Geometric Distortion	Wave Height Distortion	Hydrodynamic Time scale	Morphological time Scale
$N_\delta=(N_s N_w)^{0.4} N_\lambda^{0.8}$	$N_H=(N_\delta/N_\lambda)N_\delta$	$N_T=\sqrt{N_\lambda}$	$N_{tm}=\sqrt{N_\lambda}$

Experiments B1, B2, and B3, with normal incident waves are used for verification of modeling laws. The test wave height and period in both Experiments B1 and B2 followed the original modeling law by Wang, *et al.* (1990), whereas B3 employed the modified modeling law. In Experiments B1 and B2, two different initial profiles were used. The intent is to determine the best modeling law and to test the model sensitivity. First of all, the two dimensionality of the beach appeared to hold well in all three Experiments B1, B2, and B3 at the completion of the tests. Figure 7 shows the final profiles measured at five different cross-sections in Experiment B3.

Table 4: Test Conditions for Plane Beach Experiment.

Test No.	Incident Wave Condition			Beach Slope	
	Wave period	Wave height	Wave angle	Foreshore	Offshore
B1	1.14sec	10.5cm	0 deg	1:24	1:17.4
B2	1.14sec	10.5cm	0 deg	1:20	1:14.5
B3	1.33sec	12.5cm	0 deg	1:20	1:14.5
B4	1.33sec	12.5cm	15 deg	1:20	1:14.5

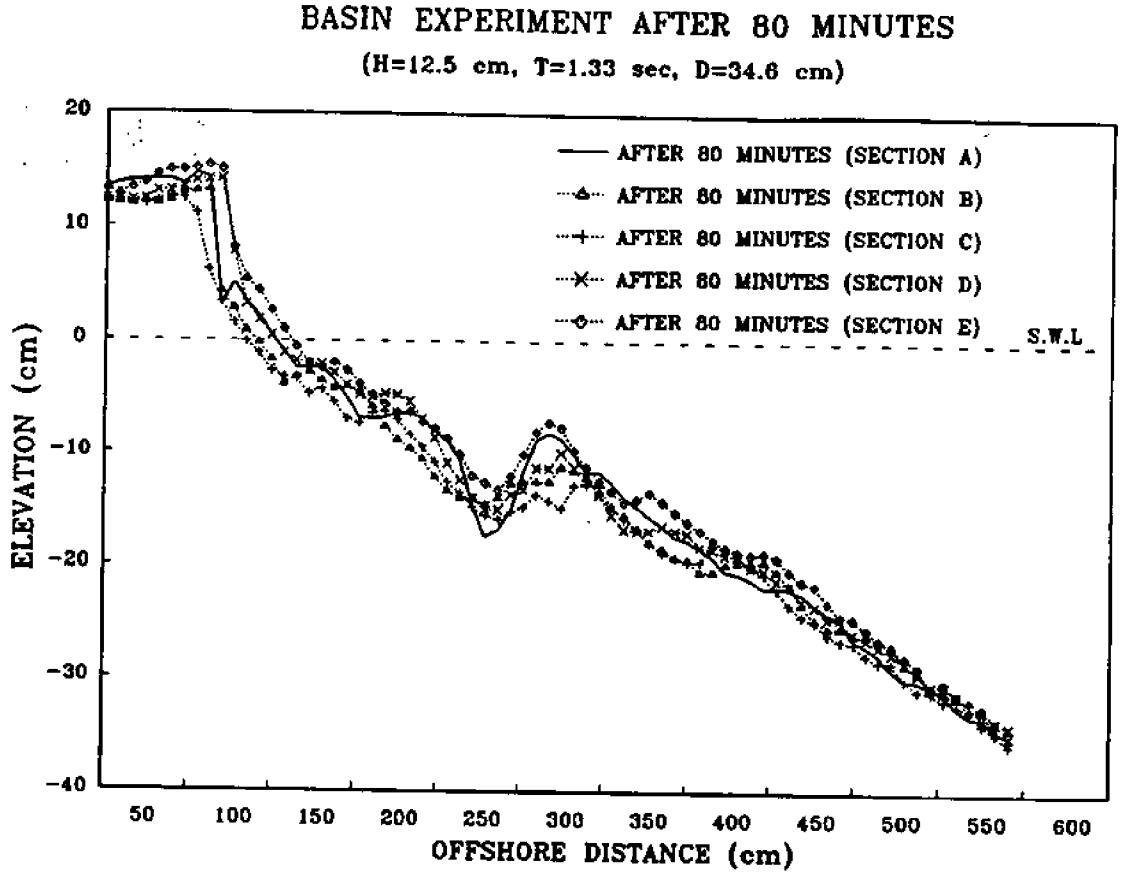

Figure 7: The Final Profiles Comparison in Experiment B3.

The experimental results showed that the proposed new modeling law has the best over all match with the GWK prototype data. Figure 8 compares the measured profiles in Experiment B3 with the GWK data based on the new modeling law. The original modeling law by Wang, *et al.* (1990) was also found to yield a reasonable match in Experiments B1 and B2. This seemed to indicate that although the new modeling law has the best overall fit, the model is not sensitive to slight variations of either wave period or height. Also since B1 and B2 have different initial profiles the end profiles are similar. In other words, the model is also not sensitive to initial profile shapes. This latter conclusion is somewhat expected since the concept of equilibrium profile has been well established.

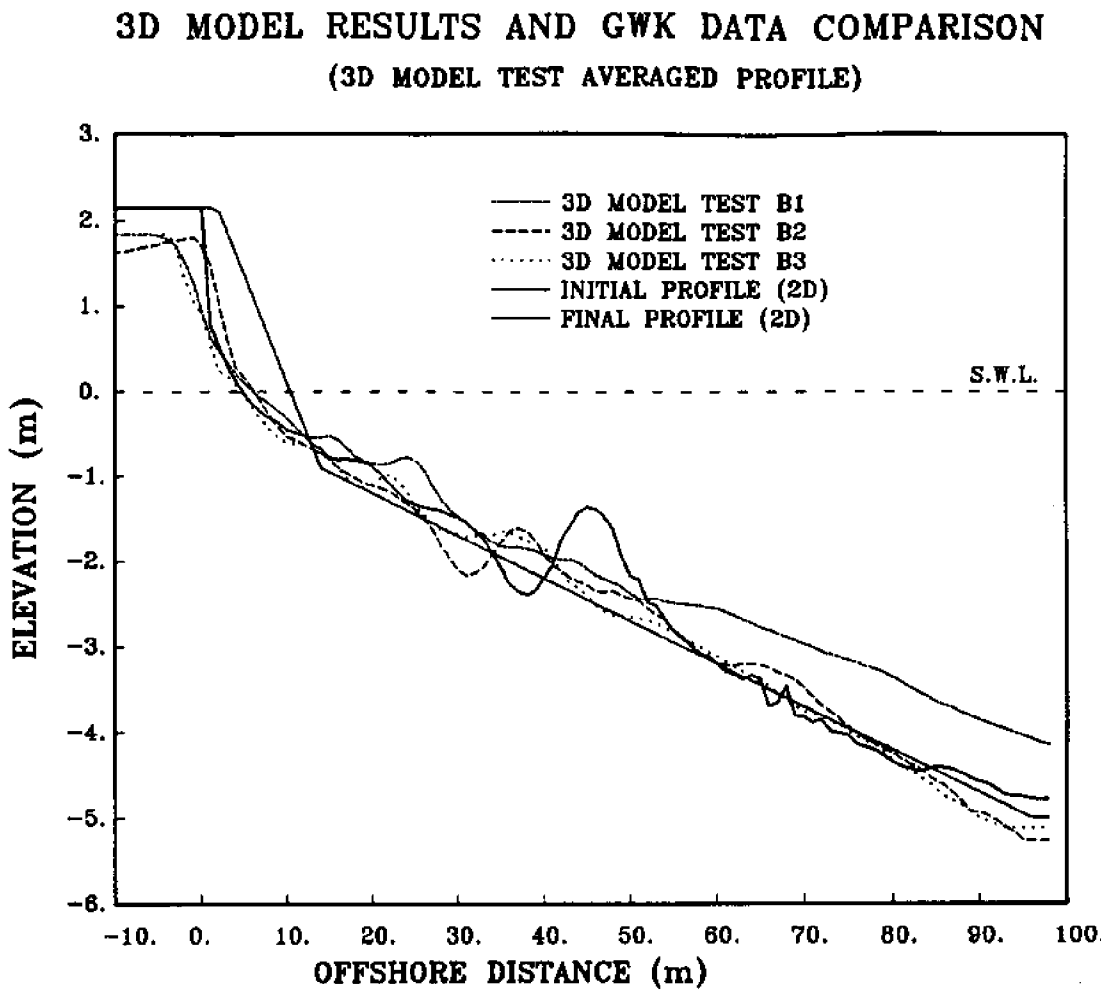

Figure 8: Comparison Between Measured Profiles in B3 and GWK Data.

Experiment B4 tested the beach model with oblique waves. The test result was utilized to check the longshore transport rate by comparing with the longshore transport formula given in SPM (1984). The measured transport rate was found to be considerably smaller than that computed by the formula. The best fit transport coefficient, K, from the laboratory data was found to be equal to 0.24, smaller than the recommended value of 0.77. The experimental value, however, is much closer to that experienced along the east coast of Florida and to some of the other laboratory experiments.

2.3 Inlet-Beach Model Design

The inlet-beach model was designed with due considerations of the constraints and the modeling laws addressed in the previous two sections. An idealized inlet of rectangular cross section was constructed cutting through a plane beach made of natural beach sand with D_{50}=0.19 mm. The overall length of the beach from updrift end to the down drift end is about 19 m. It is bounded on two sides by wave guides formed by concrete blocks. The wave guides are semi-perforated to allow flows in and out of the test section. The downdrift wave guide also has an opening near the beach end to allow downdrift littoral transport to leave the test section and to be collected in the catch channel. The plane beach consists of a flat back shore segment, a steep-slope foreshore segment and a mild- sloped offshore profile which extends seaward to about 7 m from the shoreline beach face before merging with the flat basin concrete floor. The beach profile approximates an equilibrium shape of $h=Ax^{0.8}$ (h is water depth, x is seaward distance from shoreline). Figure 9 shows this composite profile together with the curve of the equilibrium shape. The inlet is a straight rectangular channel with uniform width and depth of 1.75 m and 0.2 m, respectively. The inlet is located offset from the center towards the updrift with the updrift beach length of 4.5 m and downdrift beach length of 12 m.

For this inlet model configuration the wave generator is located about 27 m from the shoreline based on an average water depth about 0.35m. The model setup is shown schematically in Fig.10. As shown in this figure, tidal currents are generated by recirculating water through the channels as depicted. The flow discharge is controlled by the weir boxes located on the two sides of the basin. Water is supplied from the upper basin weir boxes (flood flow weirs) for flood current and from the lower basin weir box (ebb flow weir) for ebb current.

The design of sand supply from the updrift end presents a challenge. After trying several techniques it is settled with forming a curved feeder beach section at the updrift end. The sand supply to the downdrift is, therefore, purely due to wave-induced transport. This

design allows for continuous and more uniform sediment supply and the magnitude is automatically adjusted for different incident wave angles. This feeder beach has to be replenished from time to time during the intervals of conducting beach surveys.

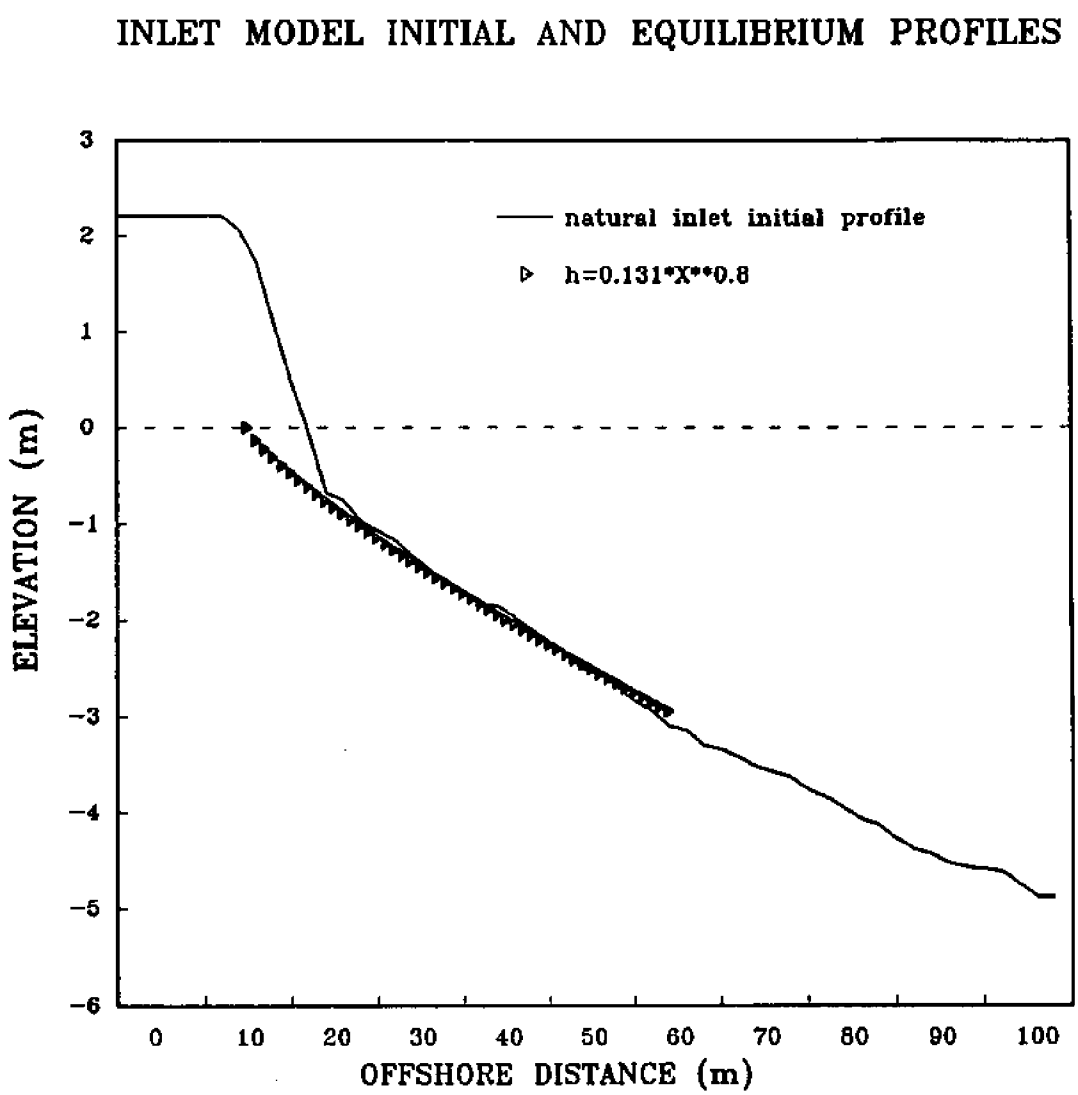

Figure 9: Initial Beach Profile and Equilibrium Profile in the Model.

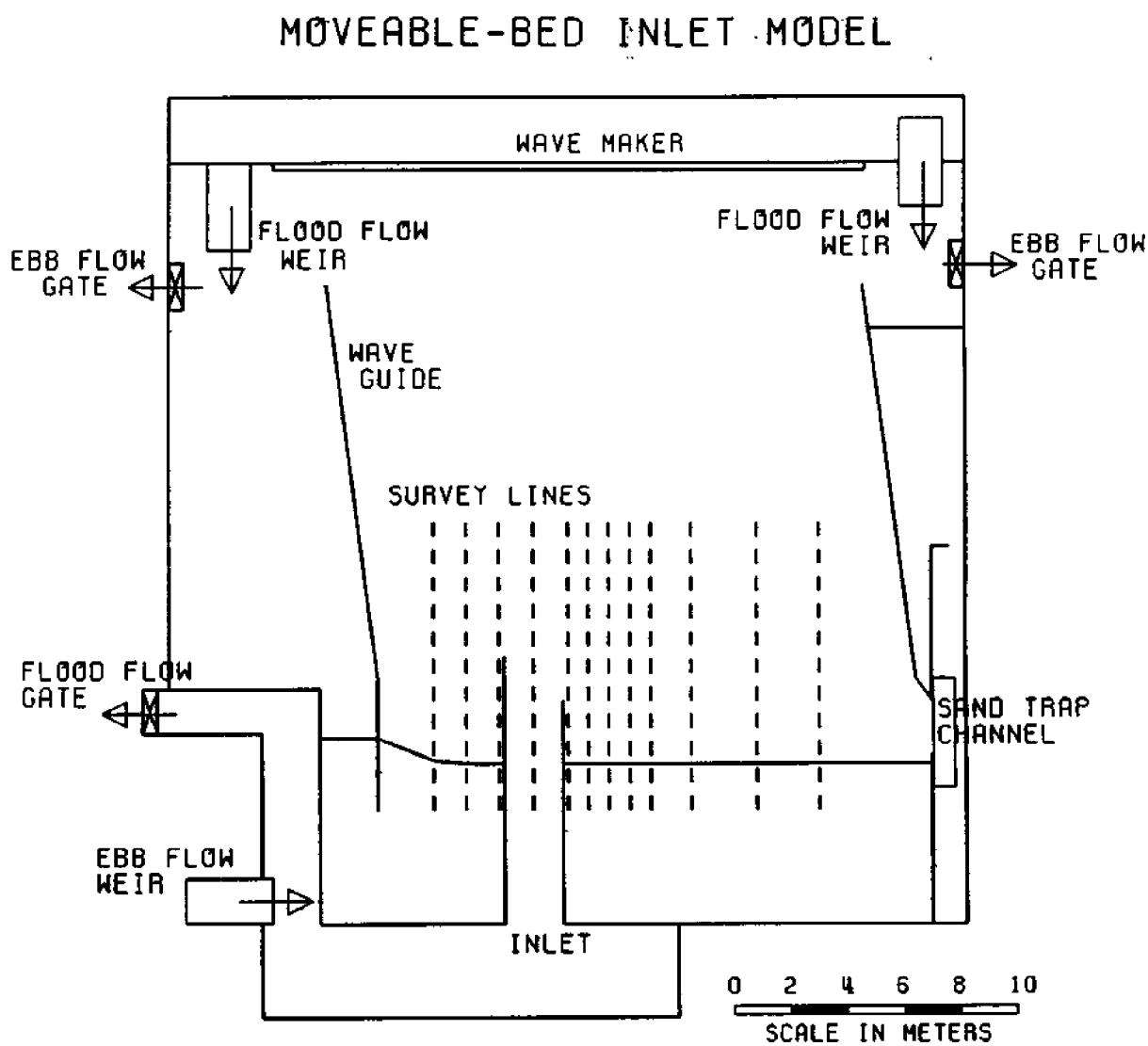

Figure 10: The Schematic Setup for Movable-Bed Inlet Model.

3. EXPERIMENTS AND TEST RESULT

3.1 Test Conditions

Three sets of experiments were carried out for the inlet-beach system. The test conditions and test run times are given in Table 5.

Table 5: Test Conditions of Inlet-Beach System Experiment.

Test No.	Water depth	Incident wave condition			Beaches slope		Jetties (Type)	Model time (min)
		Wave period	Wave height	Wave angle	Foreshore	Offshore		
C1	35 cm	1 sec	8 cm	15 deg	1:20	1:14.5	none	480
C2	35 cm	1 sec	8 cm	15 deg	1:20	1:14.5	Riprap	1600
C3	35 cm	1 sec	8 cm	7.5 deg	1:20	1:14.5	Caisson	4860

Among these three test cases, Experiment C1 is to simulate a natural inlet; C2 is to simulate a jettied inlet with riprap type jetties and C3 is to simulate a jettied inlet with caisson type jetties. The jetty geometries are the same for Experiments C2 and C3. Both updrift and downdrift jetties are straight and perpendicular to the shoreline. The length of the updrift jetty measures 1.5 m from the shoreline. The downdrift jetty is about half the size of the updrift jetty with a length of 0.7 m. The height of jetty top is about 5 cm above the flood tide water surface and the jetty width is about 20 cm. This uneven jetty geometry is common to the inlets with updrift and downdrift jetties in Florida. The major difference between riprap and caisson type jetties is that the riprap is porous and not sand tight whereas the caisson is impervious. Figures 11 to 13 show the initial topographic contours together with photos of the three different test configurations.

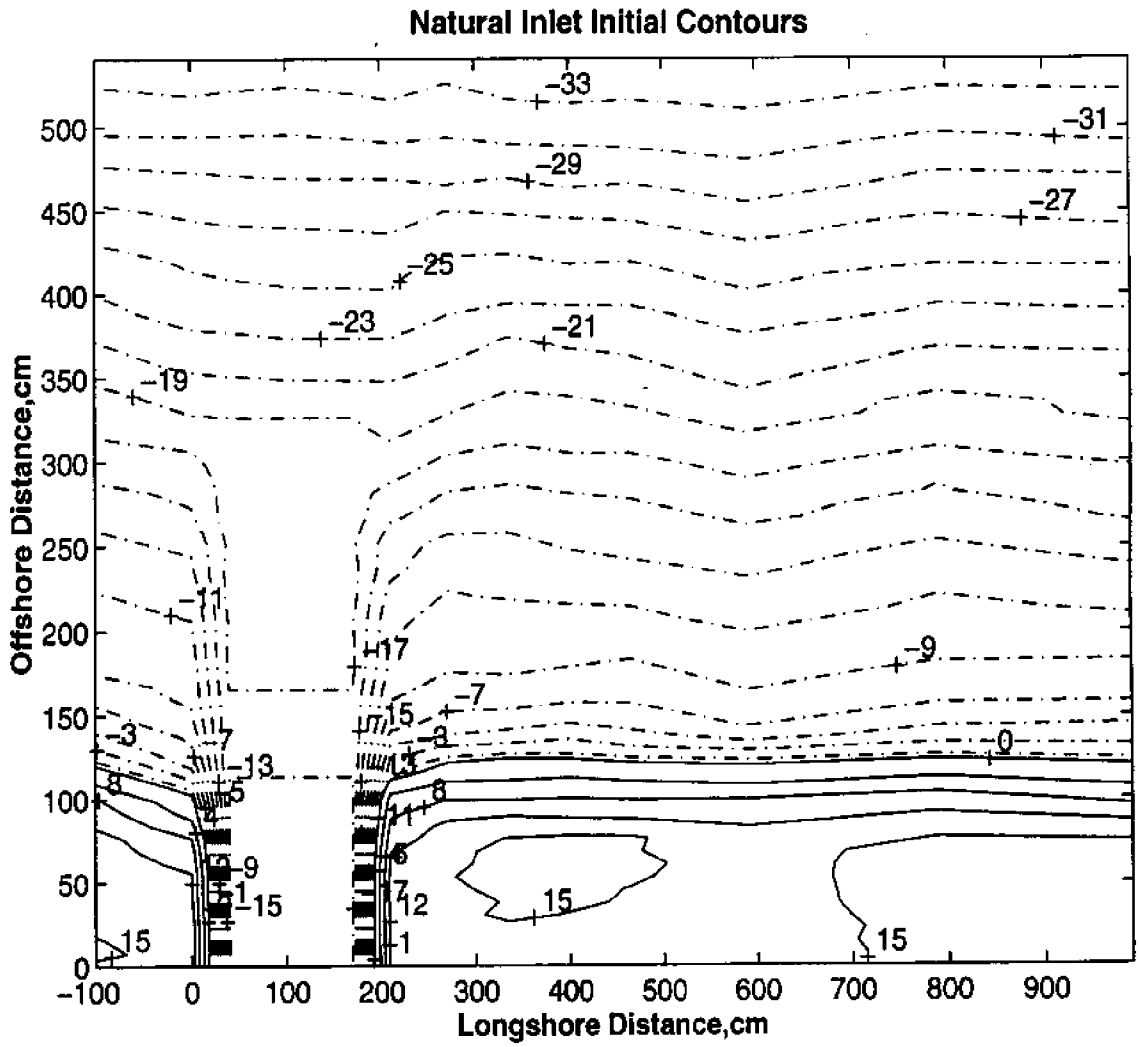

Figure 11: The Initial Topographic Contours for Experiment C1.

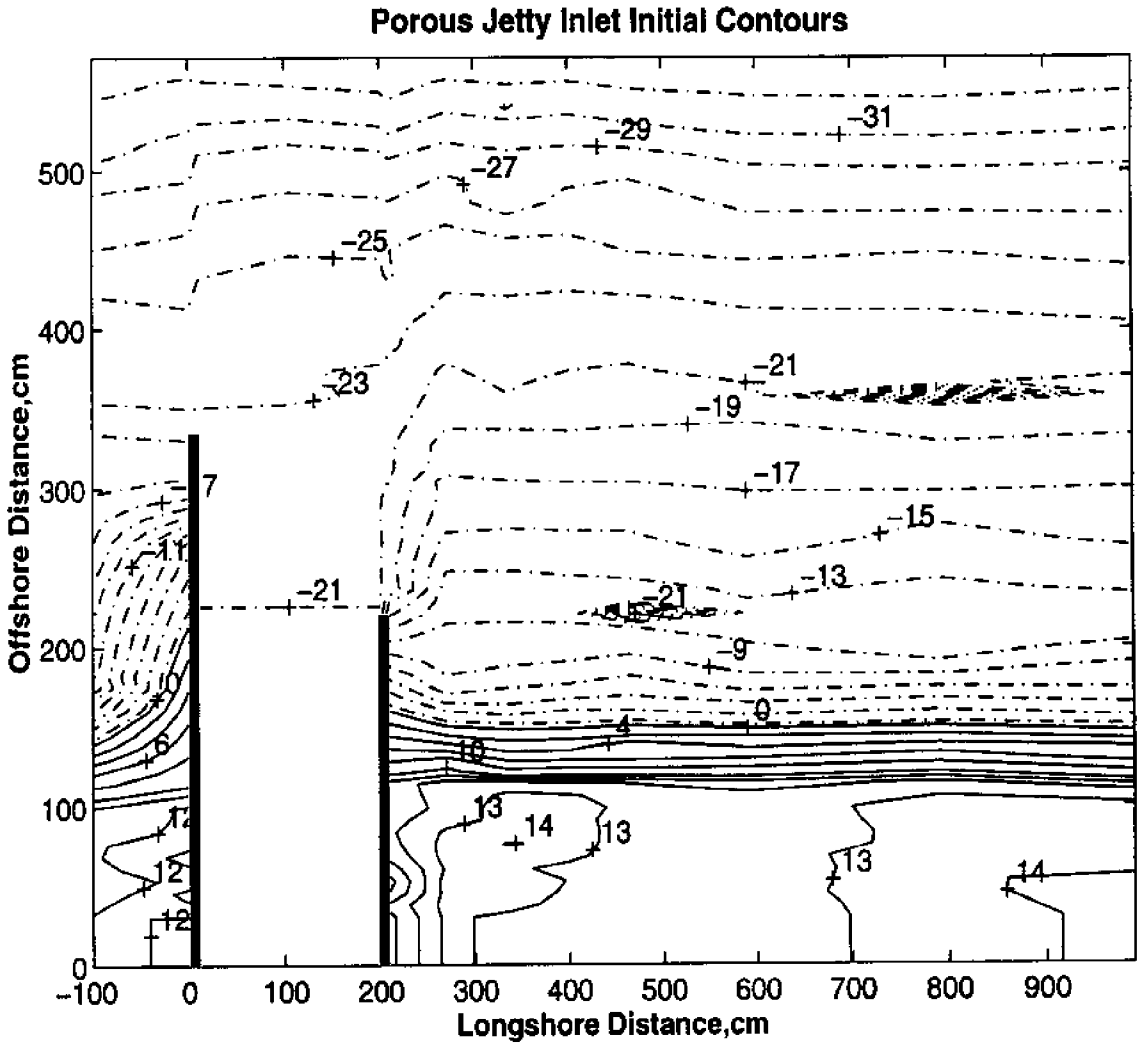

Figure 12: The Initial Topographic Contours for Experiment C2.

(a) A photo showing the initial topography

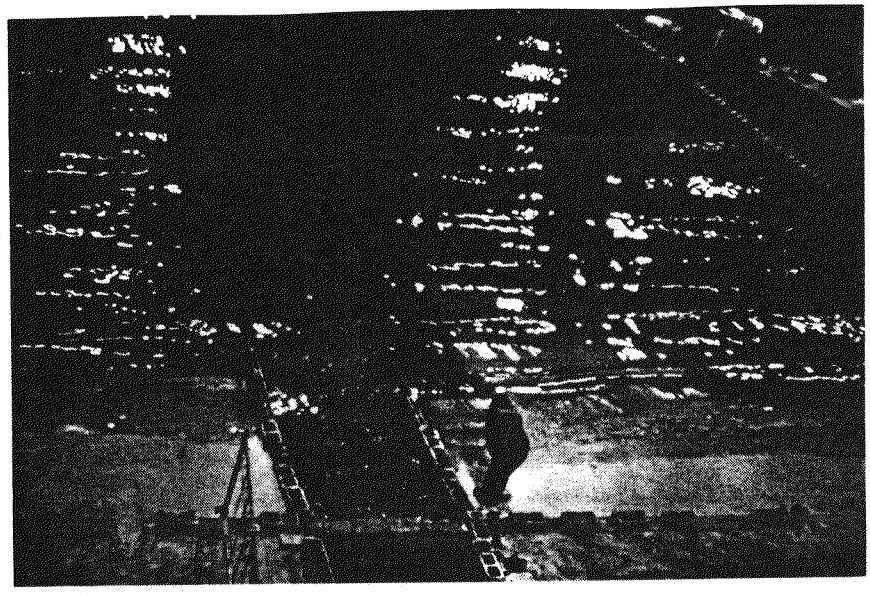

(b) Bottom contours of the initial topography

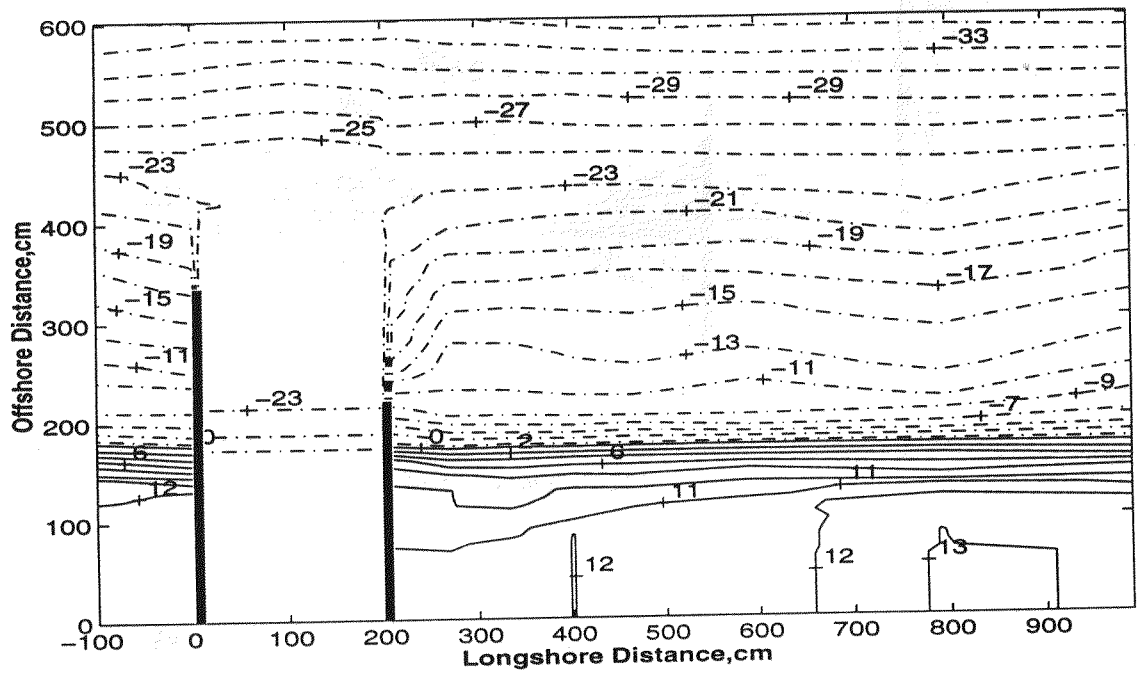

Figure 13: The Initial Topographic Photo and Bottom Contours for Experiment C3.

Incident waves utilized in the experiments are the storm waves generated by wavemaker at the offshore boundary with 8 cm in height and 1 second in period. The attacking wave direction is 15^0 in Experiment C1 and C2. After examining the results from these two experiments, it was judged that this incident wave angle was too large causing excessive channel shoaling and severe beach erosion and the experiments had to be stopped. Therefore, the incident wave angle was reduced to 7.5^0 in Experiment C3.

The tidal currents are simulated in the experiment by alternating the ebb and flood cycles at equal interval of 40 minutes. Based on Froude criterion, this time interval roughly corresponds to a semi-diurnal tidal period at 1:80 geometrical scale ratio. The tidal current condition can be simulated with a number of choices: equal flood-ebb discharge, equal flood-ebb current strength, unequal discharges or current strengths at the inlet throat. Based on field measurements at Sebastian Inlet (Wang, *et al.*, 1991) and also at other inlets equal discharge appears to be a reasonable choice and was adopted in the model test. This usually will result in stronger ebb current which is often experienced in the field. In the present study, the discharge is kept constant at 0.04 m^3/sec within each ebb and flood period. The cross-sectional averaged flood current in the inlet is 0.12 m/sec with an inlet water depth of 0.2 m. These values corresponding to ebb cycle, on the other hand, are 0.14 m/sec and 0.17 m, respectively. The ebb and flood currents were simulated alternatively in stepwise fashion, instead of sinusoidal or other types. The stepwise changes of ebb and flood currents in model experiment is deemed adequate as compared to the prototype data. Figure 14 shows the current measurements at Sebastian inlet. It is seen that the current variations within each ebb or flood can be reasonably approximated by uniform step function.

Water level is another important factor that affects beach erosion. In the present study, no attempt was made to simulate storm surges. The periodical water level change due to tidal cycles, however, was included in the test. During flood tide, water level was higher as water feeds towards the inlet whereas during ebb tide, water level was lower as water jets from the inlet. The simulated tidal range is 3 cm in the experiment.

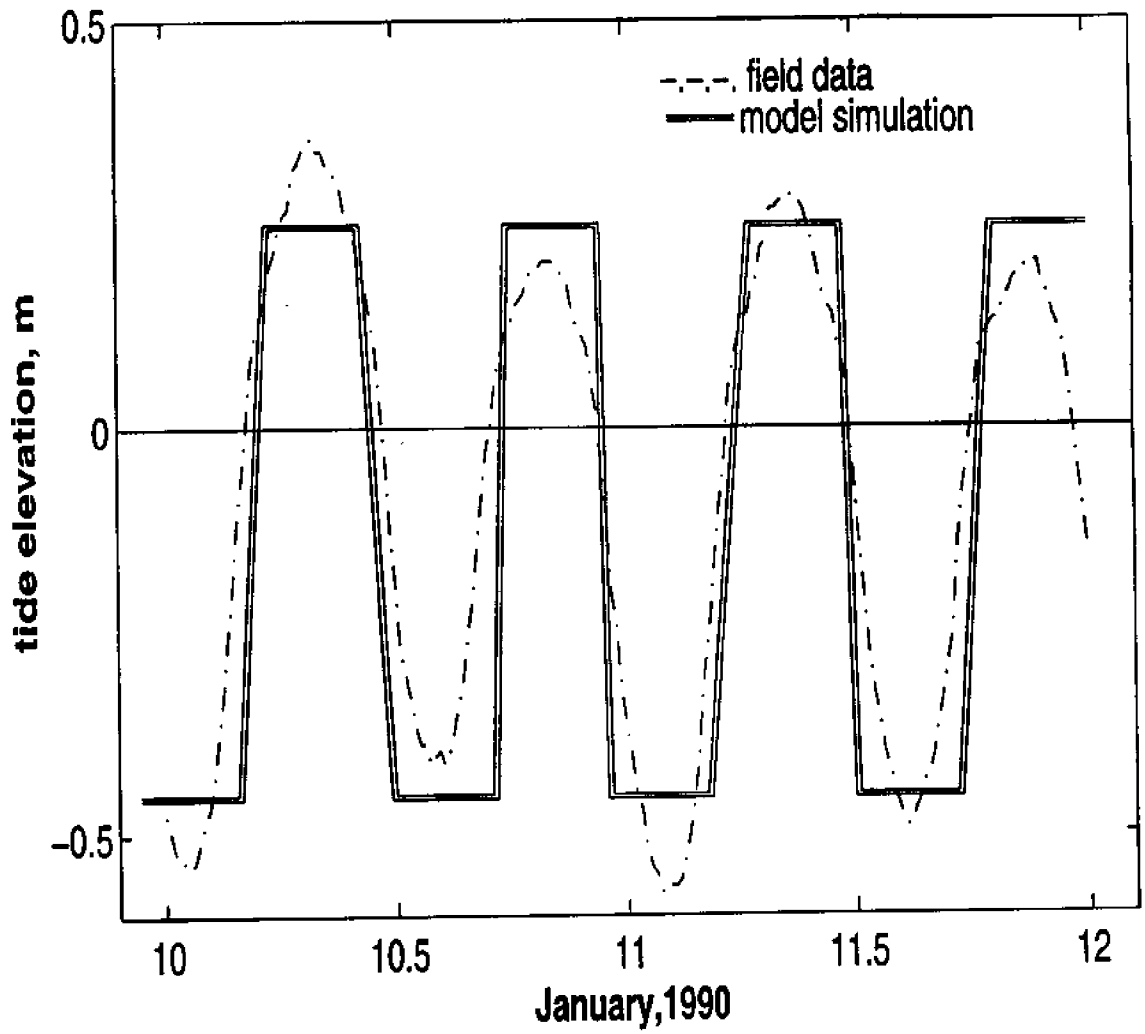

Figure 14: The Current Measurements at Sebastian Inlet..

3.2 Test Procedures

The model experiment is conducted according to the following procedures:

(1) Prepare model bathymetry.

(2) Survey initial profiles at twelve cross-sections as shown in Fig.10.

(3) Adjust water level and discharge to the specified design values. Start up the current until it stabilizes. All the tests start with ebb cycle first.

(4) Start wave generator with pre-calibrated settings. The experiment is interrupted at intervals of every 40 minutes for the change of tidal conditions between ebb and flood.

(5) Conduct bottom profile surveys at selected time intervals. The time intervals are irregular, shorter in the early stage of the experiments and progressively longer later. For example, the surveys conducted for C3 are at the time marks of 20min, 40min, 80min, 120min, 160min, 480min, 1120min, 1600min, 2240min, 3200min and 4860 min, respectively.

(6) Collect sand cumulated outside the downdrift boundary and inside the inlet.

(7) Reshape the model to its initial bathymetry for the next experiment.

In addition to the normal operating procedures described above, dye and sand tracer studies were also conducted from time to time. The dye studies were current observation and were documented by video recordings. Sand tracers were mainly used for visual examination on a sediment transport pattern. No quantitative analysis was attempted. Figure 15 shows a picture of the dye study.

In the natural inlet case of C1, the experiment was terminated at model time of 480 minutes when shoaling nearly closed the inlet entrance. In the case of C2, the experiment was stopped at model time of 1600 minutes when both inlet shoaling and downdrift beach erosion became too severe to continue. The large shoaling in inlet channel near the updrift jetty entrance was partially due to sediment transport through the porous jetties and severe downdrift erosion was judged to be caused by the large incident wave angle. In the case of C3, the experiment was run under alternate flood and ebb tidal conditions up to 1600 minutes

(a) A photo showing dye test during ebb current condition (without waves)

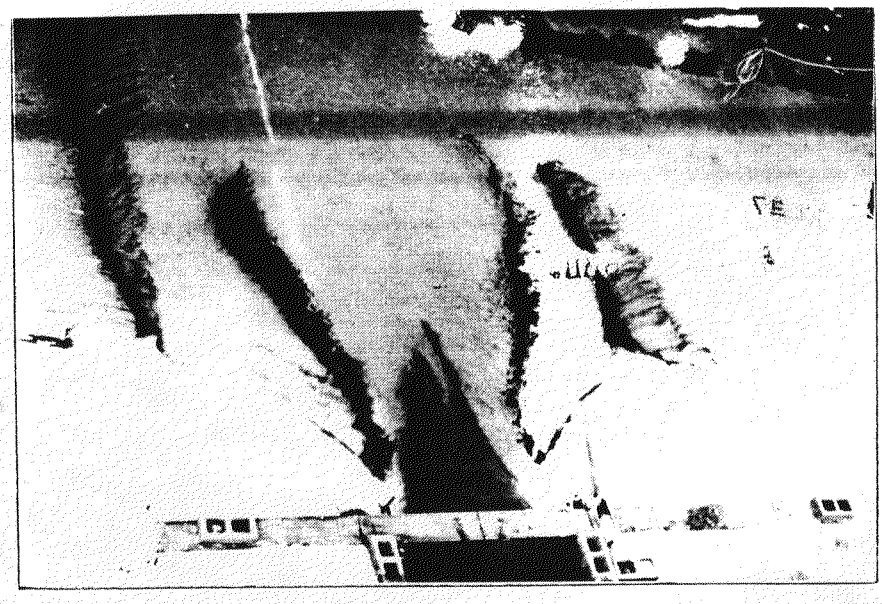

(b) A photo showing dye test during ebb current condition (with waves)

Figure 15: Dye Study of Current Pattern.

After 1600 minutes, the process of shoal development slowed down considerably. The experiment was then continued to 4860 minutes under ebb tidal condition only to extend the test duration as long as possible. After 4860 minutes the shoal began to move offshore beyond the test beach and onto the concrete floor. The experiment was terminated.

3.3 Test Results

3.3.1 Natural Inlet (Experiment C1)

The natural inlet experiment was designated as Experiment C1 in the present study. It is composed of a plane beach of straight shoreline with a rectangular tidal channel. The experiment was conducted for a total of 480 minutes or six complete tidal cycles. The experiment was not continued for a longer test time because both the downdrift erosion and channel shoaling were too severe as large waves dominated the shore erosion process. Figure 16 displays the end condition after 480 minutes test time. Bottom topographic surveys were conducted at 20, 40, 80, 120, 160 and 480 minutes, respectively. Detailed survey results including bottom topographic changes at different time intervals and profile changes were given in Appendix A.

3.3.2 Inlet with Porous Jetties (Experiment C2)

The porous jetties in C2 are of riprap type. The experiment was carried out for a total model time of 1600 min and was stopped at the end of 1600 minutes. A significant amount of sediment apparently had leaked through the porous jetties from the updrift side forming a large local shoal just inside the updrift jetty. Topographic surveys were conducted in model at every 40 minutes, i.e., at the end of each ebb or flood phase run, for the first 200 minutes. Afterwards, survey intervals were carried out at irregular and larger time intervals. Figure 17 shows the bathymetry change contours at the end of 1600 minute. Survey results including bottom topographic changes at different time intervals were given in Appendix B.

3.3.3 Inlet with Impervious Jetties (Experiment C3)

Experiment C3 is similar with C2 but with impervious jetties and a new incident

wave direction of 7.5^0. Bottom topographic surveys were again conducted at every 40 minutes in the early stage of the experiments and at larger time intervals in the later stage. Limited dye study and sand tracer experiments were also carried out. The test was continued for a total of 4860 minutes. Near the end, topographic changes became small and a more or less stable ebb tidal shoal was formed, Fig.18 shows the bathymetry change contours at the end of 4860 minute. Survey results including bottom topographic changes during different time intervals were given in Appendix C.

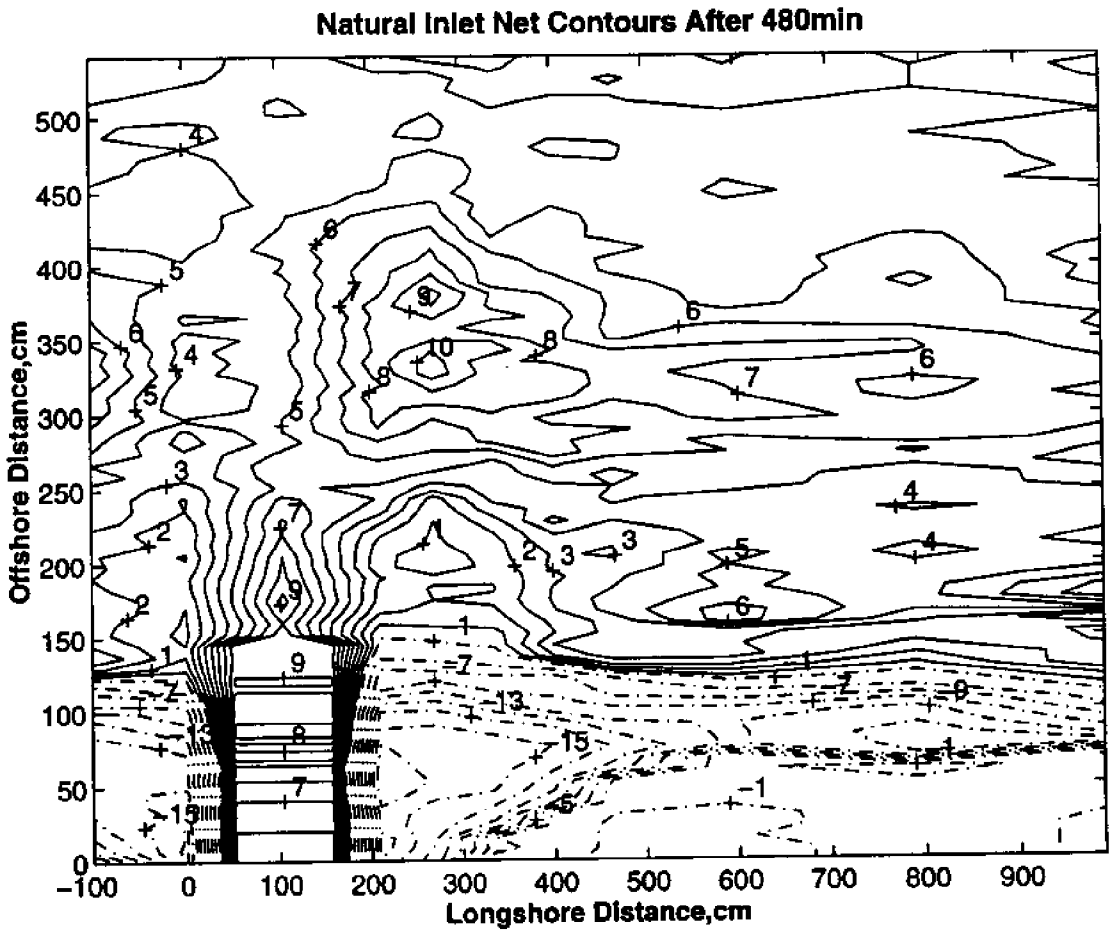

Figure 16: Natural Inlet Experiment Bathymetry Change Contours After 480 Minutes.

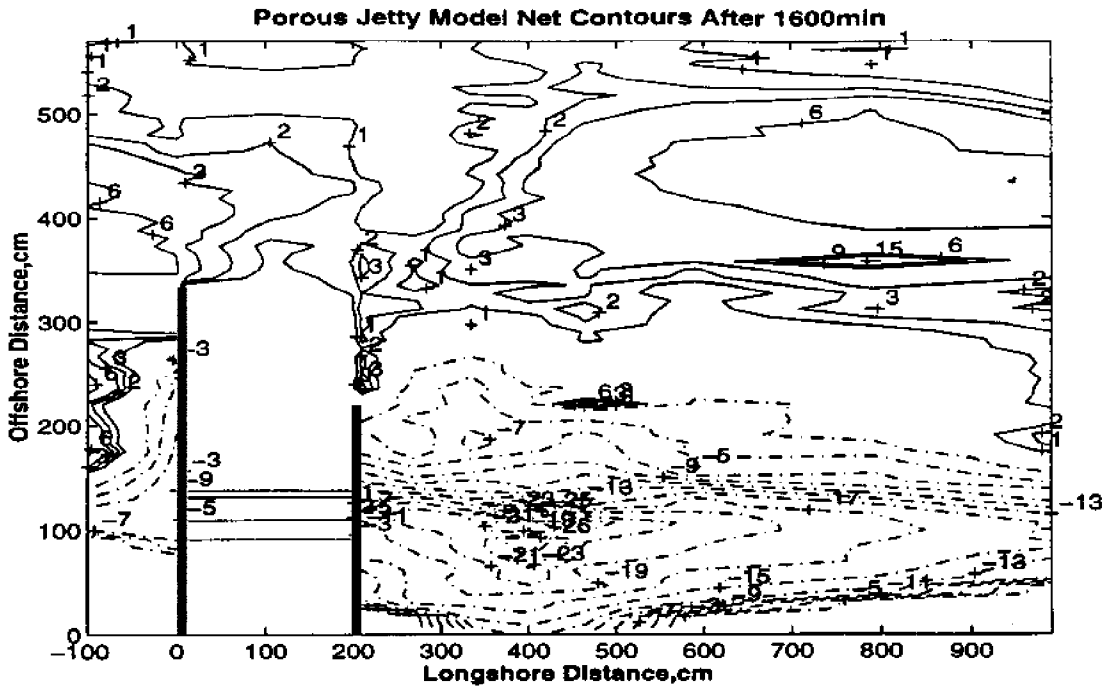

Figure 17: Porous Jetty Inlet Experiment bottom contour change after 1600 minute

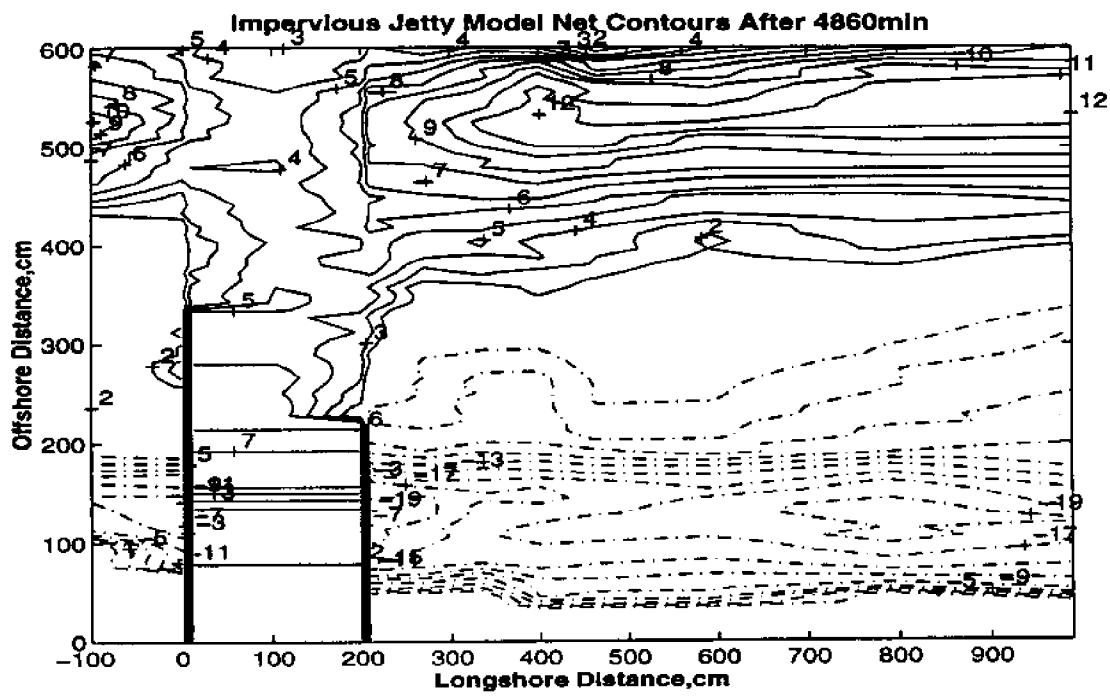

Figure 18: Impervious Jetty Inlet Experiment bottom contour change after 4860 inute.

4. SEDIMENT BUDGET AND SEDIMENT FLUX ANALYSIS

Before discussing the experimental results on ebb tidal shoal evolution, attempts were first made here to compute the sediment budget and to establish the sediment flux patterns. The sediment budget analysis will provide an overall spatial and temporal picture on the sediment losses and gains in the region of interest. The sediment flux is a dynamic property of fundamental importance towards interpretation of morphological evolution process.

4.1 Sediment Budget Computations

Two different analyses were performed for the sediment budget. The first was the time history of the overall sediment budget for the entire tested model region as shown in Fig.10. The purpose of this analysis was to determine the updrift transport rate based on the measured sediment quantities at the downdrift and channel ends and the measured net gain or loss within the region. In this analysis, the sediment transport across the offshore boundary was assumed to be equal to zero. The analyzed results for Experiments C2, and C3 are given in Table 6. The results from all Experiment C1, C2, and C3 are shown graphically in Fig.19. It is seen that for all three test cases, the experiment can be roughly divided into two stages: an initial adjustment stage followed by an evolution stage. In the first 160 minutes or so the initial inlet environment apparently underwent a major adjustment in respond to the test wave and current conditions. This is manifested by the rapid rate of changes in littoral transport and in net volume change in the domain. Afterwards, the process was stabilized with rather steady littoral drift environment. In Case 3, the cumulative net volume change inside the basin reached a constant revealing a matured environment.

The second sediment budget analysis was performed by computing sediment volume changes in seven different zones within the region as delineated in Fig. 20. Zone 1 was defined as the updrift zone which covered the area of 2 m wide and 6 m long to the left of the updrift jetty. Zone 2 corresponds to the area of 2 m wide and 3 m long inside the inlet between two jetties. Zone 3 covers the area of 2 m wide and 3 m. long offshore between two

extended jetty lines. Zones 4 and 6, each comprising 4 m × 3 m area, together correspond to the downdrift offshore region where ebb tidal shoals are generally located. Zones 5 and 7, each also comprising 4 m × 3 m area, together correspond to the downdrift nearshore region where offshore bars are generally present under storm wave conditions.

Table 6: Sediment Volume Balance Computation.

C2: Porous Jetty Inlet Experiment					
model time (min)	updrift transport (1)	downdrift transport (2)	loss to inlet (3)	offshore transport (4)	net volume (5)
40	0.011	-0.099	-0.000	0.000	-0.088
80	0.289	-0.524	-0.014	0.000	-0.249
120	0.316	-0.595	-0.014	0.000	-0.292
160	0.448	-0.835	-0.028	0.000	-0.415
480	0.463	-0.892	-0.040	0.000	-0.469
1120	0.581	-1.000	-0.062	0.000	-0.486
1600	0.597	-1.104	-0.079	0.000	-0.586
C3: Non-Porous Jetty Inlet Experiment					
model time (min)	updrift transport (1)	downdrift transport (2)	loss to inlet (3)	offshore transport (4)	net volume (5)
40	0.038	-0.071	0.000	0.000	-0.033
80	0.038	-0.354	-0.003	0.000	-0.319
120	0.109	-0.396	-0.003	0.000	-0.290
160	0.318	-0.580	-0.006	0.000	-0.268
480	0.361	-0.637	-0.017	0.000	-0.293
1120	0.375	-0.750	-0.040	0.000	-0.415
1600	0.504	-0.850	-0.057	0.000	-0.402
3200	1.188	-1.416	-0.085	-0.099	-0.413

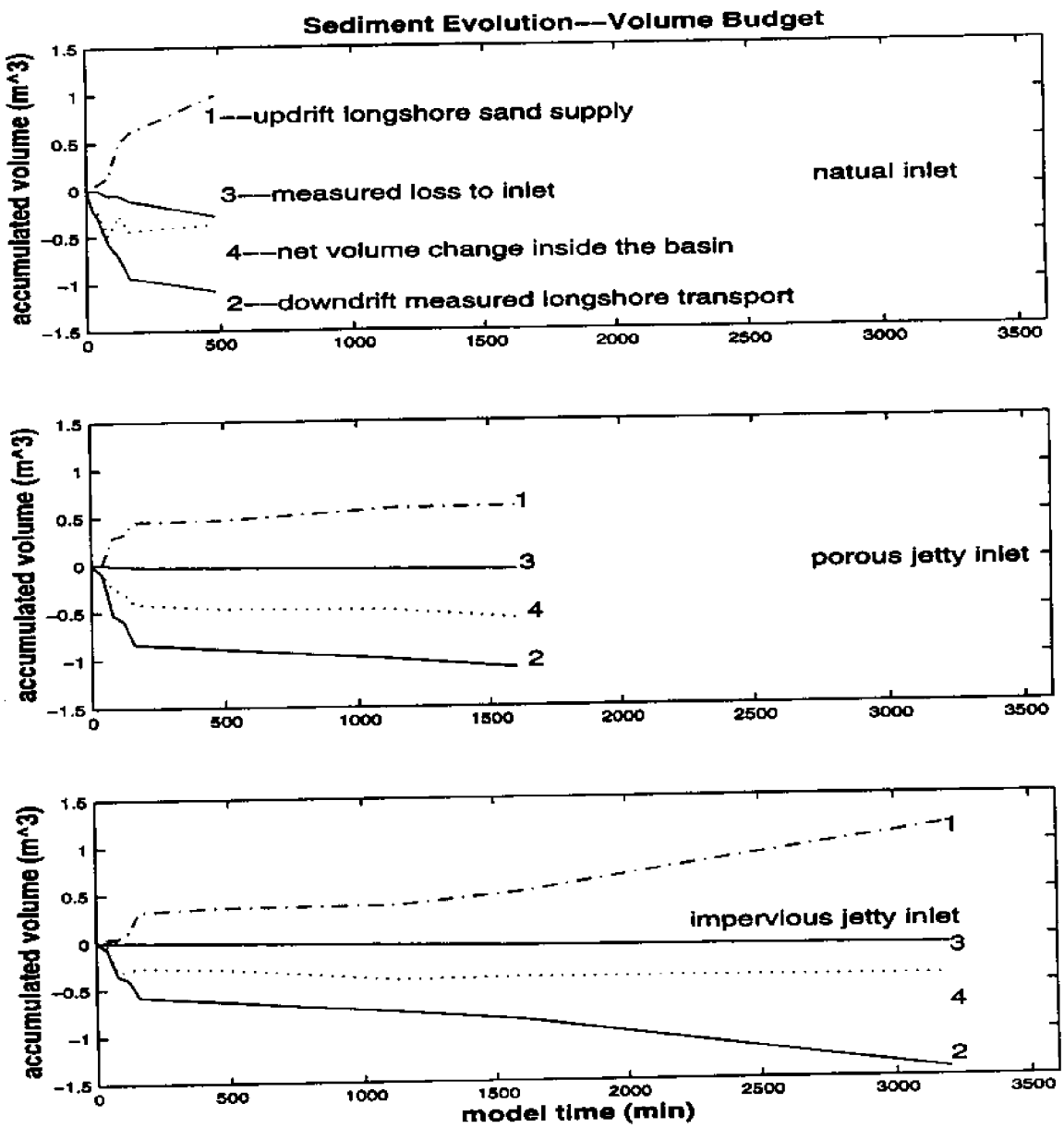

Figure 19: Sediment Budget Computation for Experiments C1, C2, and C3.

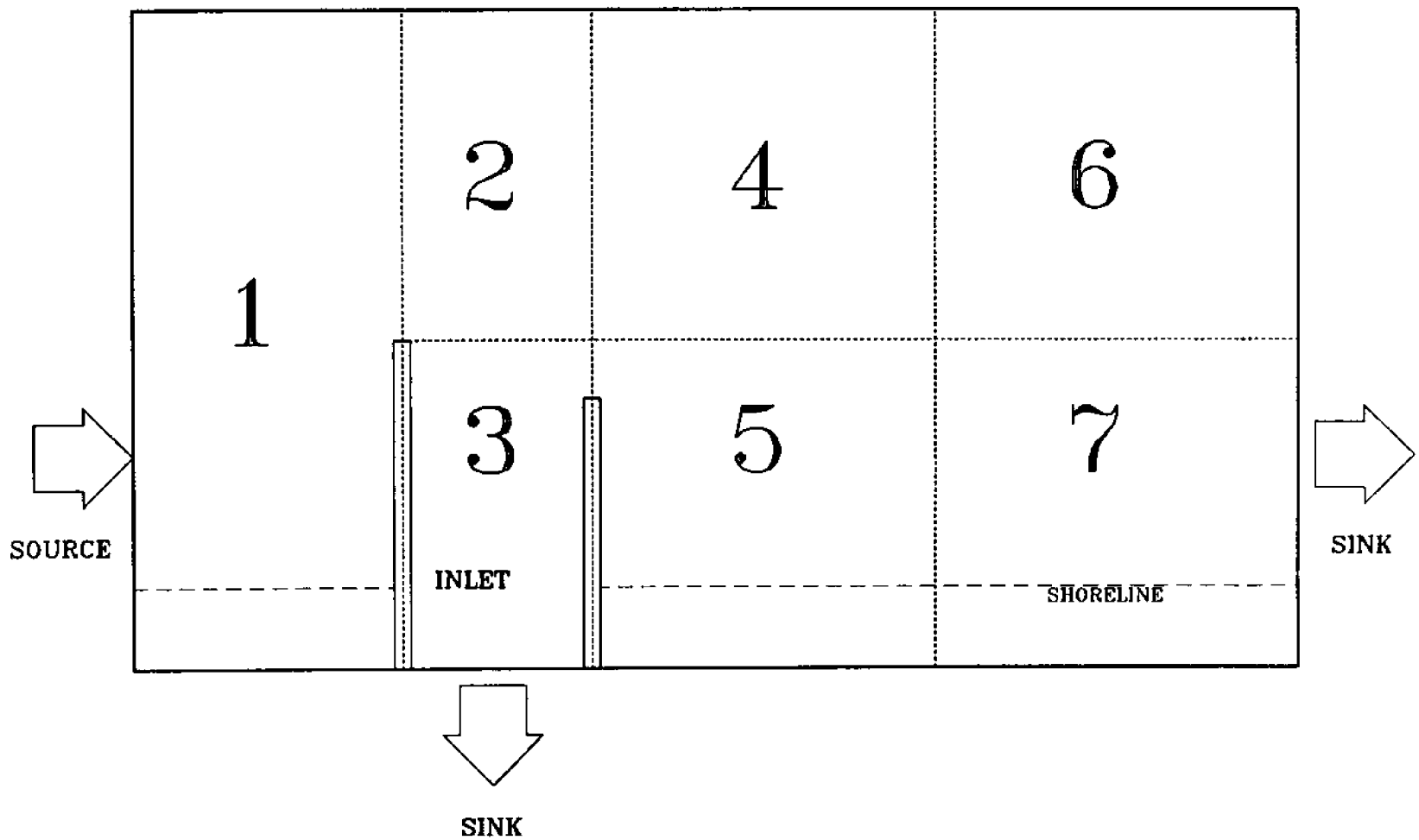

Figure 20: Seven Zones for Sediment Budget Computation.

Table 7 tabulates the results for the rate of accumulated volume changes in seven zones for Experiments C2 and C3. Figures 21, 22, and 23 exhibit the accumulated sediment volume changes with reference to the initial bathymetry for C1, C2 and C3, respectively. The patterns of sediment volume changes for Experiments C2 and C3 are shown to be similar. Using Fig.23 as an example, it is seen that the net sediment volume changes in Zone 1 were rather small. After certain initial perturbation, this zone reached a rather stable state with very little net gain or loss in the evolution process. This indicates that eventually updrift sediment was simply passing through this zone to downdrift. Zone 2 roughly represents the inlet channel within the confines of the jetties. Shoalings were rather localized and mostly occurred in the vicinity of jetties. The shoaling rate decreased steadily and bottom configuration seemed to have eventually approached an equilibrium state. Zone 3 extends from the tips of the jetties to offshore which is a zone where both channel shoal and ebb tidal shoal could occur. The total net volume change in this zone was in the same order of magnitude as that of Zone 2. It also showed that in Zone 3 sediment from the updrift was intercepted and deposited here at the initial stage and an equilibrium state appeared to have been reached in the experiment at run time around 1200 minute; afterwards, most of the sediment influx from updrift simply bypassed this zone. Zones 4 and 6 contain bulk of the ebb tidal shoal in the matured stage. They clearly represent sediment storage with rather significant volume increases in both zones, as resulted from the building and growth of the ebb tidal shoal. None of these zones appeared to have reached equilibrium state at the end of the experiment though a slower rate of volumetric increase has observed. Zones 5 and 7 represent downdrift nearshore region where both longshore sediment transport and on-off shore transport are vigorous. These zones suffered heavy sediment losses owing to severe nearshore erosion under the storm wave conditions. The rates of volume losses were quite high initially but gradually slowed down in the later stage. Equilibrium state was also not reached in these two zones at the end of the experiment. It was pointed out earlier from the results shown in Fig.19 that the cumulative volume within the entire region appeared to have reached a constant in the end. The results given in Fig.23, on the other hand, suggested that the dynamic process still caused material exchanges within the region and with the

surroundings. The patterns of exchange, however, cannot be determined without the knowledge of sediment flux.

Table 7: Sediment Volume Change Rate in Different Zones.

Model Time (min)	C2: Porous Jetty Experiment, Volume Changes Rate (m^3/min)						
	Zone 1	Zone 2	Zone 3	Zone 4	Zone 5	Zone 6	Zone 7
40	0.090	-0.025	-0.090	0.035	-0.285	0.040	-0.115
80	0.303	0.013	0.015	0.035	-0.517	0.027	-0.280
120	-0.005	0.003	-0.080	0.123	-0.160	0.157	-0.145
160	0.153	0.040	0.140	-0.070	-0.335	-0.055	-0.180
200	0.155	0.012	0.005	0.092	-0.395	0.275	-0.413
480	0.004	0.039	0.000	0.016	-0.048	0.009	-0.020
1120	-0.003	0.001	0.016	0.018	-0.040	0.031	-0.020
1600	0.008	0.004	0.004	0.007	-0.016	0.012	-0.017

Model Time (min)	C3: Non-Porous Jetty Experiment : Volume Changes Rate (m^3/min)						
	Zone 1	Zone 2	Zone 3	Zone 4	Zone 5	Zone 6	Zone 7
40	0.000	0.025	0.037	0.093	-0.262	0.135	-0.044
80	-0.125	-0.043	-0.052	-0.058	-0.268	-0.003	-0.165
120	0.015	0.053	0.110	0.052	-0.067	0.017	-0.110
160	0.032	0.020	-0.012	0.043	-0.138	0.158	-0.047
480	-0.006	0.036	0.043	0.045	-0.097	0.042	-0.070
1120	-0.010	-0.002	-0.002	-0.005	0.016	-0.009	-0.010
1600	0.009	0.001	0.001	0.008	-0.005	0.002	-0.014
3200	0.005	0.011	0.007	0.025	-0.036	0.024	-0.036

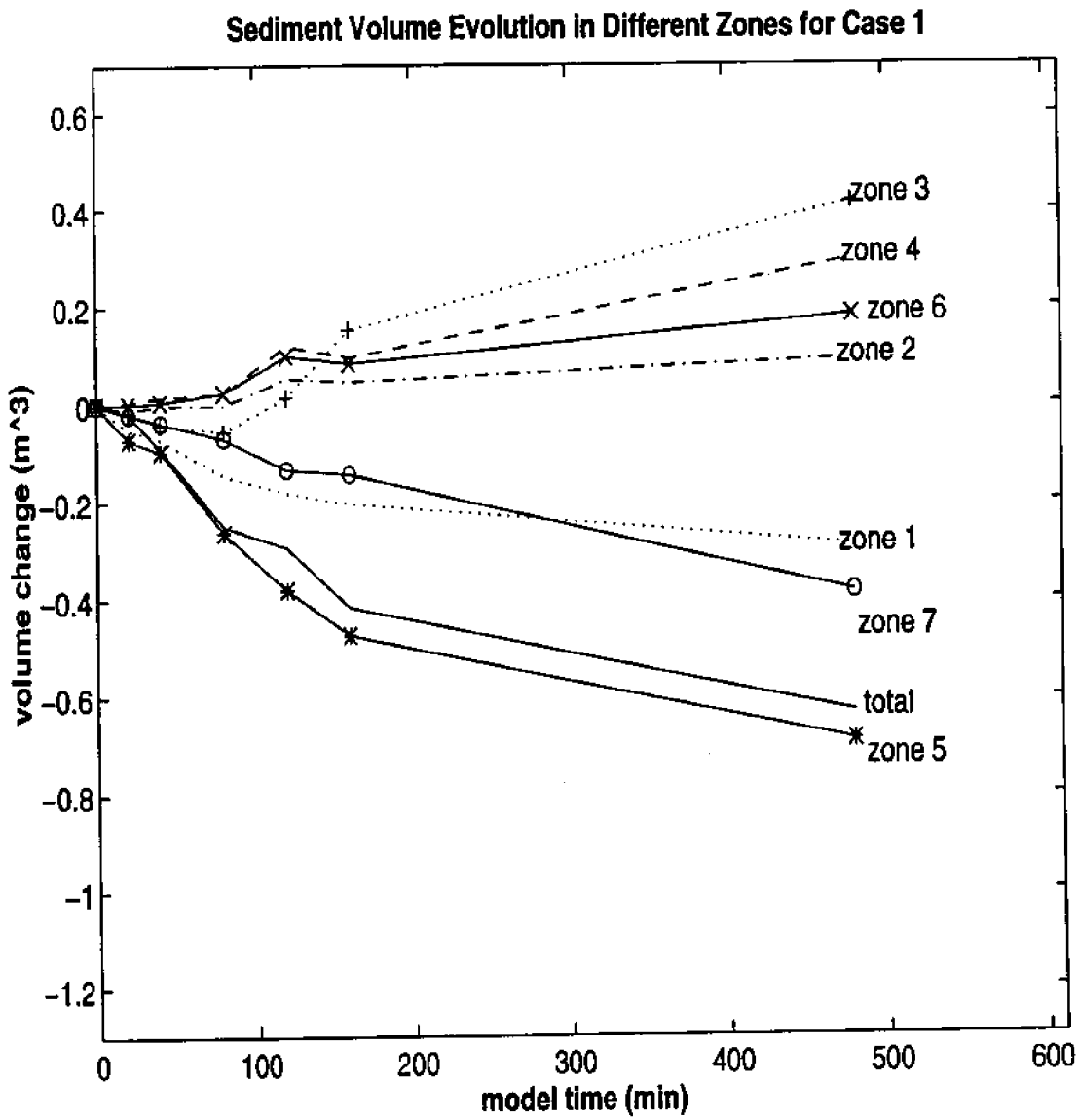

Figure 21: The Sediment Budget in Seven Zones for Experiment C1.

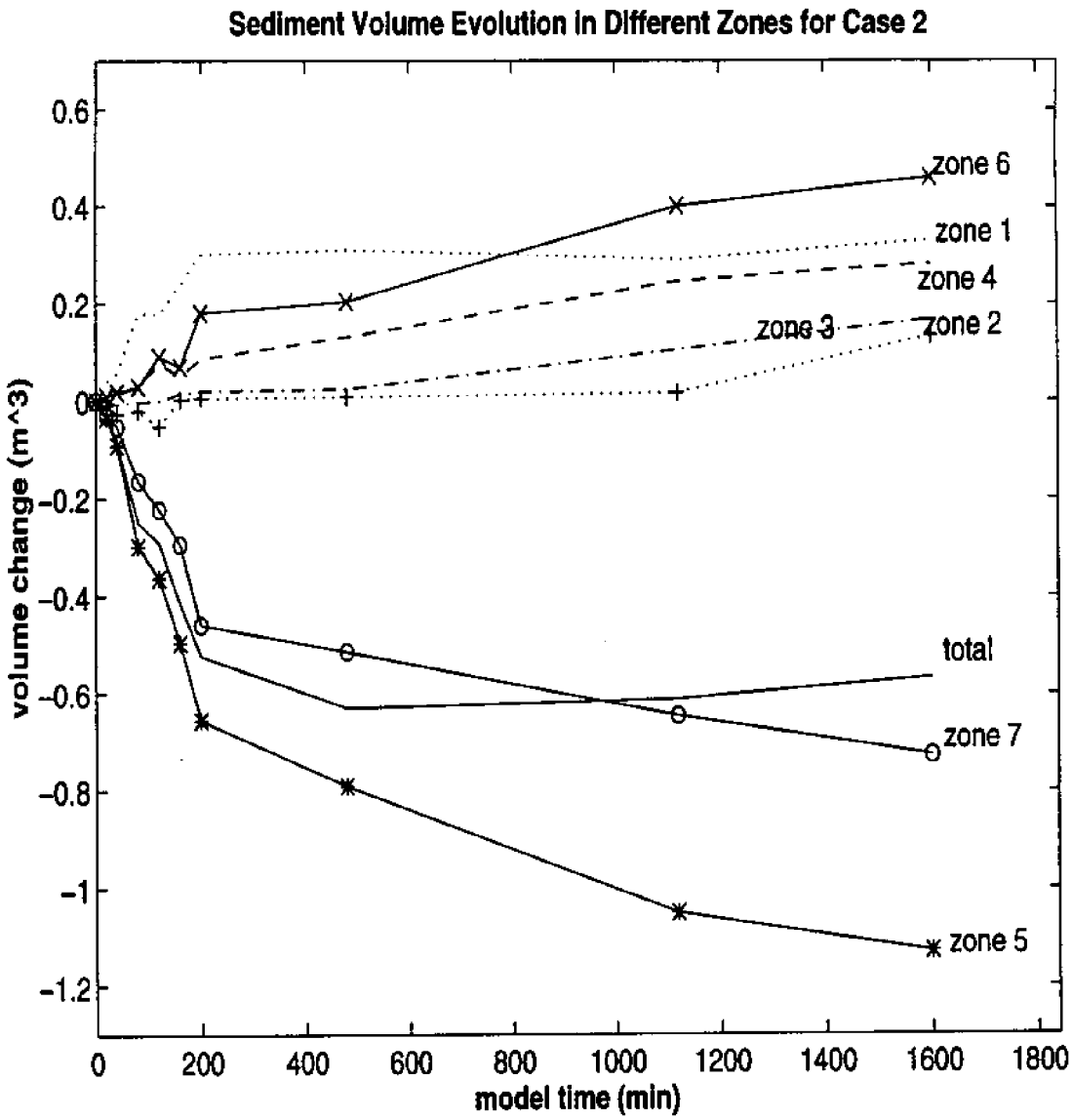

Figure 22: The Sediment Budget in Seven Zones for Experiment C2.

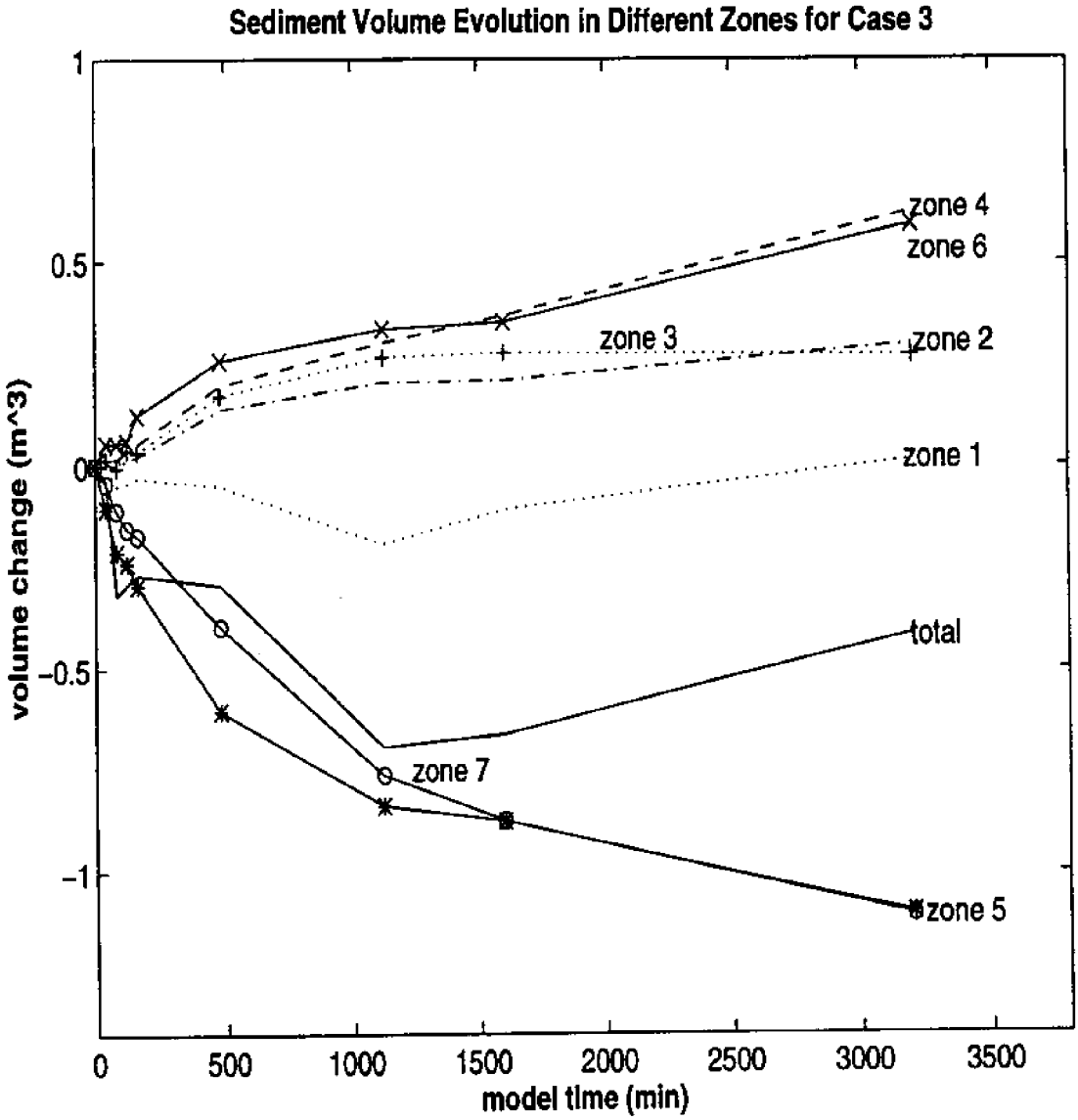

Figure 23: The Sediment Budget in Seven Zones for Experiment C3.

4.2 Sediment Flux Patterns

Sediment flux is probably the single most important parameter in sediment dynamics. However, it is generally difficult to directly measure this quantity whether in the laboratory or in the field. No direct measurement was carried out in this experiment. Attempts were made here to estimate the sediment flux using two hybrid methods relying partially on bottom survey data.

Sediment flux is defined here as the sediment transport vector, $\vec{q}=(q_x,q_y)$ in the horizontal plane. The two dimensional equation of sediment mass conservation in discrete form is:

$$\frac{\Delta q_x}{\Delta x}+\frac{\Delta q_y}{\Delta y}=-\frac{\Delta h}{\Delta t}$$

where h is the measured elevation, and t is the time. The quantity $\Delta h/\Delta t$ can be calculated from topographic surveys. To solve for q_x and q_y an additional governing equation is needed which means certain relationship must be established for either the magnitude or the direction of the flux, or certain relationship between the magnitude and the direction. This type of information unfortunately is not available and, at present, there is no easy way to acquire them through measurement. For lack of such additional information, an exploratory technique based on empirical eigen function analysis is introduced for this estimation.

The idea of using Empirical Eigen Function (EEF) theory for deriving vectors of sediment transport rates in the (x, y) plane is based on the technique of separation of variables. It is assumed here that the components of the sediment flux gradient at any fixed time can be expressed by the following series forms of the product of two functions $f(x)$ and $g(y)$.

$$\frac{\partial q_x}{\partial x} = \sum_{n=1}^{\infty} \alpha_n f(x)_n g(y)_n$$
$$\frac{\partial q_y}{\partial y} = \sum_{n=1}^{\infty} \beta_n f(x)_n g(y)_n$$

where $f(x)$, $g(y)$ are orthogonal functions and α and β are weighting factors. Substituting the above quantities into the mass conservation equation given in finite difference form,

$$\frac{\Delta q_x}{\Delta x} + \frac{\Delta q_y}{\Delta y} = \sum_{n=1}^{\infty} \alpha_n f(x)_n g(y)_n + \sum_{x=n}^{\infty} \beta_n f(x)_n g(y)_n = -\frac{\Delta h(x,y)}{\Delta t} \qquad at \quad t=t_k$$

The above Equation can be also written as:

$$\sum_{x=n}^{\infty} w_n f(x)_n g(y)_n = -\frac{\Delta h(x,y)}{\Delta t}$$

where

$$w_n = \alpha_n + \beta_n$$

The Empirical Eigen Function technique is then employed here to obtain $f(x)_n$, $f(y)_n$ and w_n for given $\Delta h/\Delta t$. For a finite grid size of $I \times J$ (a grid of $I \times J$ points in x and y directions, respectively), the series expressions have to be truncated with the maximum number of eigen vector, w, to be the smaller of the two grid sizes, say, for the present case to be I, *i.e.*,

$$\frac{\partial q_x}{\partial x} = \sum_{n=1}^{N} \alpha_n f(x)_n g(y)_n$$
$$\frac{\partial q_y}{\partial y} = \sum_{n=1}^{N} \beta_n f(x)_n g(y)_n$$

for $N \leq I$.

The x and y direction flux components at grid point (x_i, y_j) can be given as

$$q_x(x_i, y_j) = \Sigma_n^N \alpha_n F(x_i)_n g(y_j)_n + d(y_j)$$
$$q_y(x_i, y_j) = \Sigma_n^N \beta_n f(x_i)_n G(y_j)_n + e(x_i)$$

with

$$F(x_i) = \int_0^{x_i} f(x_i)dx, \qquad G(y_j) = \int_0^{y_j} g(y_j)dy$$

and is subject to

$$\alpha_n + \beta_n = w_n$$

It should be noted here that the flux components so obtained are volumetric discharge per grid width. The EEF method can be applied to the entire region as a whole or to different subregions and then matching the subregions at the boundaries.

To explain the procedure, application to the entire region is used as an example. The grid system for the entire region is $I = 19$ (longshore direction) with Δx=65.54 cm and J =80 (on-offshore direction) with Δy=7.62 cm. Therefore, in theory, a maximum of 19 pairs of eigen values, f(x) and g(y), together with 19 eigen vectors, w, can be solved. To solve for α and β, additional constraints must be specified through boundary conditions. The choices of boundary conditions are the following:

1) No flux (impervious) or given flux (porous) normal to jetties.
2) Given flux distribution on updrift boundary (calculated from sediment budget analysis presented in the previous Section).
3) Given flux distribution on downdrift boundary (measured in the laboratory).
4) No flux (shoreline) or given flux (inlet) on shoreward boundary.

To solve for all the α_n and β_n and the integration coefficients of $d(y_j)$ and $e(x_i)$ a total of $N+I+J$ conditions needs to be given. In EEF analysis, one routinely truncates the eigen vectors to retain only a few dominant terms. In this case, the required conditions can also be

reduced. On the other hand, if all boundary conditions listed above are specified, the system will be over constrained. For over constrained system, one either has to relax the system or seek approximate solution.

It is natural to require no flux condition at the jetties and to specify the total sediment influx at the updrift boundary and no flux at the shoreline while leave the downdrift and offshore boundaries open. The sets of equations to be solved simultaneously are given in the following:

1) Eigen function relationship:

$$\alpha_n + \beta_n = w_n \qquad n = 1 \ to \ I$$

$$\Sigma_{j=1}^{J} \Sigma_{n=1}^{N} \alpha_n F(x_1)_n g(y_j)_n + d(y_j) = q_{in}(x_1, y_j)$$

2) Known updrift input flux:

3) Shoreline no flux and inlet known flux conditions:

$$\Sigma_{n=1}^{N} \beta_n f(x_i)_n G(y_s)_n + e(x_i) = 0, \quad for \ shoreline$$
$$\Sigma_{n=1}^{N} \beta_n f(x_i)_n G(y_s)_n + e(x_i) = q_{inlet}, \quad for \ inlet \qquad i=1 \ to \ I$$

4) Jetties no flux condition:

$$\Sigma_{n=1}^{N} \alpha_n F(x_{jetty})_n g(y_{jetty})_n + d(y_j) = 0 \qquad j = a \ to \ b$$

where a and b mark the beginning and end of the jetty locations, respectively, and is assumed to contain K grid points. Therefore, altogether there are $I + J + K + 1$ equations for $I + J + N$ unknowns. If $K + 1$ is larger than N, the system is over constrained. One then must devise a scheme to relax the constraints. A method used in the present analysis is to represent the spatial distribution of the influx by a polynomial with $K + 1 - N$ degrees of freedom. The set of equations can then be solved for all the α's, β's and the coefficients of the polynomial.

For a domain with no structure inside such as the natural inlet case, additional boundary conditions must be specified to replace the missing no flux condition at the structure. In the present study, the sediment influx at the updrift boundary is fitted with an empirical distribution curve.

4.3 Temporal Changes of Sediment Flux Patterns

Two cases were examined in this section for temporal changes of sediment flux patterns, the natural inlet case and the case with impervious jetties. For the natural inlet case, the flux patterns for the first ebb and flood cycles obtained from EEF analysis are shown in Figs. 24 and 25, respectively. In both cases, longshore sediment transport in the nearshore zone dominated. The longshore drift was also seen to shift shoreward in the inlet region causing rapid topographic changes near the entrance. The experiment was terminated at 480 minutes. The total resultant sediment flux pattern is given in Fig.26. Again, nearshore longshore transport dominated. Sediment was also seen to be diverted to offshore due to the combined ebb current and storm wave effects.

For the impervious jetties, the experiment was conducted for a total of 4860 minutes which is equivalent to 40.5 days in prototype at a geometrical scale ratio of 80. A few cases were examined here to reveal the sediment flux patterns at different stages in the experiment.

First, the flux patterns in individual tidal cycles were examined for the first ebb (0-40 minutes) and the first flood (40-80 minutes) cycles. In the EEF computation, the domain was divided into two regions, one updrift region and one downdrift region as shown in Fig 27. Computation was performed for the updrift region as a first step. The computation then proceeded to the downdrift region using the output from the first region as the input boundary condition. Figures 28 and 29 display the results of the computed flux patterns for the first ebb and flood cycles. Figure 28 shows that during the first ebb cycle material from updrift was carried around the updrift jetty, across the channel then towards offshore by the

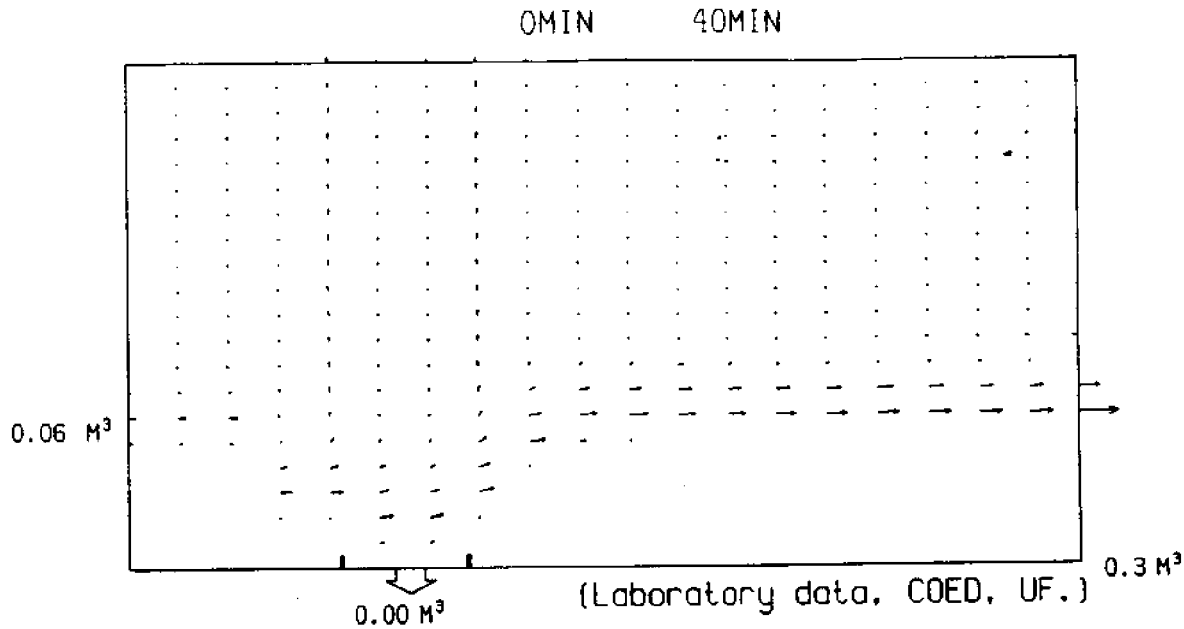

Figure 24: Sediment Transport Flux Pattern for the First Ebb Cycle in Natural Inlet Case.

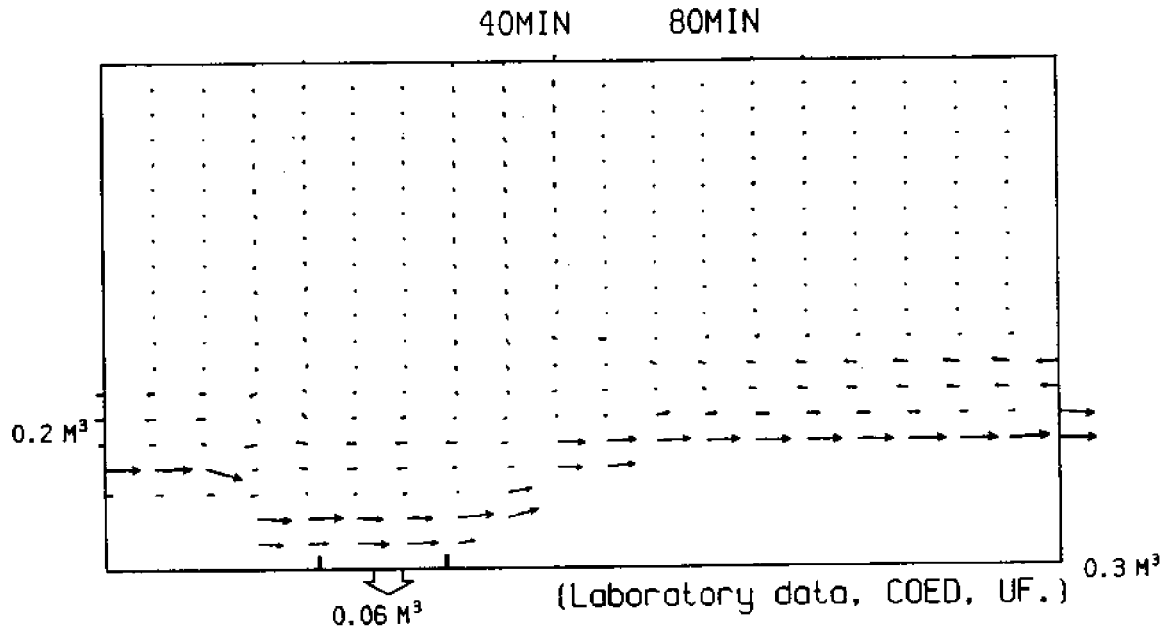

Figure 25: Sediment Transport Flux Pattern for the First Flood Cycle for Natural Inlet.

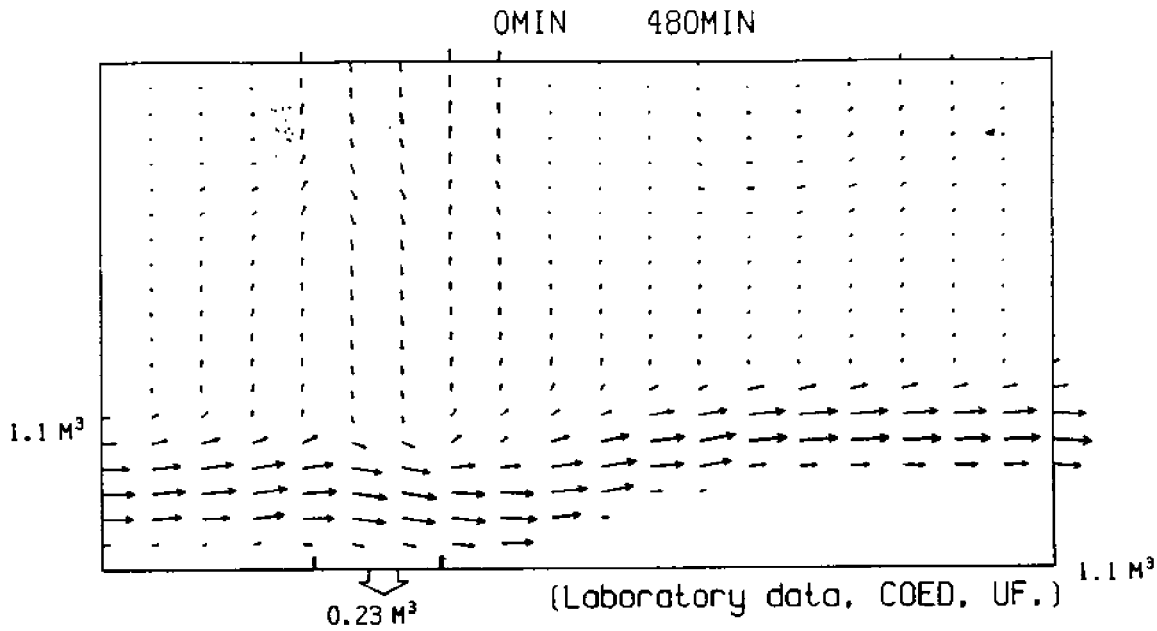

Figure 26: Sediment Transport Flux Pattern After 480 min. for Natural Inlet Experiment.

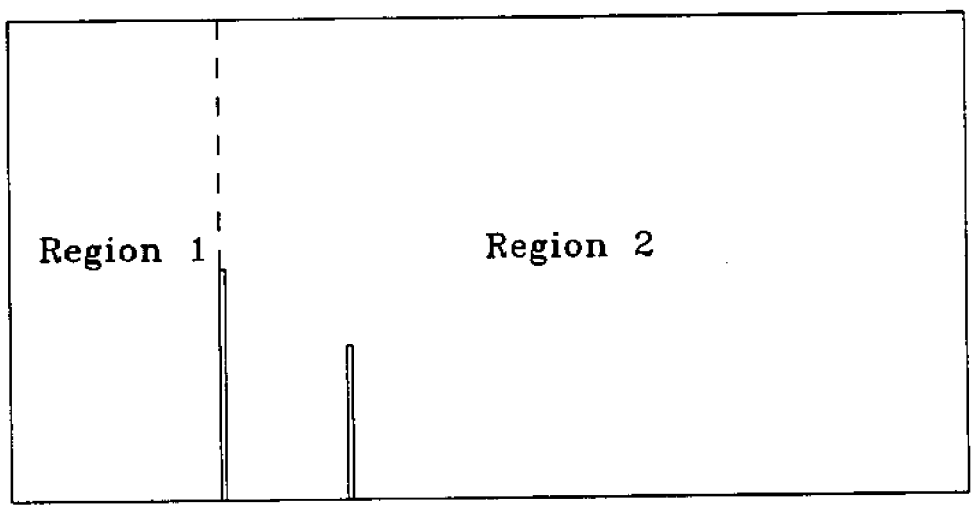

Figure 27: Two Regions for The EEF Computation.

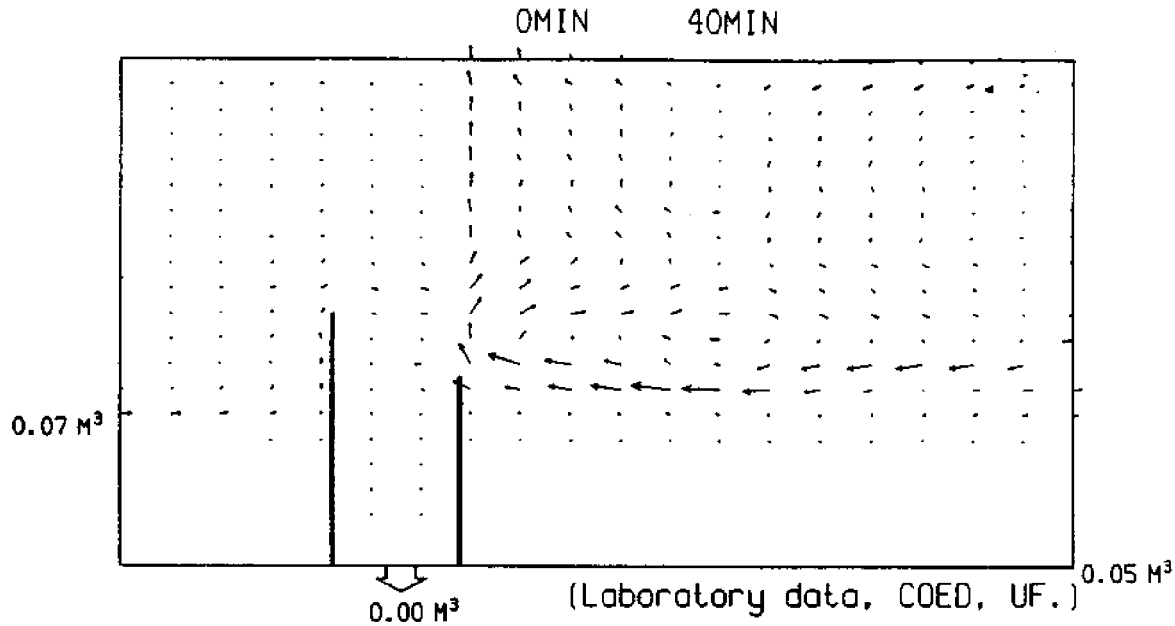

Figure 28: Sediment Transport Flux Pattern for the First Ebb Cycle in Experiment C3.

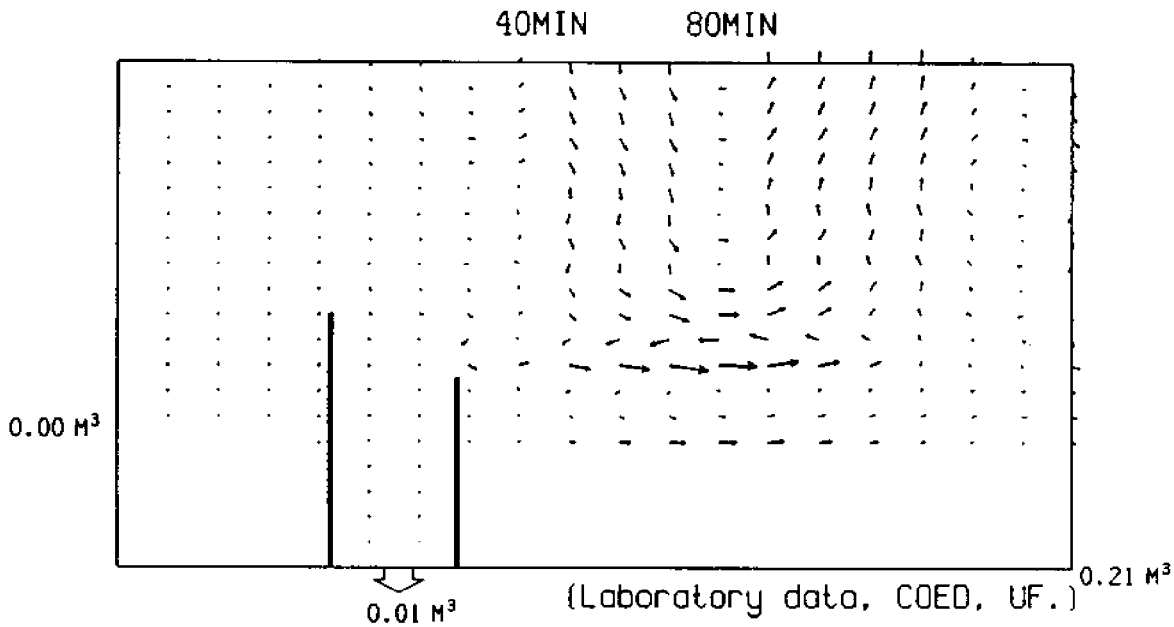

Figure 29: Sediment Transport Flux Pattern for the First Flood Cycle in Experiment C3.

ebb tidal current. Downdrift sediment motion is far more active than the updrift side owing to the energetic fluid motion caused by current wave interaction. Material eroded from the beach was largely carried offshore. Strong drift reversal was detected and material was entrained into the ebb current towards offshore. Clearly, the strongest offshore transport was offset to the downdrift side of the channel under the influence of the oblique incident wave angle. Both updrift and downdrift material contribute to this offshore transport. Shoals were developed in regions where the flux gradients were strongly negative. The validity of the flux solutions can be checked to insure that input bottom contours can be recovered from the computed flux distribution. Figure 28 shows the comparisons of the original input contour map with the recovered one for the ebb cycle case. In the subsequent flood cycle, the results given in Fig.29 showed strong downdrift components in the nearshore zone and over the shoals formed during the ebb cycle. It appeared that ebb flow tended to build up shoals whereas flood flow tended to destruct the shoals but promote longshore transport. Similar situations were also observed in subsequent tests. The cumulative effect, however, was growth of shoals.

To examine the cumulative sediment flux patterns, the test duration is artificially divided into two stages: the adjustment stage covering the initial 4 to 6 tidal cycles and the evolution stage covering the remaining period. The EEF analysis was applied to these two stages. Figure 30 displays the computed sediment flux patterns from 0 to 480 minutes when a rather stable ebb shoal can be identified. During this stage, net nearshore sediment transport was more active than offshore region. Longshore transport was strong. Drift reversal near a downdrift jetty was evident. Figure 31 displays the results from 480 to 1600 minutes. During this period, the total magnitude of a transport rate was considerably smaller than the initial 480 minute periods. Net littoral transport slowed down significantly. Relatively speaking the on/offshore flux component became more important than longshore component. Sand loss too offshore was evident. Channel bypassing and channel shoaling were also evident during this later stage.

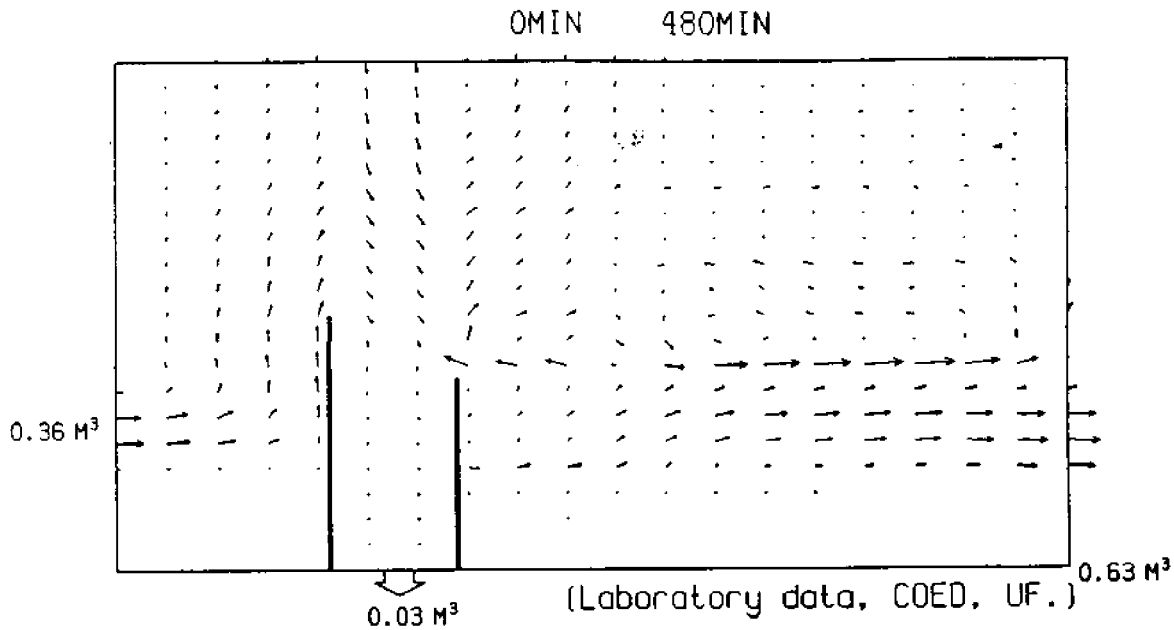

Figure 30: Sediment Transport Flux Pattern for 0 to 480 minutes in Experiment C3.

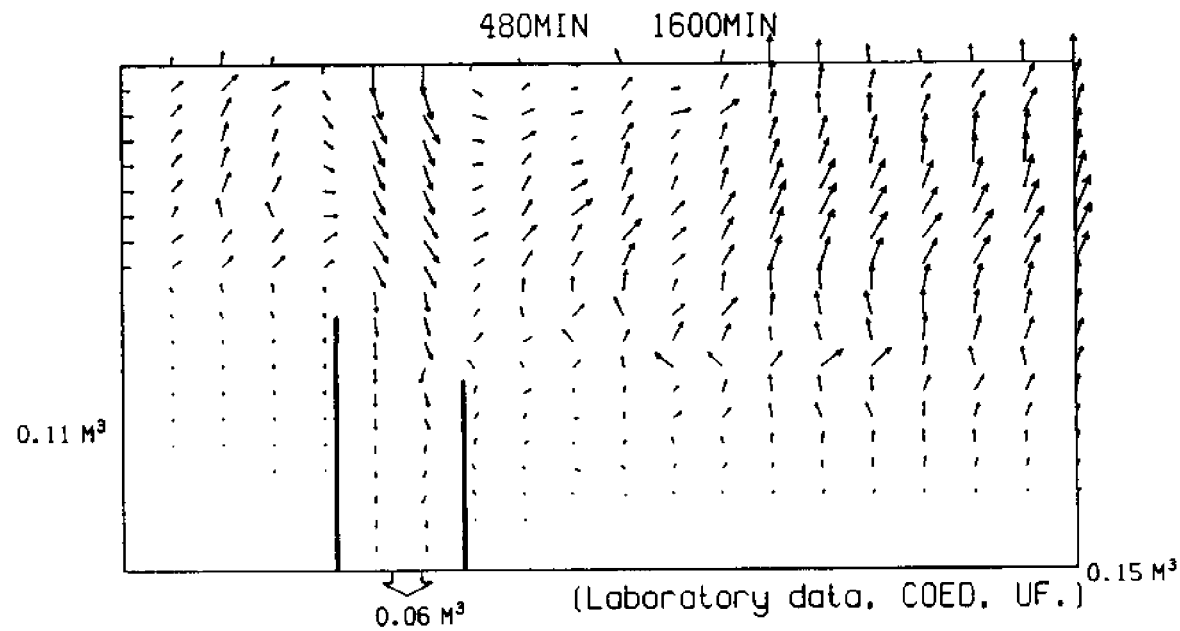

Figure 31: Sediment Transport Flux Pattern for 480 to 1600 minutes in Experiment C3.

5. EBB TIDAL SHOAL EVOLUTION PROCESS

The ultimate goal of the present study is to examine the ebb tidal shoal evolution process. Current laboratory results concerning this process are discussed in this Chapter.

5.1 Defining Ebb Tidal Shoal in the Laboratory

In order to quantify the test results with regard to ebb tidal shoal growth it is necessary to define the ebb tidal shoal first. In theory, ebb tidal shoal is the excess sediment material accumulated in a zone under the influence of ebb tidal current. In reality, there exist two difficulties to quantify an ebb tidal shoal; one is to determine the zone of influence and the other is the selection of a reference bottom contour above which one defines as ebb tidal shoal.

In examining the accretive pattern from the test results, a number of main accretive features in topographic changes are identified. These features are defined here as: channel shoals, ebb tidal shoals, breaking bars and downdrift accretion. Since they mutually affected each other, separation of them at times could be subjective. For instance, in the early stage shoaling could began in the channel. As the channel shoal grew, it might breakup in the offshore direction to initiate ebb shoal. To separate them, the channel shoal is considered as the material deposit inside the inlet channel or in the vicinity of the inlet entrance whereas ebb tidal shoal is the material deposited in the offshore region roughly coincide with the ebb tidal flow path. In the later stage, the down drift accretion which was influenced by the downdrift boundary in the laboratory would gradually encroach into the ebb tidal shoal. In this case, the contribution to ebb tidal shoal due to downdrift encroachment must be separated. In the late stage, it was also possible that the ebb tidal shoal would expand into the channel to link with the channel shoal. Therefore, the separation of these accretive features became rather subjective at times.

Our main interest is to examine the ebb shoal and channel shoal development. To define the boundaries of either shoal, reference planes must be defined. In the laboratory, the initial bottom configuration would be a natural choice provided that the initial configuration does not deviate too much from a quasi-equilibrium shape. The shoal is then the positive elevation change with respect to the reference. In the present experiment, it is found that using initial configuration as reference to define ebb tidal shoal is impractical as the outlines of zero net elevation change was rather diffused as well as confused. This situation is illustrated in Fig.32 using the case of ebb shoal generated in the natural inlet experiment. Therefore, to identify and construct ebb tidal shoal in a consistent and manageable manner, a net increase in elevation with more coherent contour can serve better as the reference plane. In the natural inlet experiment, for instance, the net +2 cm elevation was selected as the reference. The shoal below this level is extrapolated based on an assumed angle of repose of 25^0 (for fine median sand). An improved picture describing ebb shoal pattern based on this net +2 cm elevation in the natural inlet experiment is shown in Fig.33. In the jettied inlet experiments, the experimental durations were considerably longer. In these cases, one could find that even the +2 cm contours became too diffused. Under such condition one would have to select a higher elevation to outline a coherent shoal. The procedure of extrapolating to the zero contour remains the same as discussed using 25^0 angle of repose. In this manner, the shoals are identified. Other derived quantities such volume, location, perimeter, areas, etc., are then computed based on the constructed shoals.

5.2 Ebb Tidal Shoal Evolution For the Natural Inlet Experiment

In Experiment C1, the test was conducted under storm wave condition beginning with an ebb current cycle. The beach responded immediately from the wave attack; beach and foreshore material was rapidly carried offshore to form breaking bars. As expected, beaches on both sides of the inlet entrance sustained severe erosion. Material from the updrift beach was pushed towards the inlet and downdrift by the strong wave action. Inside the breaking line, a small shoal began to form immediately near the entrance and inside the breaker line. Outside the breaking line, where the wave motion was stronger, material was carried across

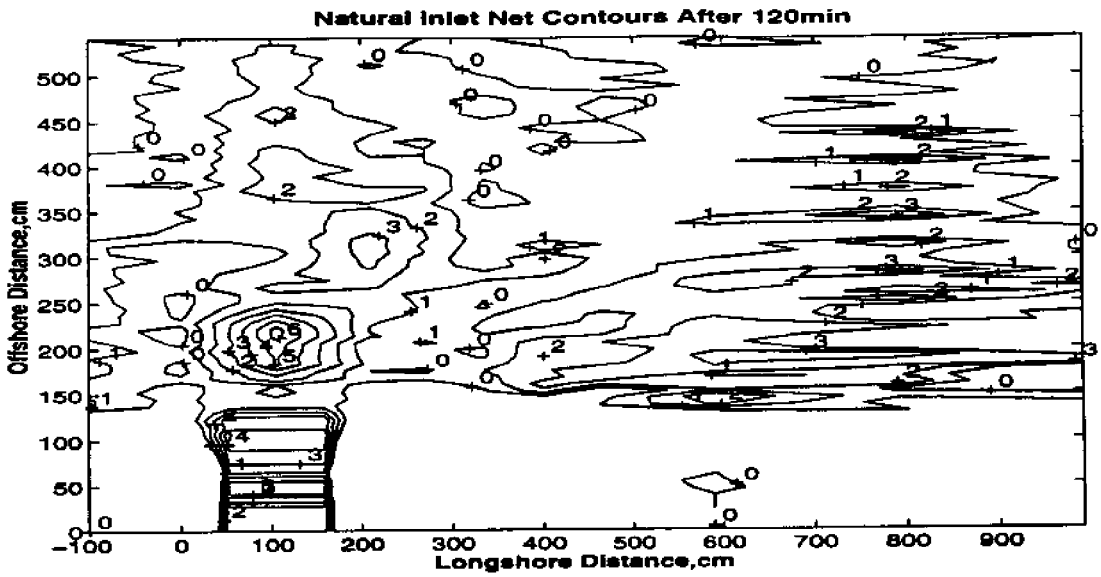

Figure 32: Description of Ebb Shoal Pattern Using net +0 cm Elevation in Experiment C1.

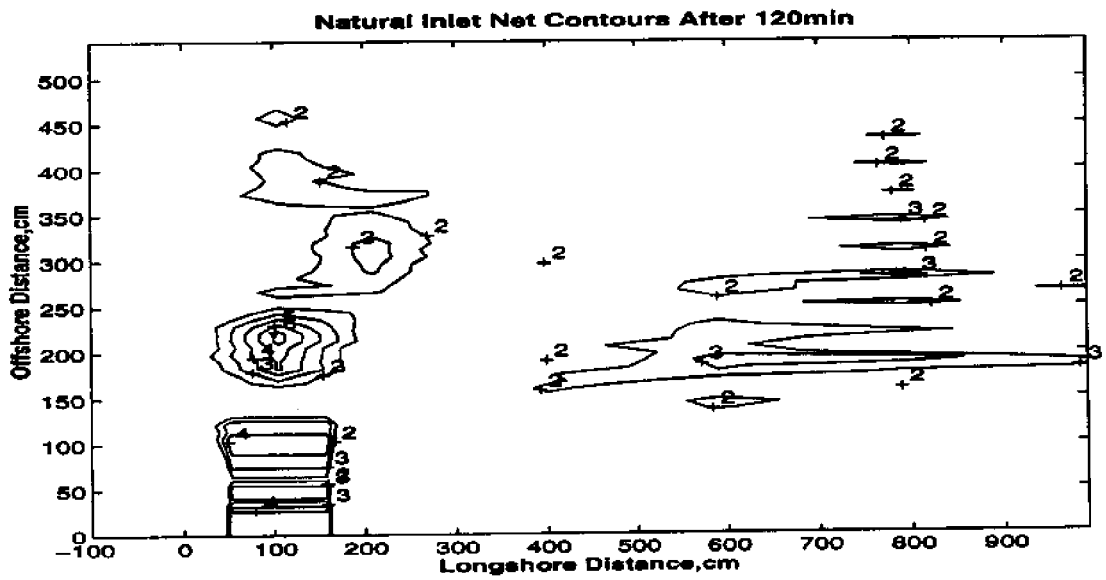

Figure 33: Description of Ebb Shoal Pattern Using net +2 cm Elevation in Experiment C1.

the channel and deposited immediately downdrift of the channel outside the surf zone. Meanwhile, downdrift erosion began near the entrance and gradually expanded towards downdrift. Part of the eroded material was carried downdrift in the littoral zone but part of the material was carried offshore to form breaking bars. Figure 34 shows the net sediment erosive and accretive patterns at the end of the first ebb tidal cycle as compared with the initial bathymetry.

In the following flood cycle, material from the updrift was pushed into the channel by the combined strength of current and waves. The small channel shoal initiated during the preceding ebb cycle was observed to grow both into the inlet and towards offshore. Shoreline erosion was significant in the immediate updrift and downdrift beaches. On the downdrift side the rate of littoral drift increased significantly as the flood current not only aided in the incident wave to the downdrift but also caused more flooding on the dry beach. Figure 35 shows the sediment erosive and accretive patterns during this flood tidal cycle in the experiment. In the subsequent cycles, one observed the breakup of shoals into what generally referred to as channel shoals and ebb tidal shoals. The experiment was stopped after another three complete tidal cycles (480 minutes) as both the channel shoaling and shoreline erosion became excessively severe. Figure 36 shows a photo of the model topography at the end of the experimnet. An inlet channel shoaling was clearly noticed. Figure 37 displays the final shoreline configuration in the experiment. Both the updrift and the downdrift shoreline erosions were significant with the most severe erosion occurred next to the inlet, and shoreline erosive patterns were nearly symmetrical with respect to the inlet center.

Figure 38 displays the generation and growth of the ebb tidal shoal in Experiment C1 using the net +2 cm as the base contour. It is seen that shoaling began at the channel entrance and grew in both directions towards offshore and into the channel. The offshore shoaling eventually broke off from the channel shoaling. After 120 minutes, channel shoaling

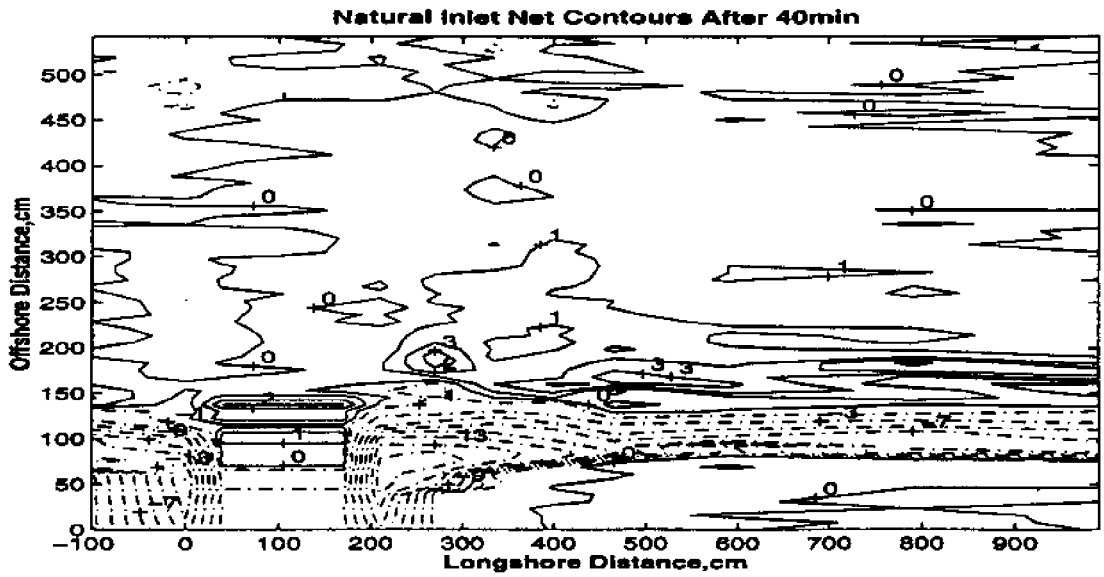

Figure 34: Accretion and Erosion Pattern during 0-40 minutes in Experiment C1.

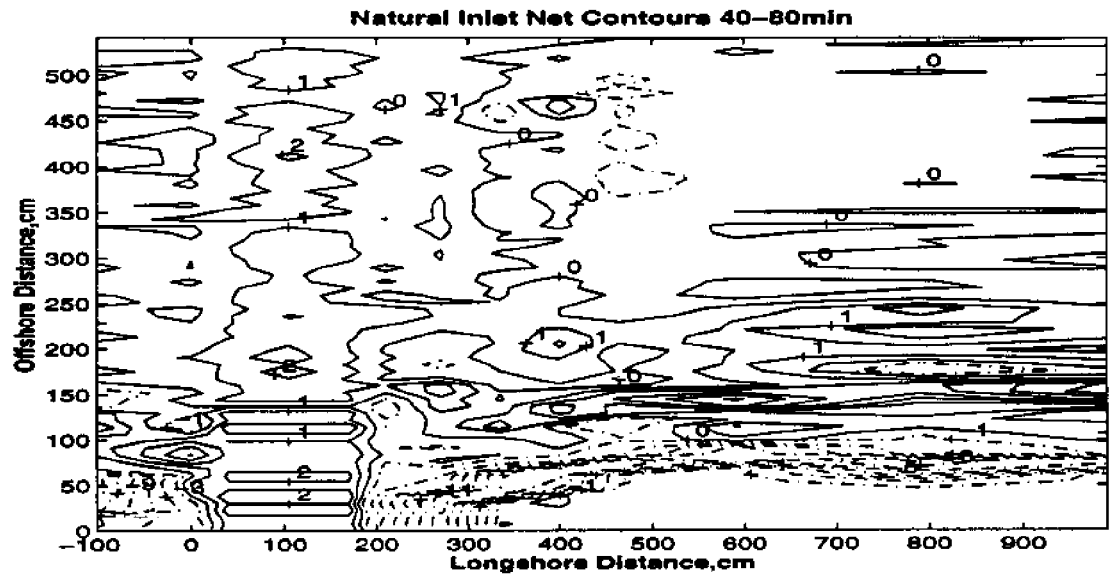

Figure 35: Accretive and Erosive Patterns during 40-80 minutes in Experiment C1.

Figure 36: A Photo Showing the Model Topography after 480 minutes in Experiment C1.

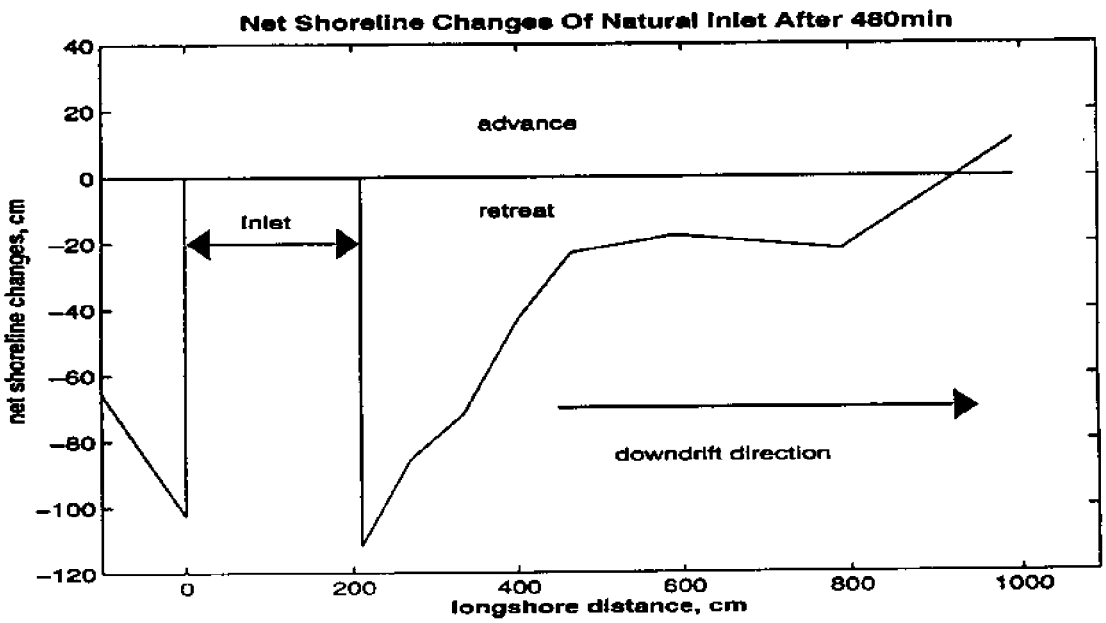

Figure 37: Shoreline Change after 480 minutes in Experiment C1.

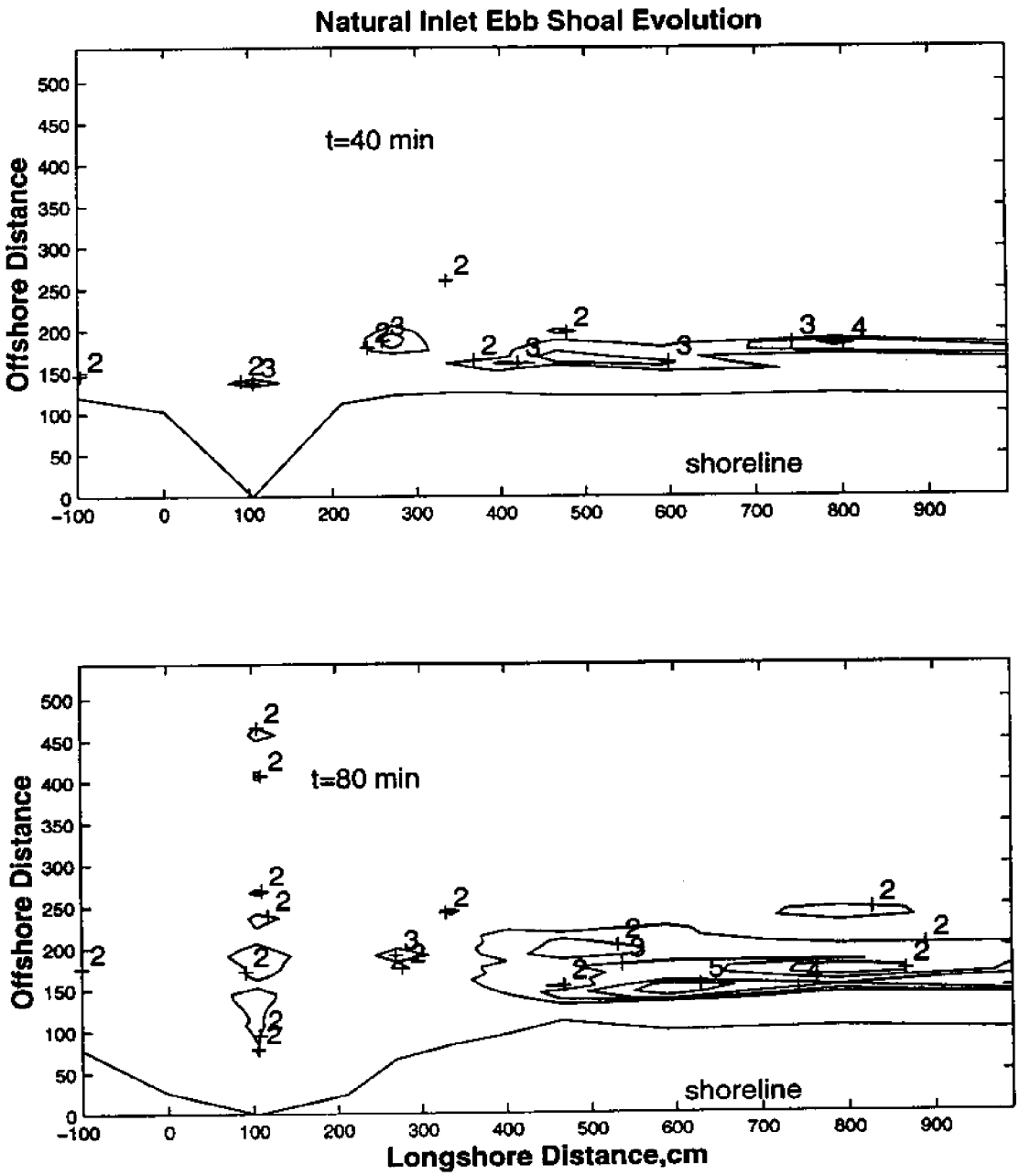

Figure 38: Description of Generation and Growth of EbbShoal in Experiment C1.

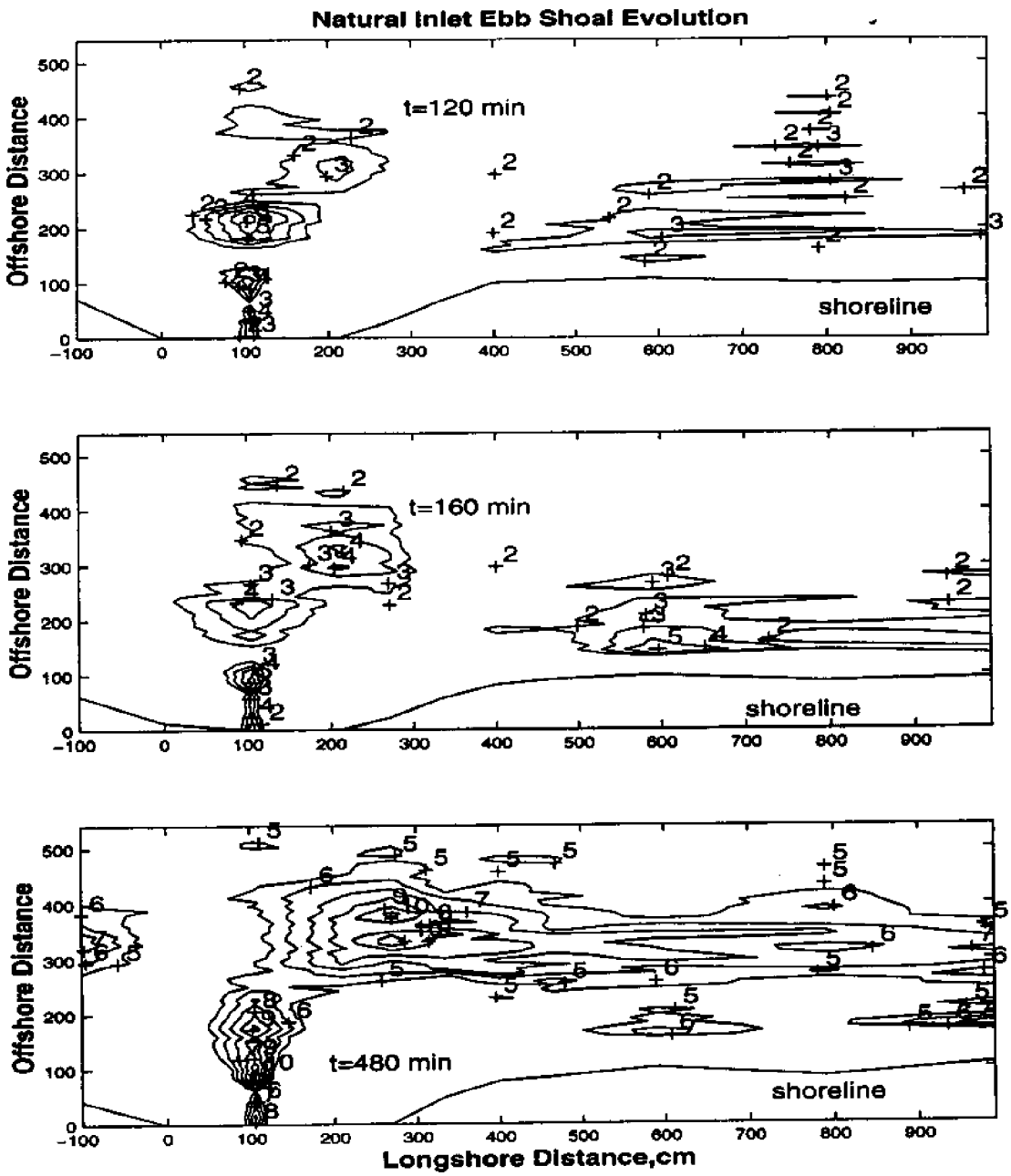

Figure 38: Description of Generation and Growth of Ebb Shoal in Experiment C1 (Continue).

And ebb tidal shoal can be separately identified. The ebb tidal shoal began to shift towards downdrift after this stage. At the end of 480 minutes, the ebb shoal was seen to grow to a considerable size while the channel shoaling also grew to reconnect with the ebb shoal. A number of parameters are defined here to quantify the ebb tidal evolution process; they are the ebb tidal shoal volume, the volumetric centroid and the areal of spreading. The ebb tidal shoal volume is the volume of the synthesized shoal above the initial profile. The geometrical centroid is referenced to the Cartesian coordinate system with x- and y-axis coinciding with the initial shoreline and the updrift jetty, respectively. The areal of spreading is simply the area above the initial profile. Values of these parameters are given in Table 8 for the natural inlet experiment.

Table 8: Natural Tidal Inlet Ebb Shoal Characteristics.

Experiment C1: Natural Tidal Inlet Experiment				
Model Time (min)	Ebb Shoal Characteristics			
	volume (m^3)	Centroid of Volume		spreading radius of volume, R_c (m)
		X_c (m)	Y_c (m)	
40	0.0005	1.05	1.35	0.35
80	0.0085	1.05	1.75	0.75
120	0.0312	1.35	2.60	1.35
160	0.0520	1.95	3.05	1.65
480	0.2532	2.95	3.55	2.05

5.3 Ebb tidal Shoal Evolution for Jettied Inlets

Both Experiments C2 and C3 were conducted under storm wave conditions beginning with an ebb current cycle. The wave incident angle in Experiment C2 was 15^0 which is twice as large as in Experiment C3. Experiment C2 has riprap type porous jetties and C3 has caisson type impervious jetties.

In the initial tidal cycle the general sediment transport patterns in both C2 and C3 were similar. Sand accretions occurred at the tips of both updrift and downdrift jetties. In subsequent time, the transport patterns became different. In C2, the updrift jetty tended to attract sediment owing to the structural porosity. Consequently, sediments were heavily deposited on both sides of the updrift jetty around its tip. In C3, on the other hand, the updrift sediment began to bypass the jetty and deposited in the channel. On the down drift side of the inlet beach erosions were severe, particularly in C2 owing to the large incident wave angle. Bars were formed in both cases due to offshore sediment transport. Figures 39 and 40 show the net contour changes after the first ebb cycle for C2 and C3, respectively. In the following flood cycle, the porous jetty in C2 attracted more sediment and resulted in substantial growth of shoaling around the tip of the updrift jetty. In C3, more sediment bypassed the inlet and was transported downdrift into the littoral zone. Beach erosions were seen to be more severe than ebb cycle on both sides of the inlet due to higher flood water level. The sand eroded from the downdrift beach was carried out offshore as well as along the shore direction. Unlike the natural inlet case, channel shoaling was not severe at this stage. Figures 41 and 42 show the sediment erosive and accretive patterns during this flood cycle interval for C2 and C3, respectively.

For C2, the porous jetty case, test was stopped at 1600 minutes when shoaling around the updrift jetty grew so large that the channel was nearly blocked. This is shown in the net contour change plot in Fig 43. Owing to this result, the testing wave angle in the subsequent impervious jetty case, C3, was reduced to half that C2. For C3, the test was stopped at 4860 minutes. Figure 44 shows the net contours change pattern for C3 at 4860 minutes. It was found that in C3 the bottom changes became less drastic and the development of shoals were more orderly.

Based on the same procedures described earlier, the shoal evolution sequence can be constructed for C2 and C3. The results are presented in Figs. 45 and 46 for C2 and C3, respectively. It is seen that the porous updrift jetty behaved like a magnet that drew large

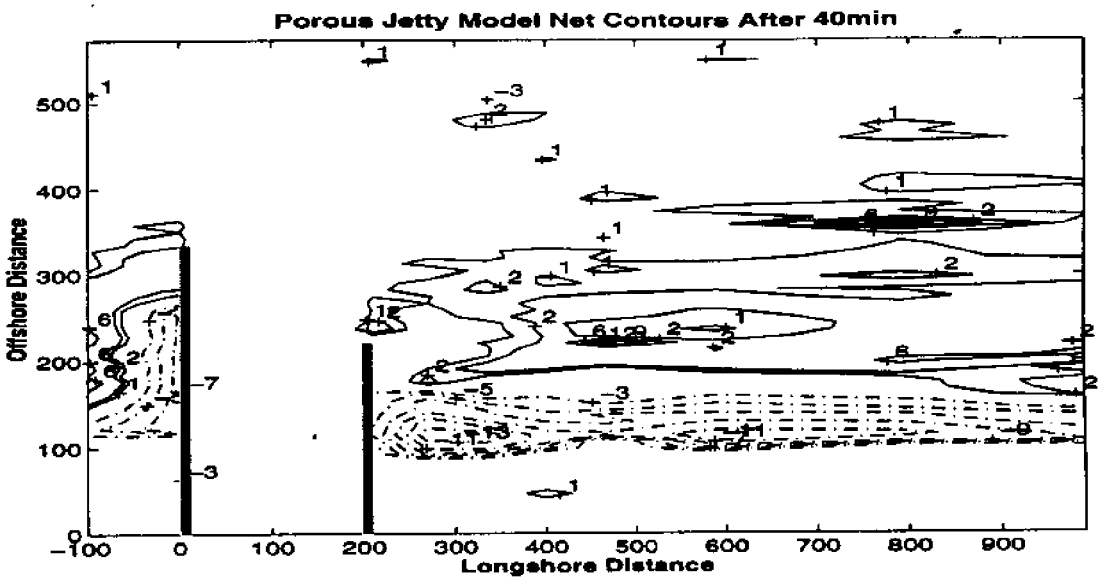

Figure 39: Accretive and Erosive Patterns during 0-40 minutes in Experiment C2.

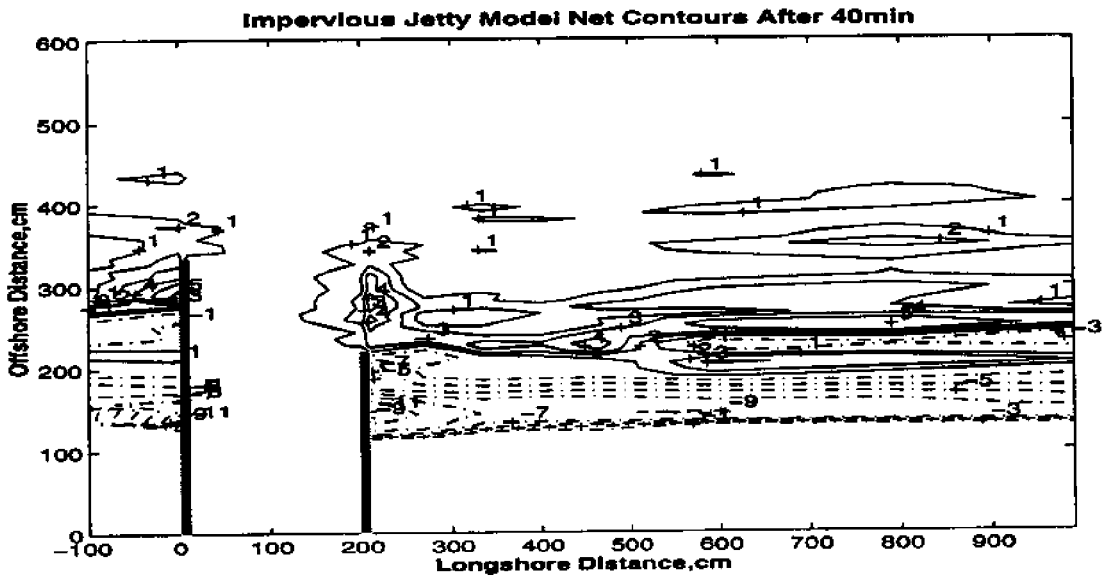

Figure 40: Accretive and Erosive Patterns during 0-40 minutes in Experiment C3.

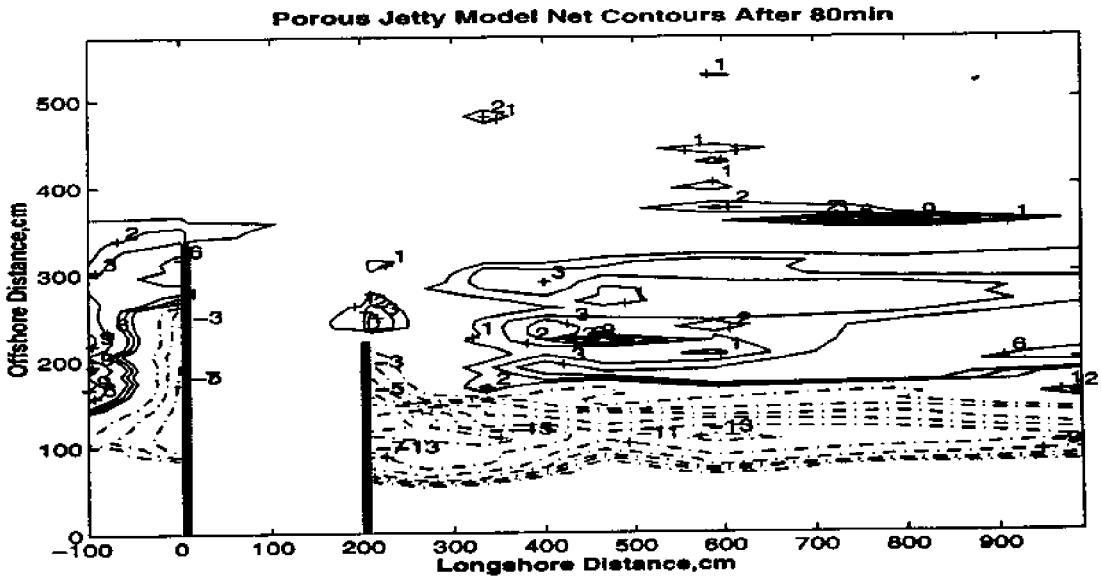

Figure 41: Accretive and Erosive Patterns during 40-80 minutes in Experiment C2.

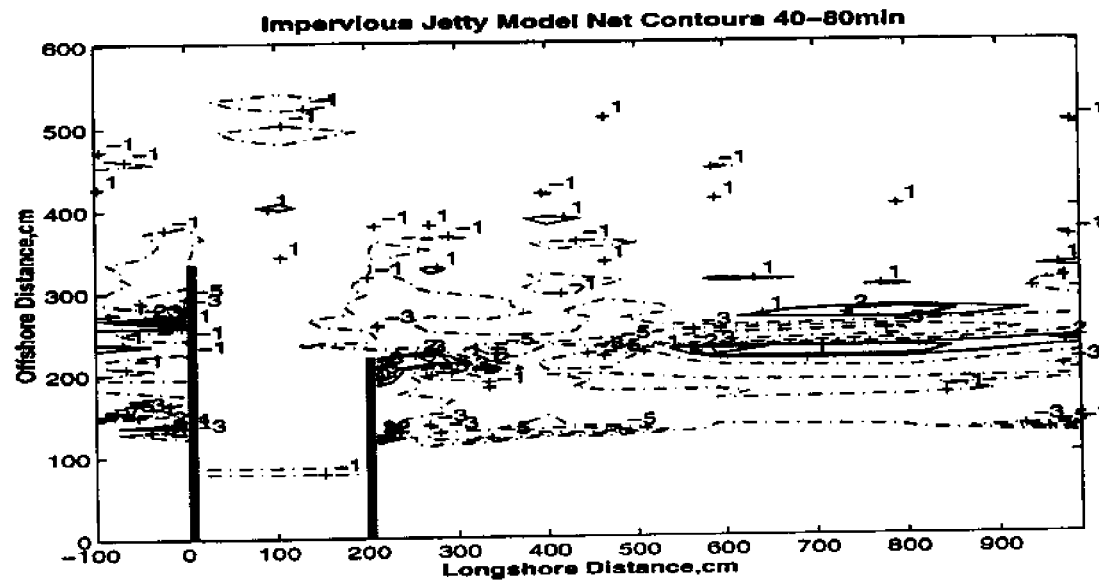

Figure 42: Accretive and Erosive Patterns during 40-80 minutes in Experiment C3.

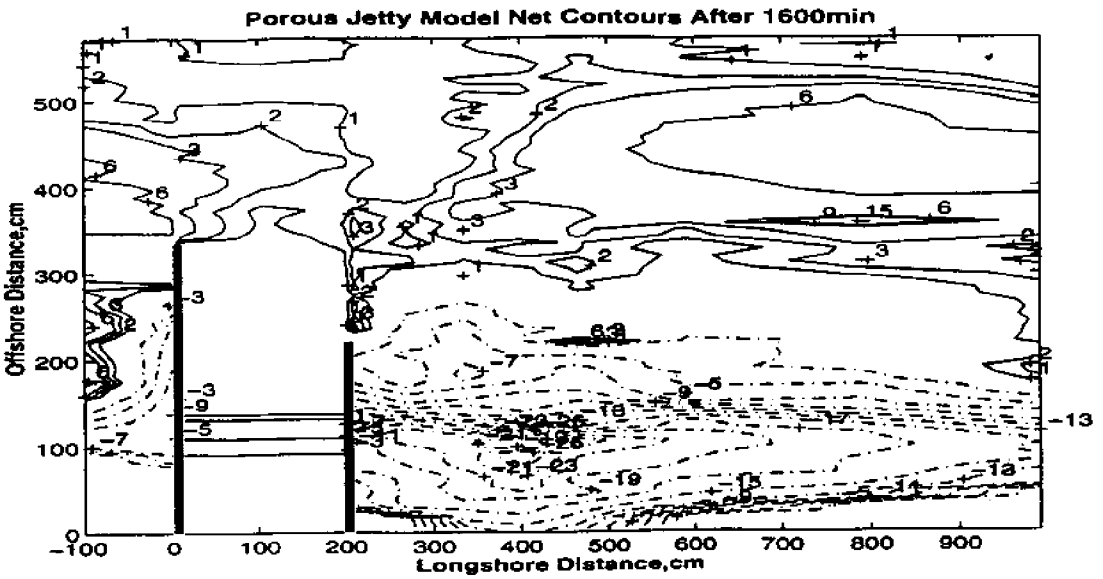

Figure 43: Accretive and Erosive Patterns during 0-1600 minutes in Experiment C2.

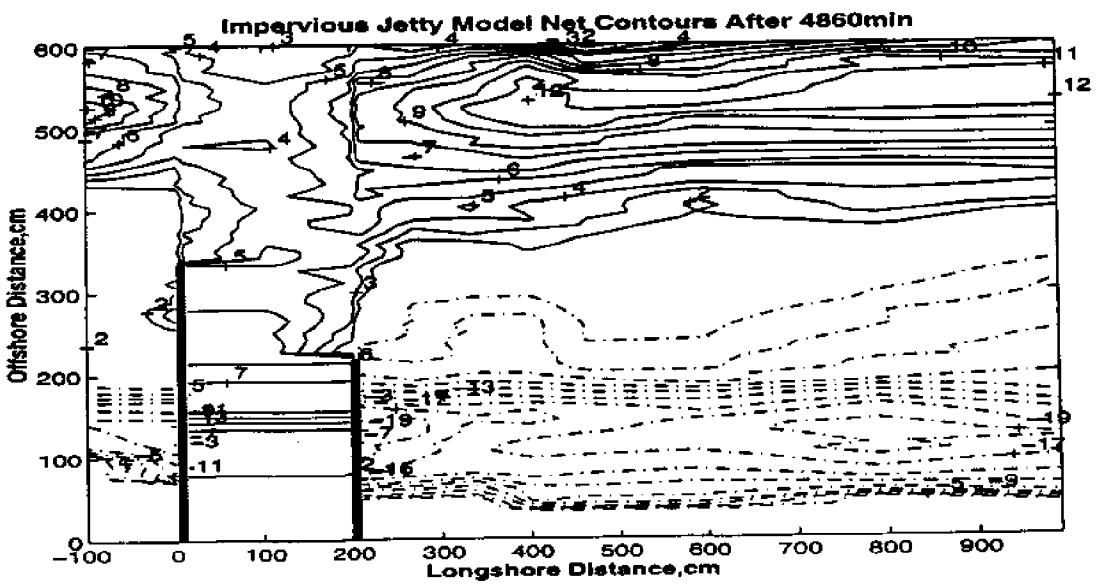

Figure 44: Accretive and Erosive Patterns during 0-4860 minutes in Experiment C3.

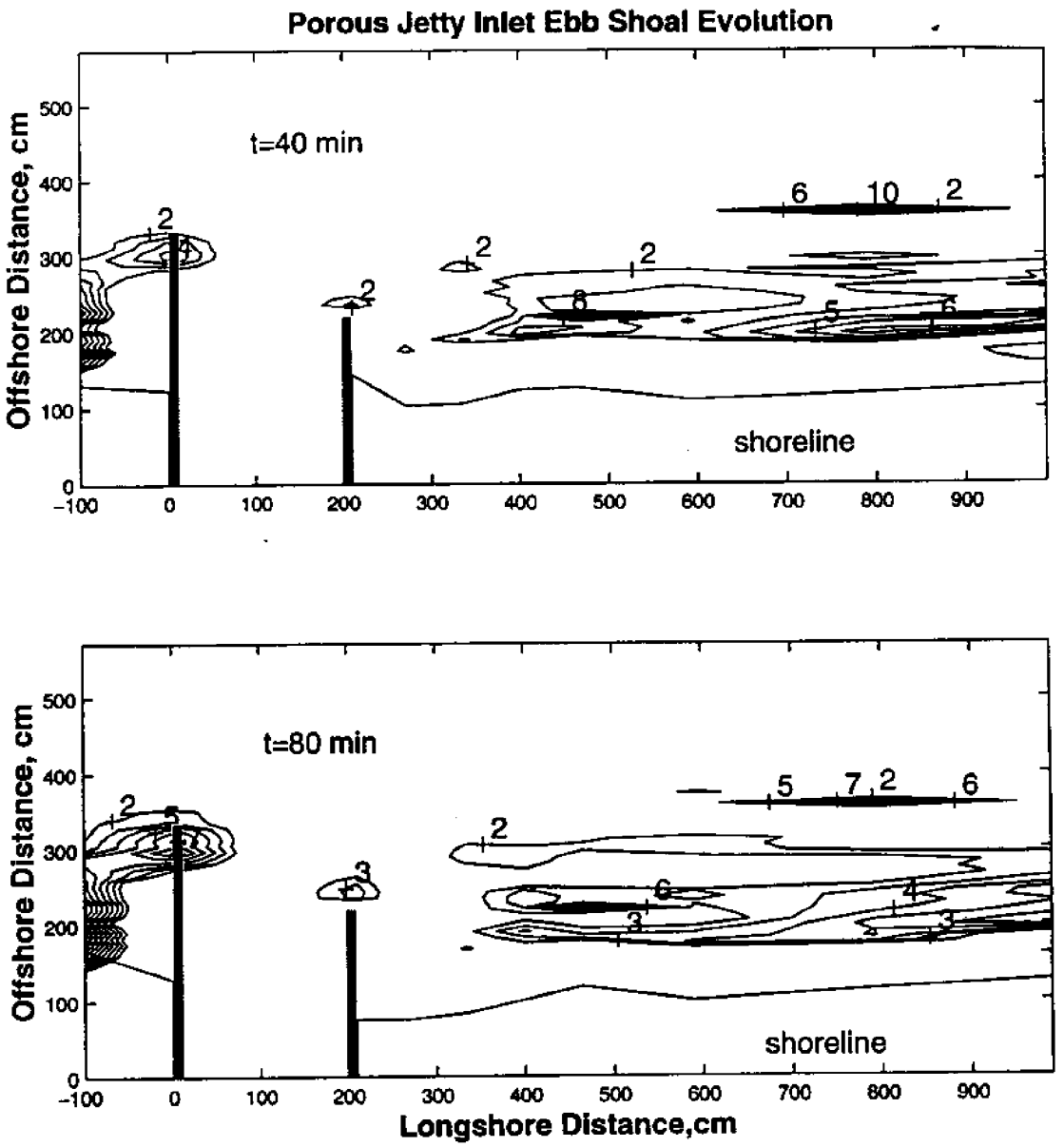

Figure 45: Description of Generation and Growth of Ebb Shoal in Experiment C2.

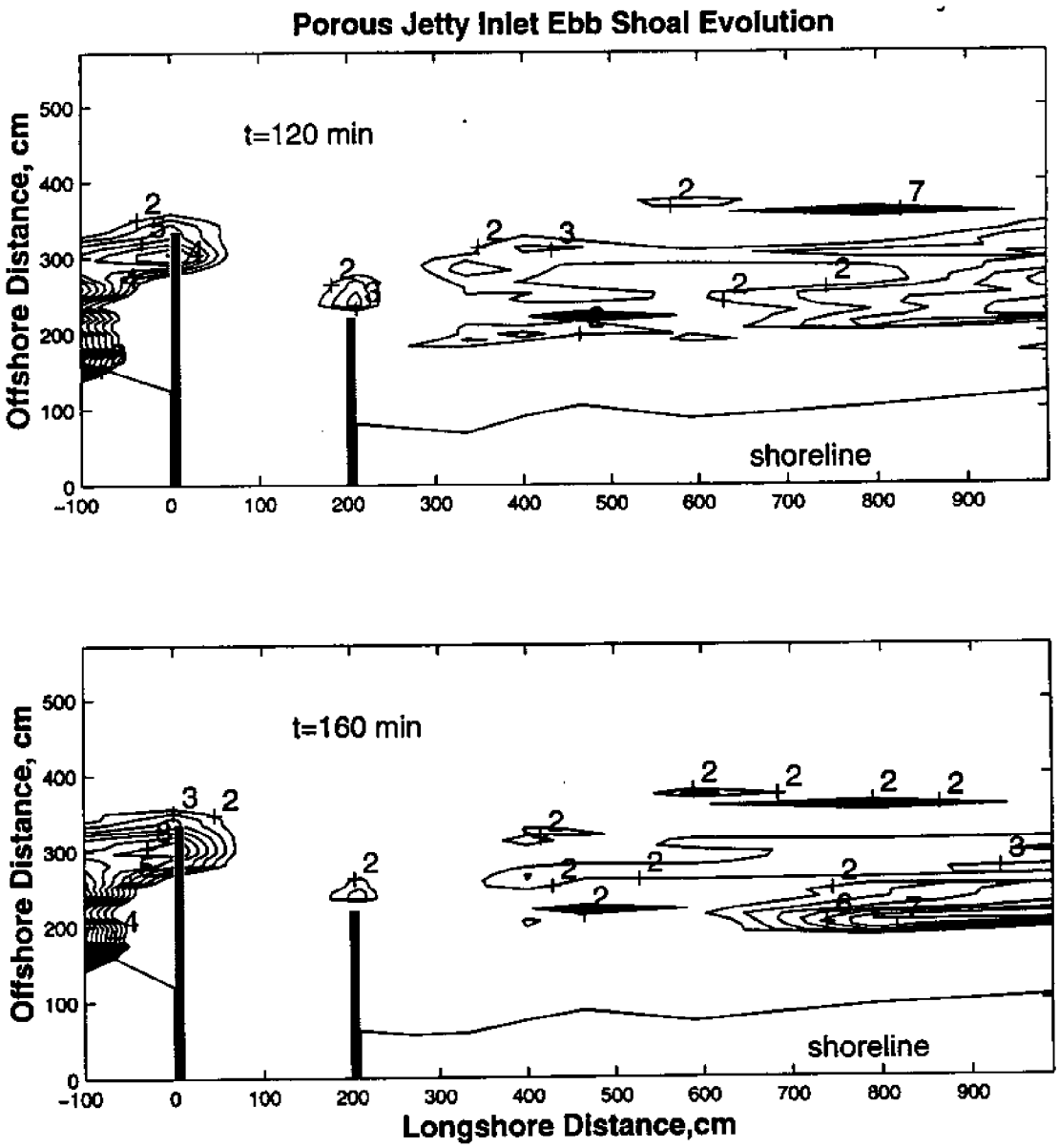

Figure 45: Description of Generation and Growth of Ebb Shoal in Experiment C2 (Continue).

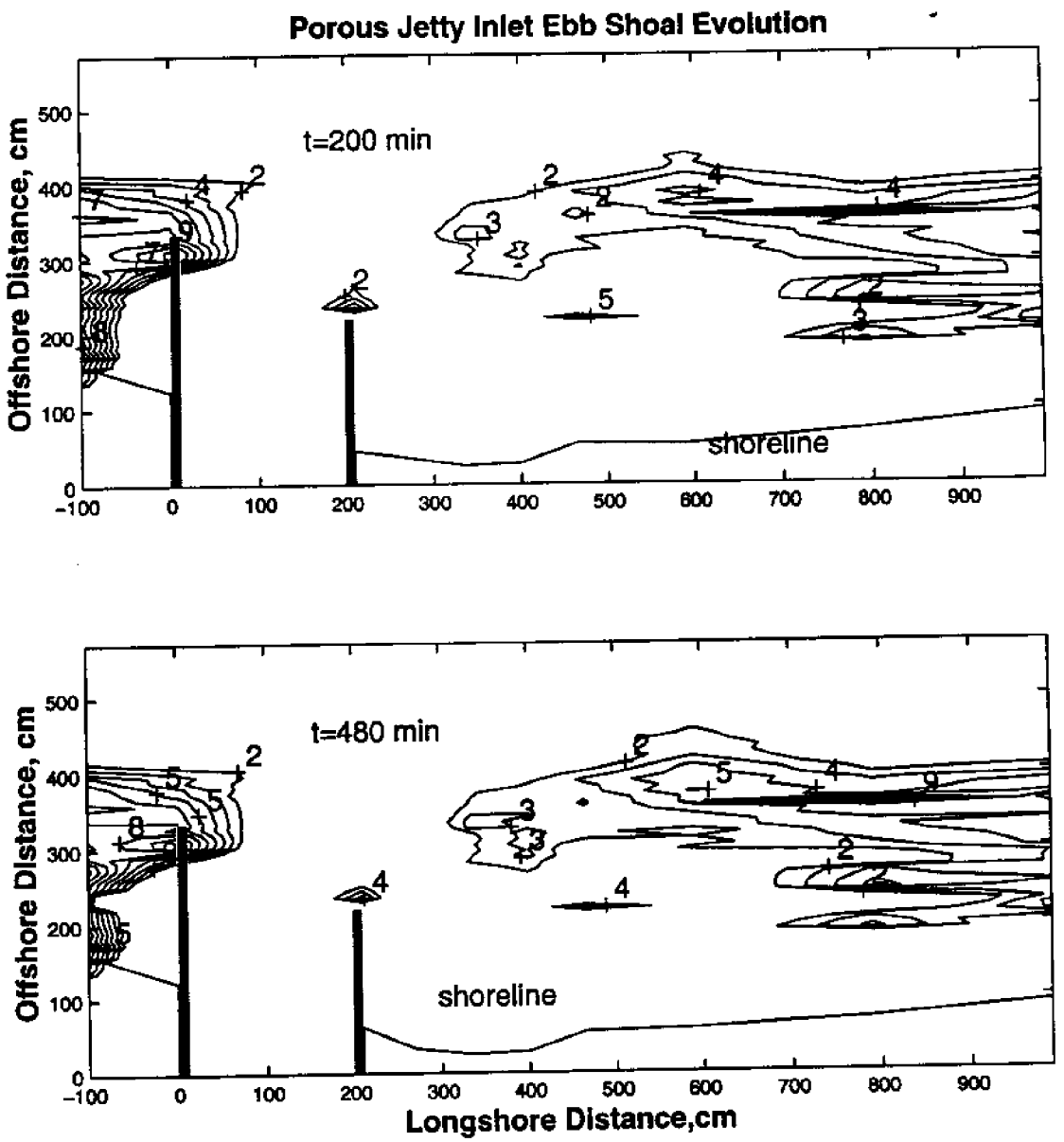

Figure 45: Description of Generation and Growth of Ebb Shoal in Experiment C2 (Continue).

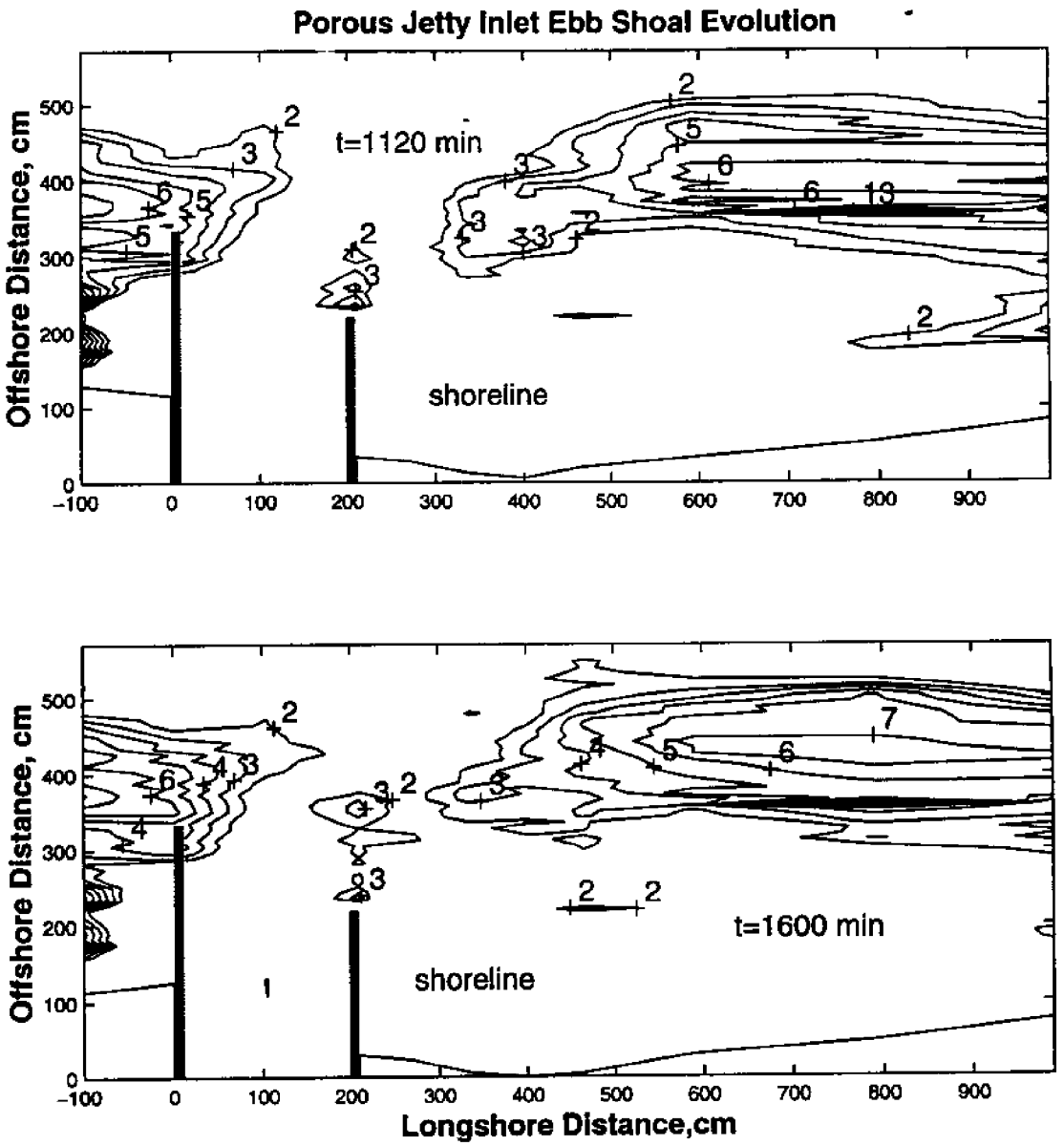

Figure 45: Description of Generation and Growth of Ebb Shoal in Experiment C2 (Continue).

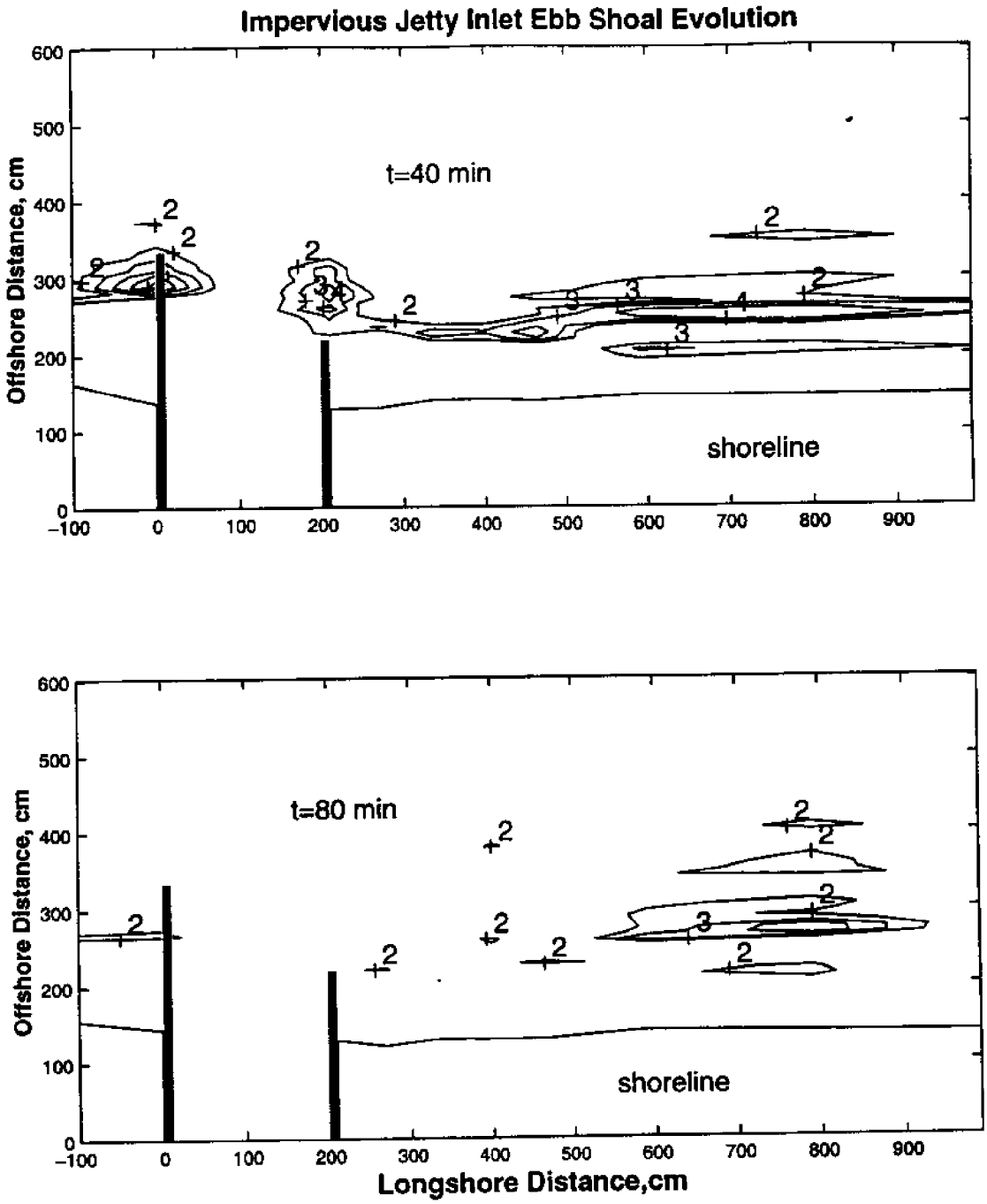

Figure 46: Description of Generation and Growth of Ebb Shoal in Experiment C3.

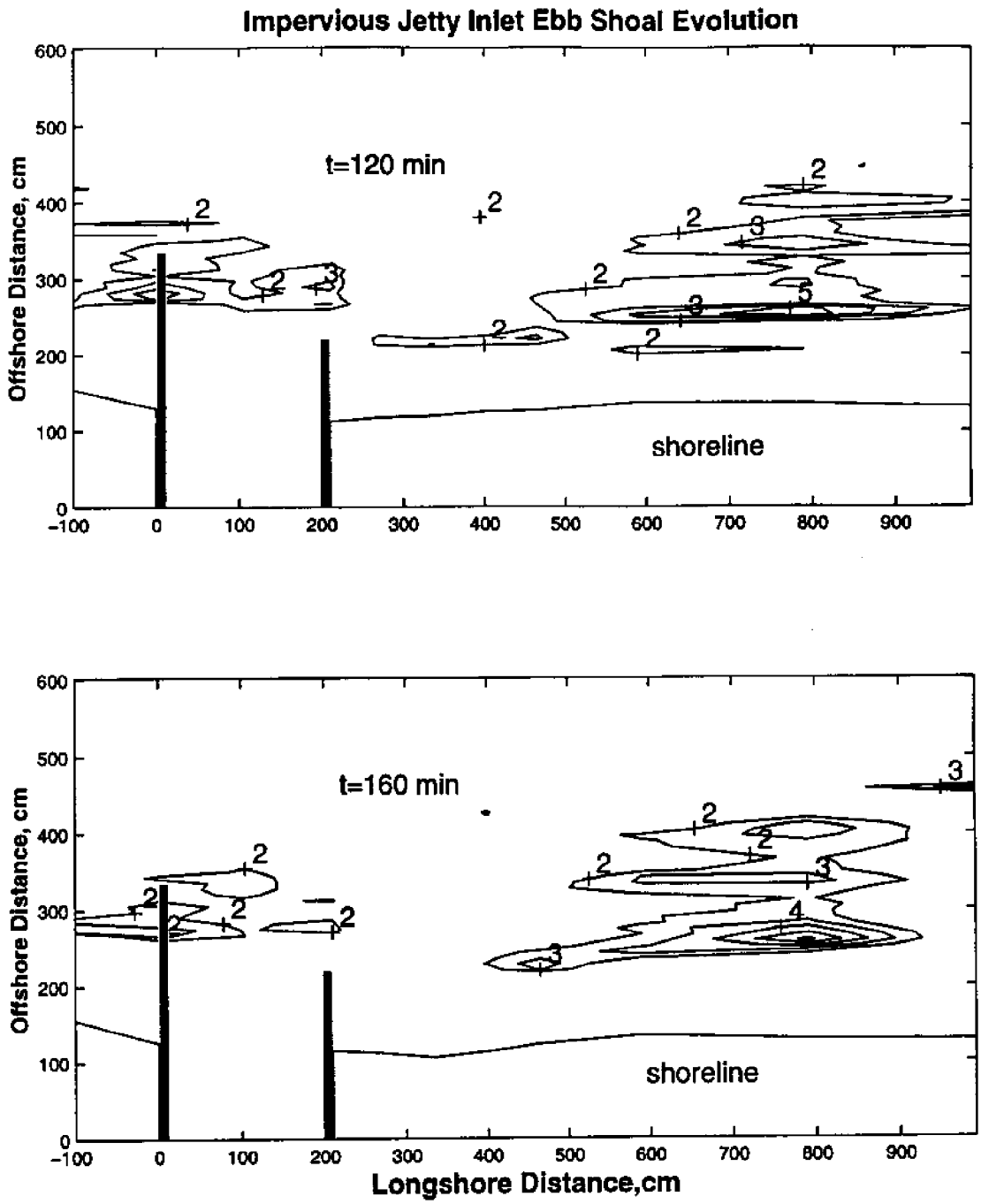

Figure 46: Description of Generation and Growth of Ebb Shoal in Experiment C3 (Continue).

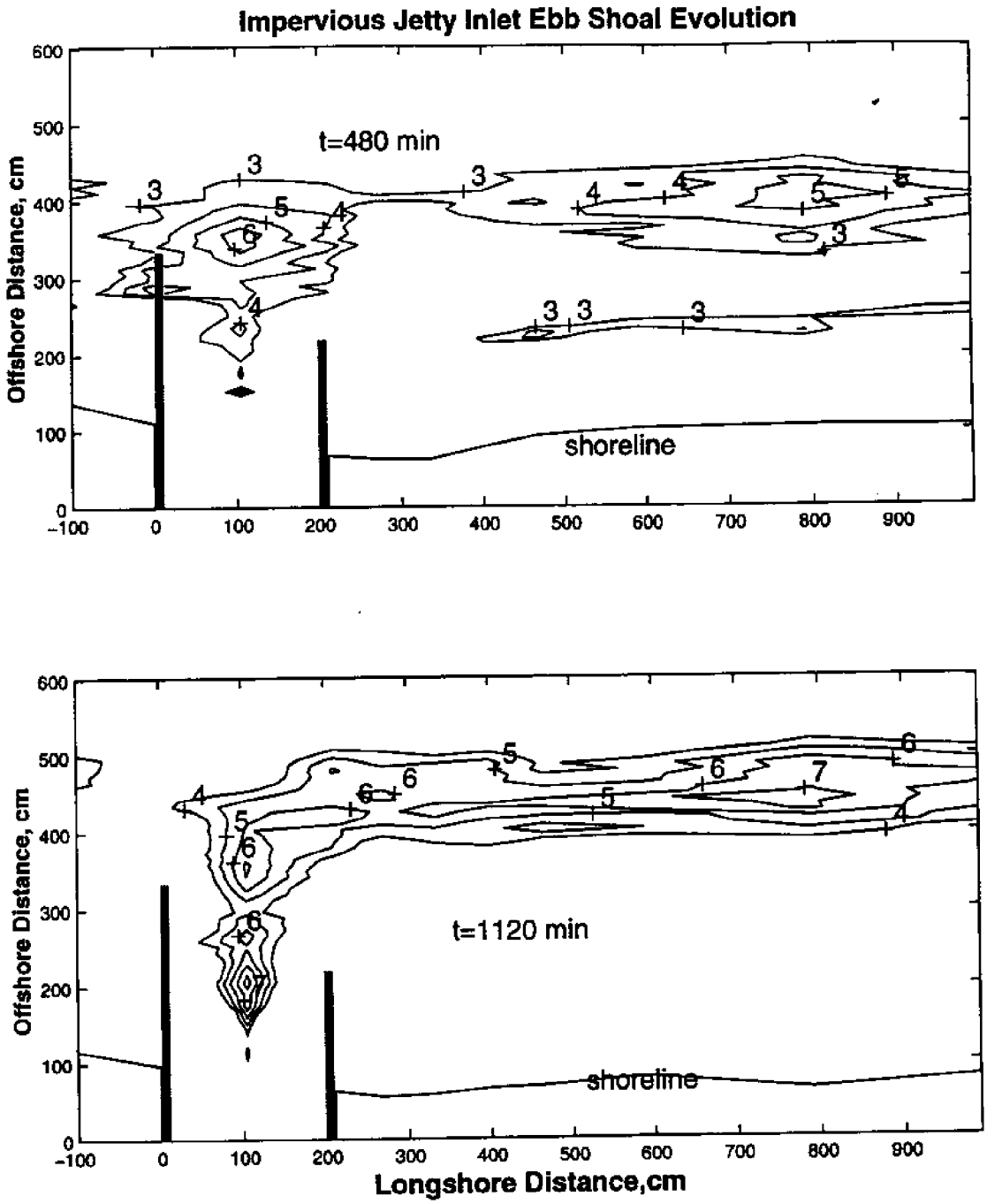

Figure 46: Description of Generation and Growth of Ebb Shoal in Experiment C3 (Continue).

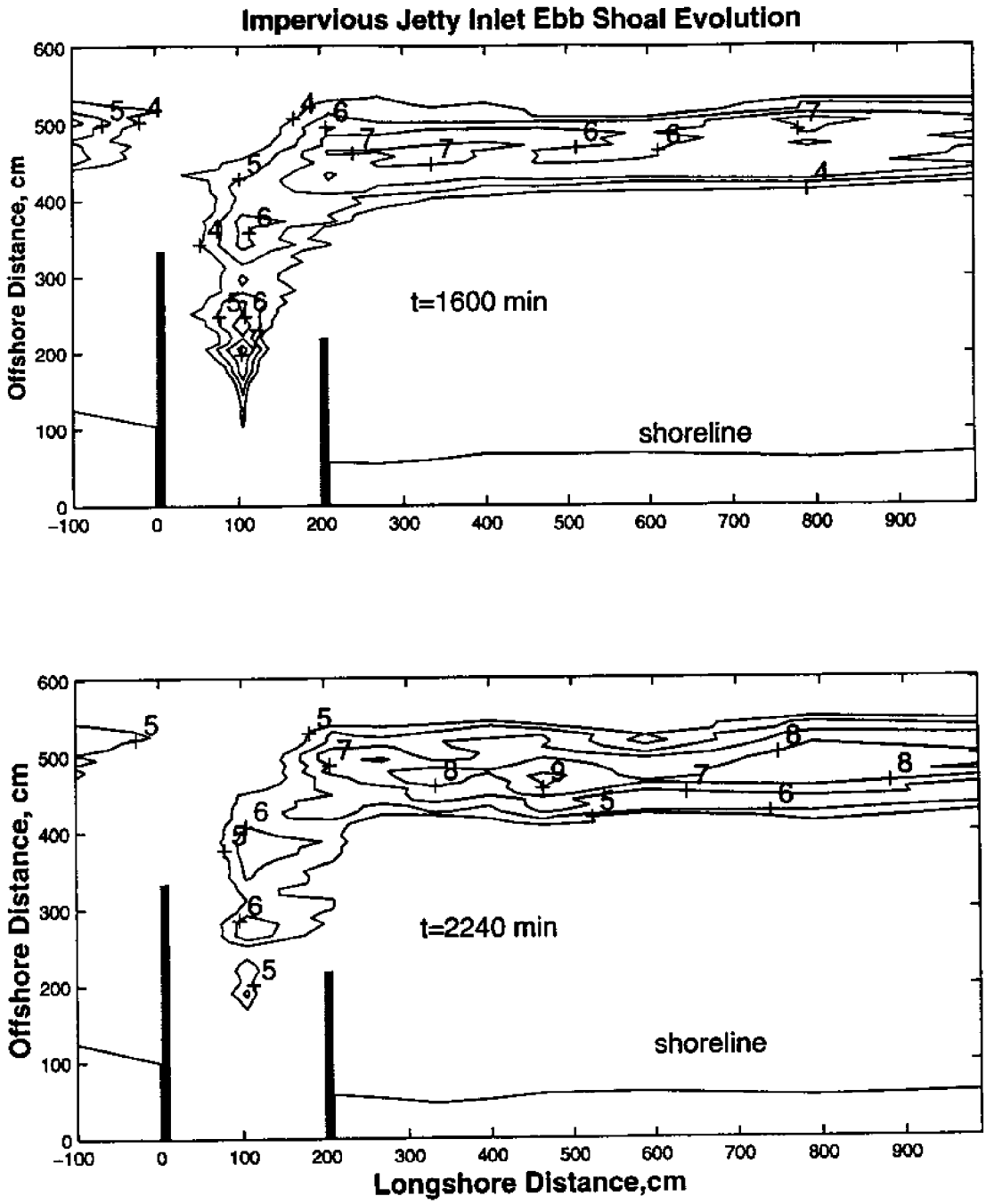

Figure 46: Description of Generation and Growth of Ebb Shoal in Experiment C3 (Continue).

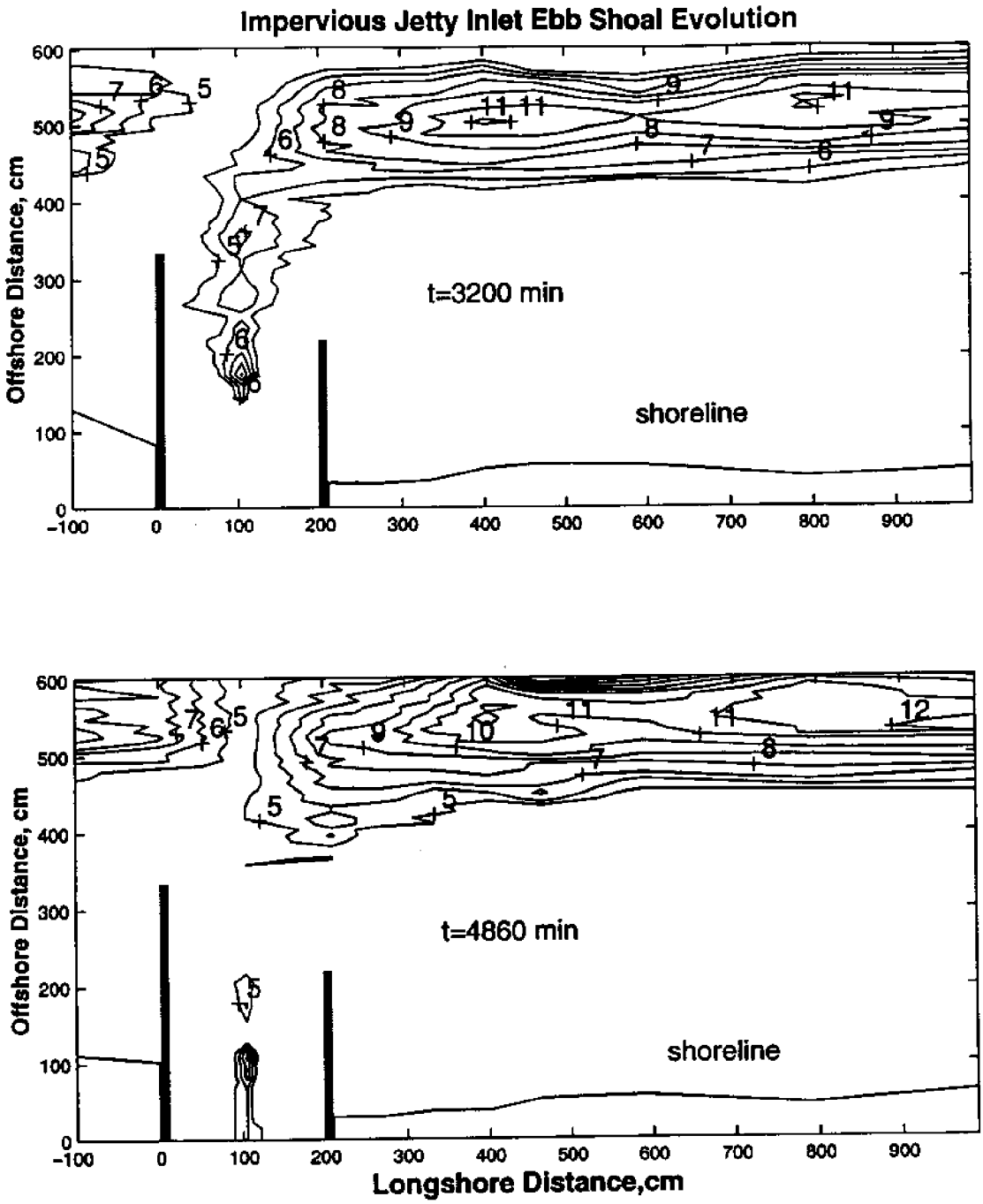

Figure 46: Description of Generation and Growth of Ebb Shoal in Experiment C3 (Continue).

amount of sediment deposition. The rate of channel shoal was considerably slower than the natural inlet case. However, as time progressed, the channel was eventually blocked when shoaling from the updrift jetty expanded towards downdrift. The formation of ebb tidal shoal was not evident until a later stage (outlined at 200 and 480 minutes). From the locations of the ebb tidal shoal and the sequence of topographic changes, it is hard to judge how the ebb tidal shoal was formed, whether it was directly from updrift bypassing, or from offshore transport of nearshore material or from growth of downdrift accretion.

In Experiment C3, updrift sediment tended to bypass the imperious updrift jetty instead of accumulating around the tip. The bypassed material first formed channel shoals which eventually moved further downdrift and drew into a substantial ebb shoal. The ebb shoal was a large elongated body of sand somewhat resembled to that observed in nature downdrift of improved inlets.

The ebb tidal shoal volume, the volumetric centroid and the areal of spreading of the ebb shoal were also calculated for C2 and C3. The results were given in Table 9. The ebb tidal shoal volume changes as well as the areal of spreading for C1, C2, and C3 are plotted in Fig.47. In the early stage, the growth of ebb tidal shoal was unsteady for all the experimental cases; first grew during ebb cycles but shrunk during flood cycles. After the first few cycles, the ebb tidal shoal grew steadily, almost in a linear fashion. The process was much rapid for the natural inlet case than the jettied case. In the case of porous jetties, the smallest ebb shoal as the material was largely accumulated near the updrift jetty. The impervious jetty experiment had the longest test time. The rate of growth apparently slowed down at a later stage.

5.4 Ebb Tidal Shoal Dynamics

With the aid of the shoal evolution plots together with the sediment flux program presented in Section 4.2, one is able to shed some light on the dynamic process of ebb tidal

Table 9: Jettied Inlet Ebb Shoal Characteristics.

Experiment C2: Porous Jettied Inlet Experiment				
Model Time (min)	Ebb Shoal Characteristics			
	volume (m^3)	Centroid's of A volume		spreading radius of volume, R_c (m)
		X_c (m)	Y_c (m)	
40	0.0010	2.10	2.35	0.25
80	0.0029	2.10	2.50	0.55
120	0.0060	2.15	2.50	0.75
160	0.0050	2.10	2.55	0.60
200	0.0210	3.70	3.45	1.05
480	0.0329	4.25.	3.55	1.85
1120	0.0483	4.75	3.75	2.45
1600	0.0693	5.95	4.25	2.95

Experiment C3: Impervious Jettied Inlet Experiment				
Model Time (min)	Ebb Shoal Characteristics			
	volume (m^3)	Centroid of Volume		spreading radius of volume, R_c (m)
		X_c (m)	Y_c (m)	
40	0.0092	2.00	2.75	0.45
80	0.0005	2.40	3.00	0.10
120	0.0130	1.00	3.00	0.95
160	0.0077	1.00	3.10	0.75
480	0.0597	1.05	3.50	1.95
1120	0.0942	1.10	4.35	2.05
1600	0.1709	2.55	4.50	2.30
2240	0.2346	2.95	4.75	2.95
3200	0.3908	4.05	5.05	3.95

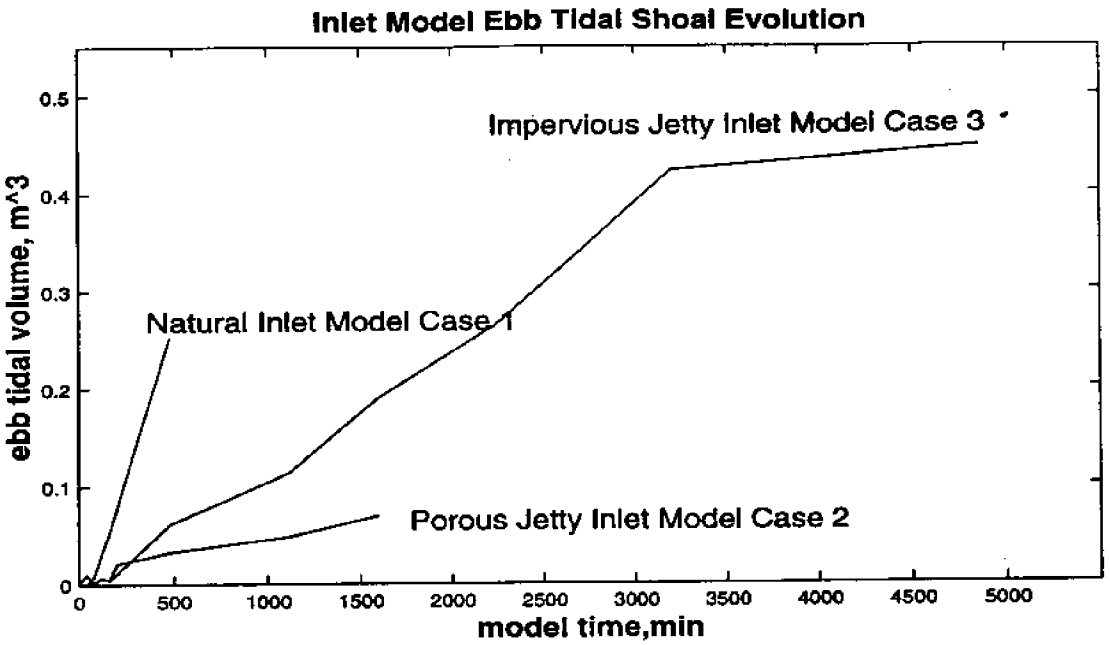

Figure 47: Accretive Change of Ebb tidal Shoal Volumes in Experiments C1, C2, and C3.

shoal evolution. Experiments of natural inlet and the non-porous jetty case are used here for discussions. The objective is to determine the source origins and the flux rate during the ebb tidal shoal evolution process. The basic procedures used consist of the following two steps.
Step 1: Delineate shoal regions. The regions and grids of ebb tidal shoal and channel shoal are constructed based on the results given in Section 5.3.
Step 2: Prepare a sediment flux diagram: The sediment flux program is applied to regions of separate shoals to construct a sediment flux diagram.

The case of the natural inlet experiment is discussed first with a few representative flux patterns. Figure 48 shows the sediment flux pattern around the initial shoaling region just outside entrance. As can be seen this initial shoaling was formed by offshore sediment

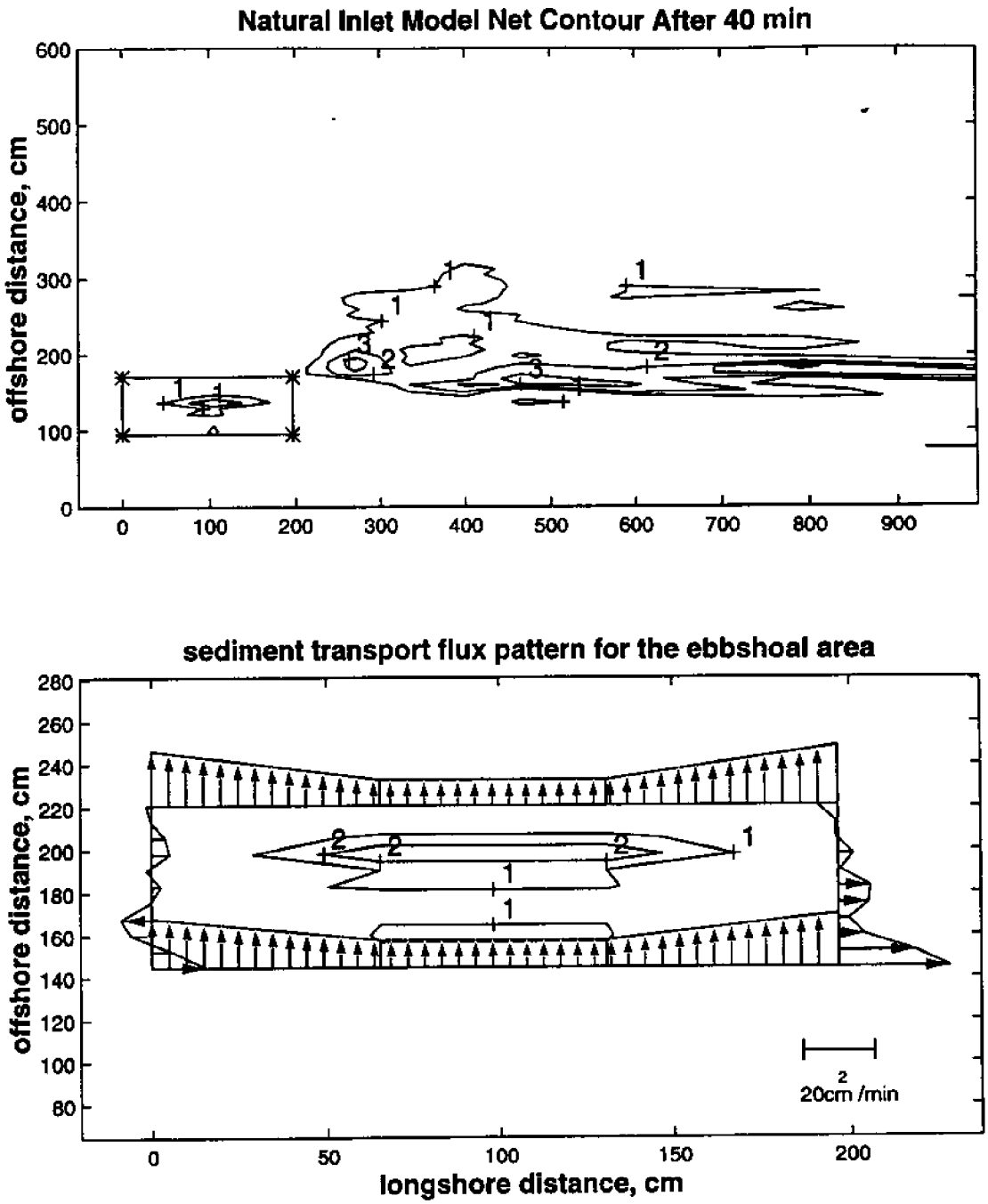

Figure 48: Sediment Flux Pattern in the Initial Shoaling Region in Experiment C1 (0-40 minutes).

flux instead of directly from the updrift transport. In the subsequent flood tidal cycle, the shoal growth was clearly diffused (Fig.49). In the ebb tidal shoal region, longshore drift reversal was detected from the flux pattern. To examine the overall shoal growth patterns for the duration of the experiment, flux patterns from two regions were constructed, one in the channel region and one in the offshore regions on the downdrift side. The flux pattern for the channel shoal is shown in Fig. 50. It appeared that there was a significant net onshore component contributing to the shoal growth even though the original sand source might still be from the updrift sediment. The longshore component was much larger but its net contribution to shoal growth might not be more important than the on/offshore component. The shoal growth in the offshore region, as shown in Fig.51, was clearly due to the material from the nearshore region. It is suspected that it was simply a part of an over grown offshore bar in the laboratory and was not an ebb tidal shoal in the true sense.

In the case of impervious jetty inlet experiment, both longshore and offshore components contributed to the initial accretion at the jetty's tips during ebb tidal cycle as shown in Fig. 52. It is seen that contributions came from various components in this development stage. In the subsequent flood tidal cycle, the accretion at the updrift jetty simply diffused (Fig. 53) similar to that in the natural inlet case. Sediment motion was more active near the downdrift jetty. And the flux pattern was almost opposite to that obtained during the ebb cycle and, again, caused shoaling diffusion. In these initial cycles sediment transport was very active as can be judged by the magnitude of the mean flux values.

As discussed earlier that the topographic response in the experiment can be roughly divided into an initial adjustment and response stage followed by a steady development stage. Figure 54 displays the net pattern in Experiment C3 from 0 to 480 minutes which roughly represents the initial stage. A clearly identifiable shoal was developed in this stage. The supplies to the shoal region were from three main sources: updrift longshore influx, updrift

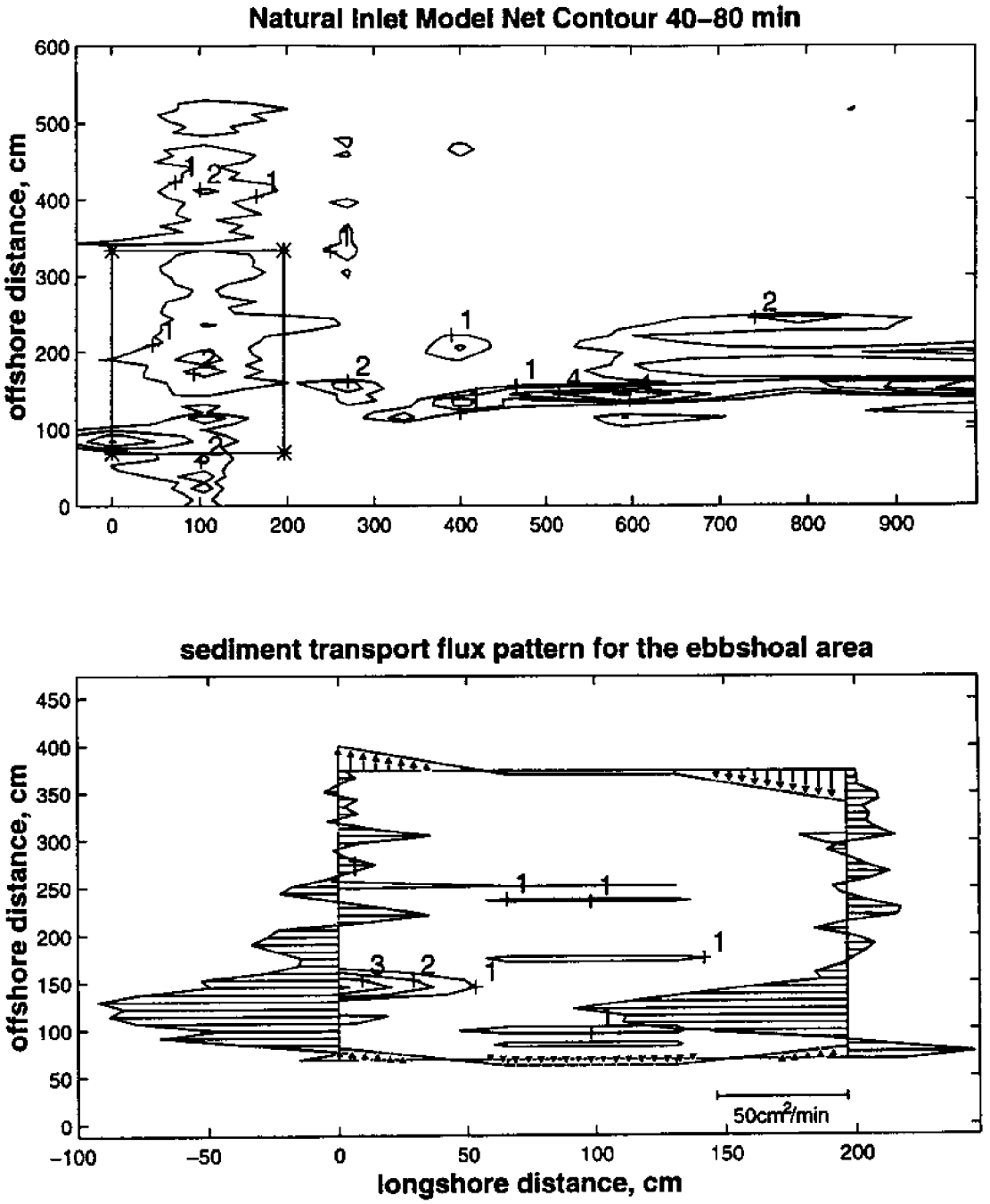

Figure 49: Sediment Flux Pattern in the Initial Shoaling Region in Experiment C1 (40-80 minutes).

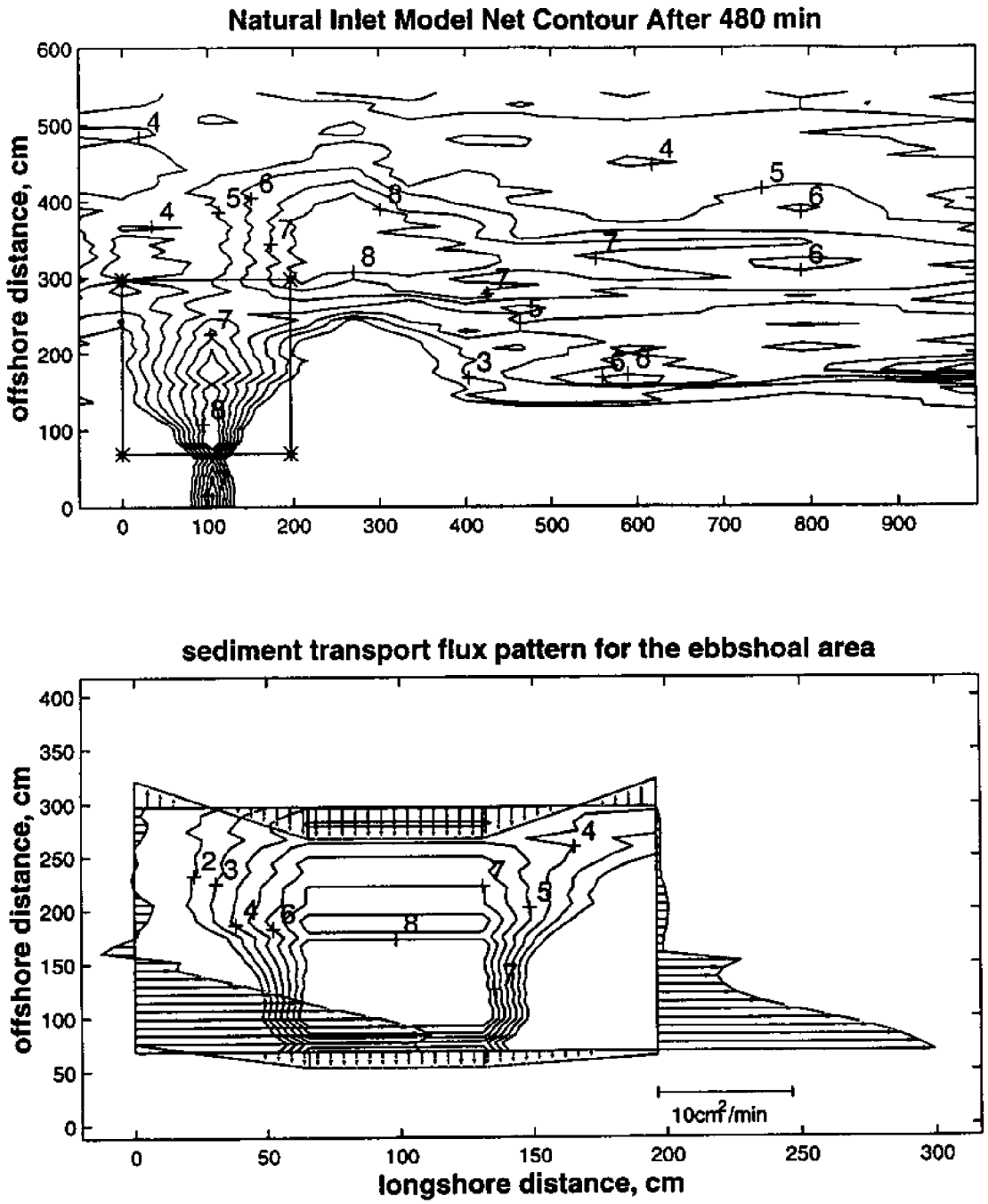

Figure 50: Overall Sediment Flux Pattern in Channel Shoaling Region in Experiment C1 (0-480 minutes).

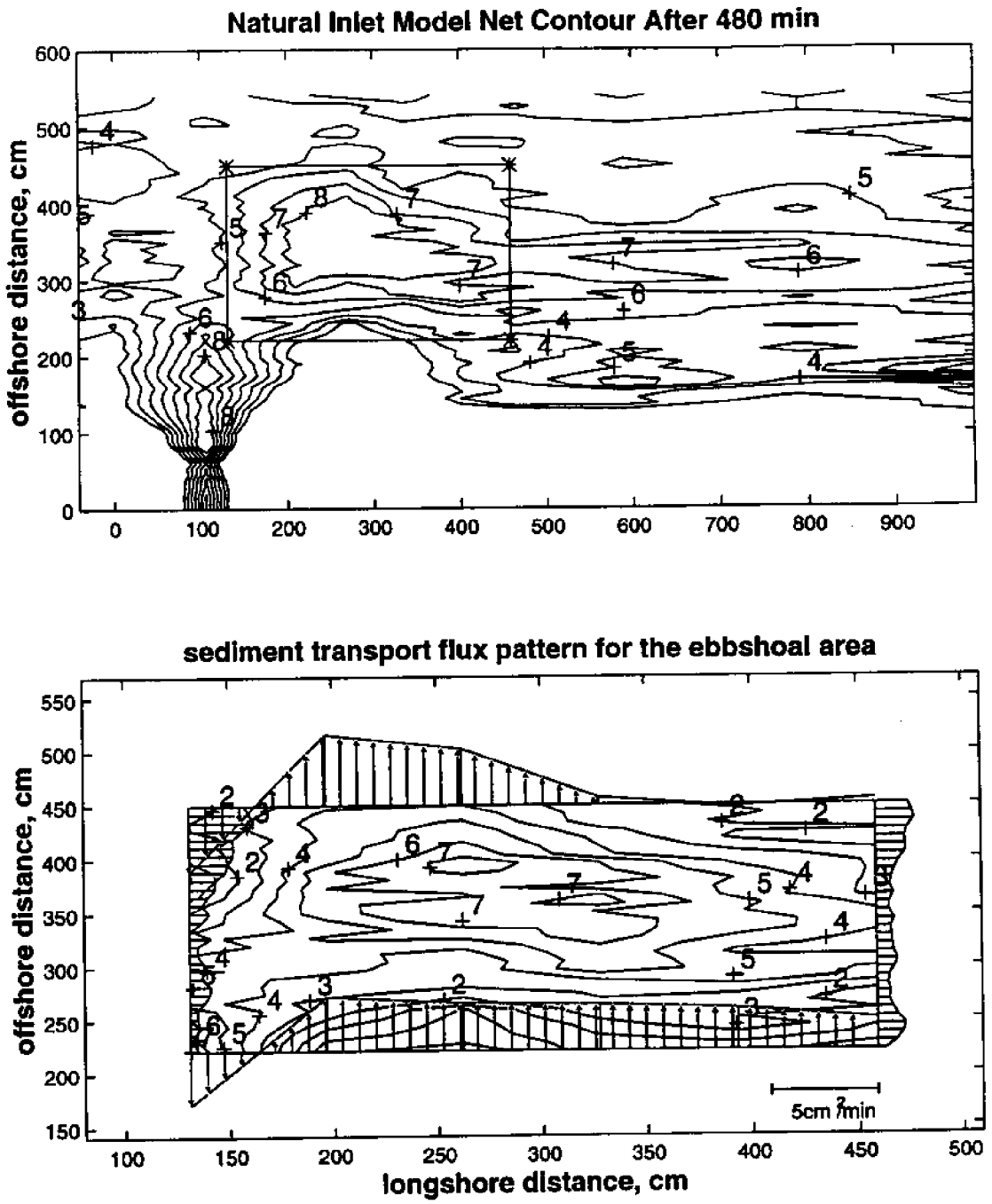

Figure 51: Overall Sediment Flux Pattern in Offshore Shoaling Region in Experiment C1 (0-480 minutes).

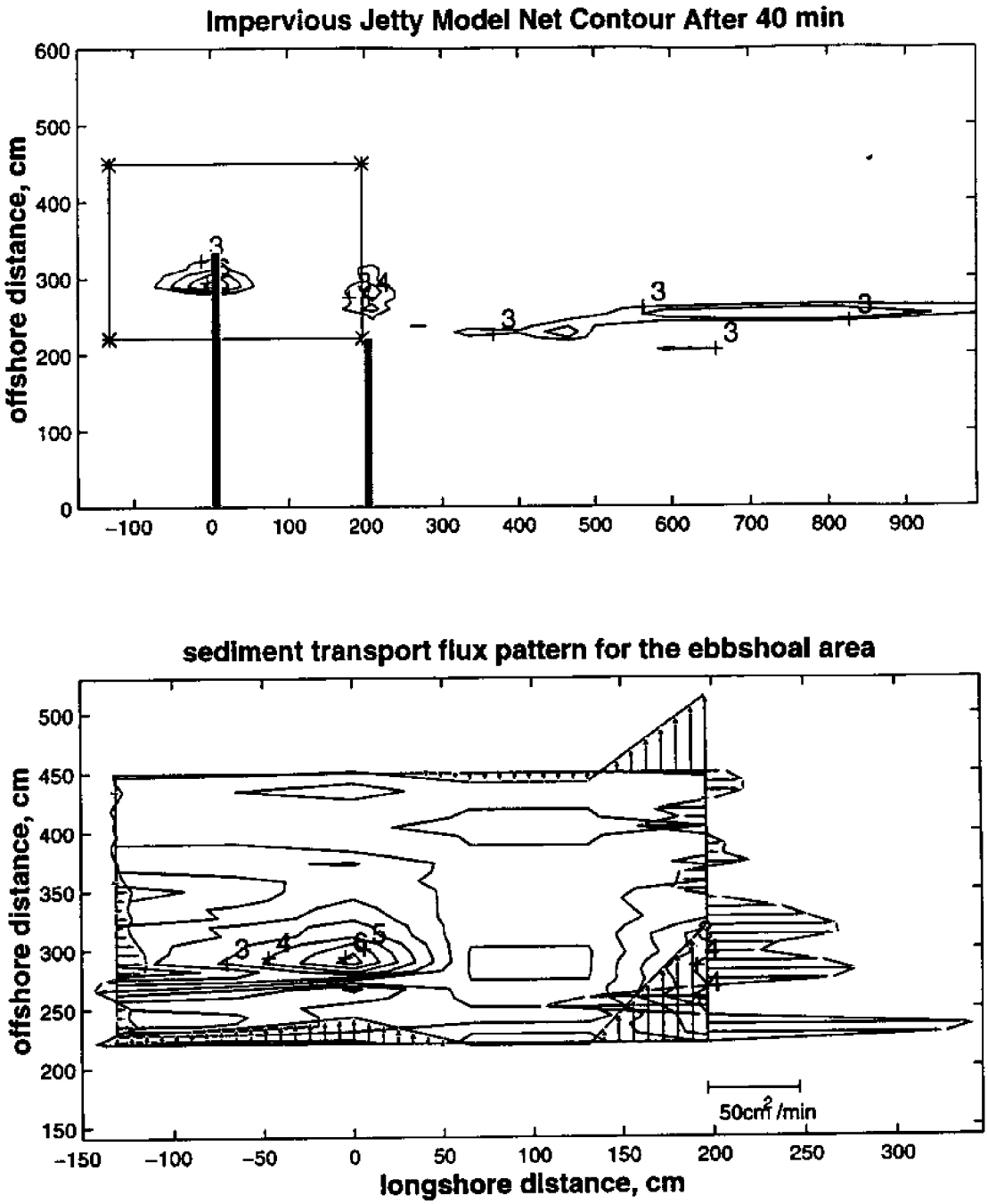

Figure 52: Sediment Flux Pattern in the Initial Shoaling Region in Experiment C3 (0-40 minutes).

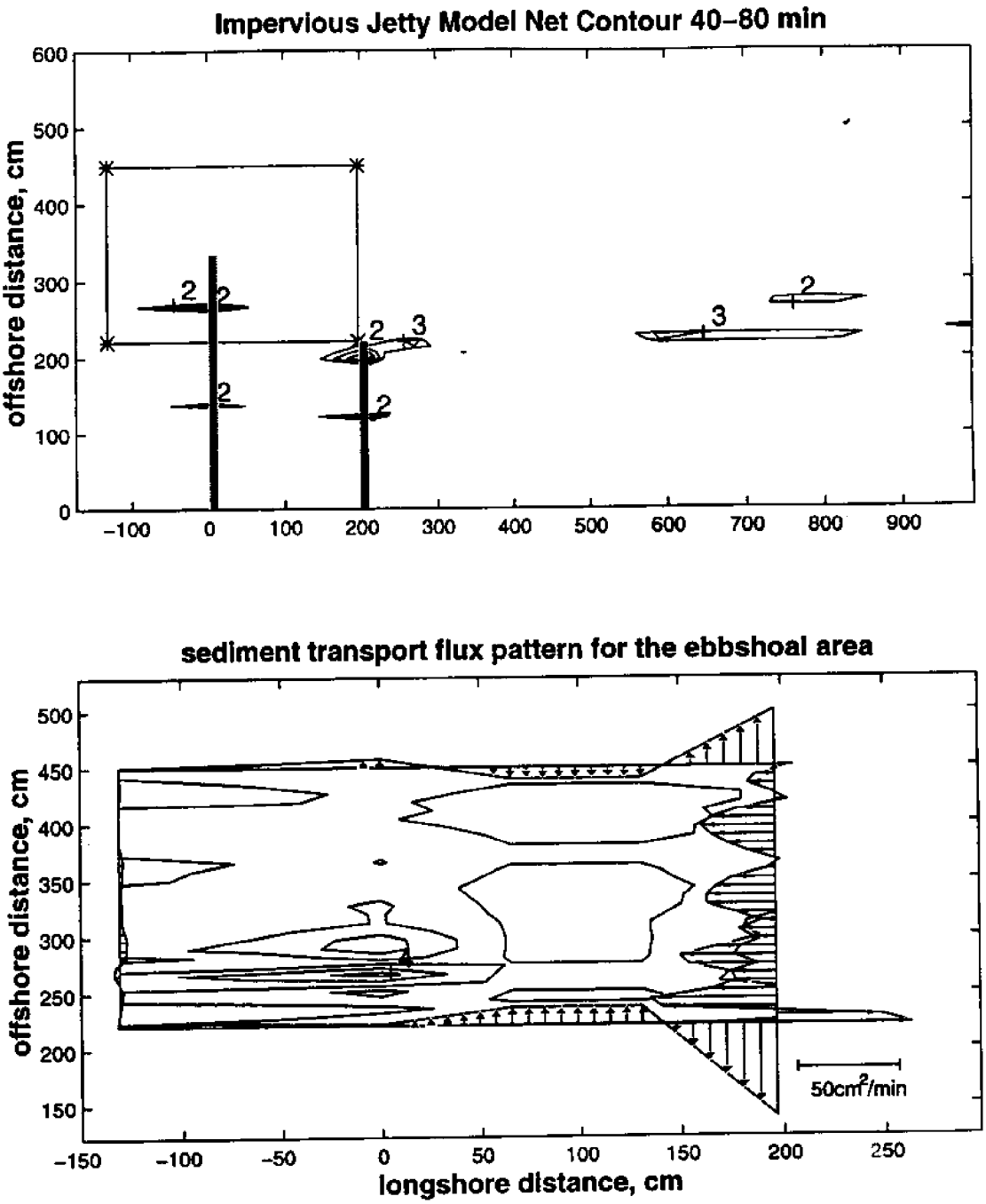

Figure 53: Sediment Flux Pattern in the Initial Shoaling Region in Experiment C3 (40-80 minutes).

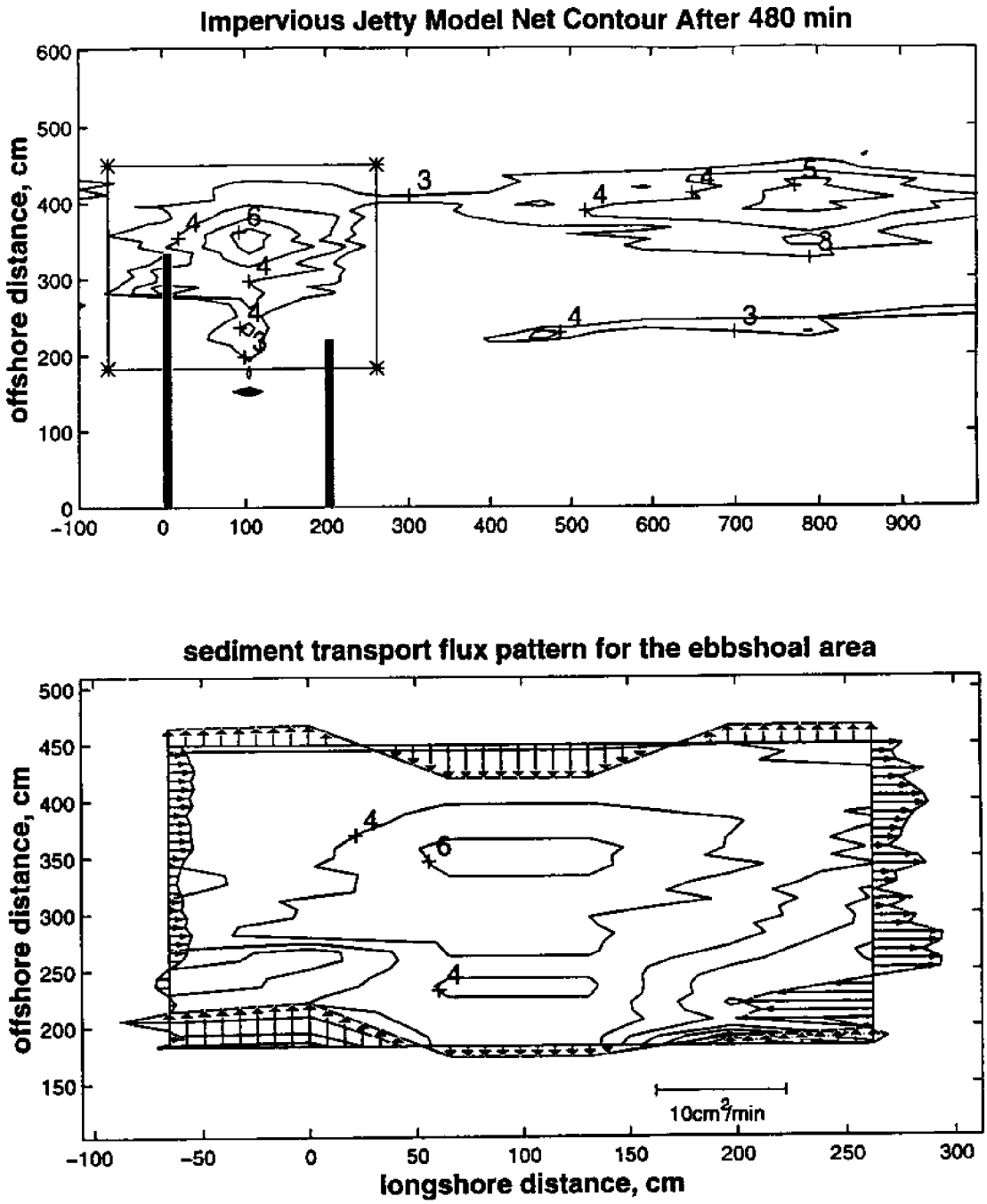

Figure 54: Sediment Flux Pattern in the Initial Shoaling Region in Experiment C3 (0-480 minutes).

offshore influx and influx from offshore in the channel confinement. Drift reversal at the downdrift end also contributed to the region but was mainly compensated by the loss into the channel.The magnitude of the mean flux values was much smaller than those in the initial cycles. In the following development stage the shoal formed in the initial stage began to grow into two directions, one into the channel and the other towards downdrift offshore. Two shoal regions were, therefore, delineated to examine the growth pattern for the duration from 480 to 1600 minutes. The computed net sediment flux pattern during this period for the channel shoal region is given Fig.55. In this case, clearly the main contribution was from influx into the channel which in a way provides the validation of the EEF method. The results for the offshore shoal region are shown in Fig. 56. In this region, longshore influx almost balanced by the outflows. The shoal growth appeared to be due to offshore influx from the channel region and material supplied from downdrift nearshore zone. The magnitude of the mean flux for the channel shoal growth was about one fourth of that for the offshore shoal indicating that the channel shoal became matured much earlier.

The test results can be extrapolated to prototype values based on the proposed scaling law. Result from C3 is used here for illustrative purposes. Values based on two horizontal scales, 60 and 80, were computed and tabulated in Table 10. By comaring with the values of ebbshoal volume in Fig.1, it is clear that the model tests have not reached the final shoal development stage.

Table 10: Comparison of Model and Prototype Scales for Experiment C3.

Prototype to Model Scale Ratio					Inlet Width (m)	Wave Height (cm)	Wave Period (sec)	Tidal Prism (m^3)	Ebb Shoal Volume (m^3)
N_λ	N_δ	N_H	N_T	N_W					
1	1	1	1	1	1.7	8	1.0	98.4	0.5
60	35	20	7.7	2	102.0	163	7.7	1.24×10^7	63,000
80	44	24	8.9	2	136.0	193	8.9	2.77×10^7	140,800

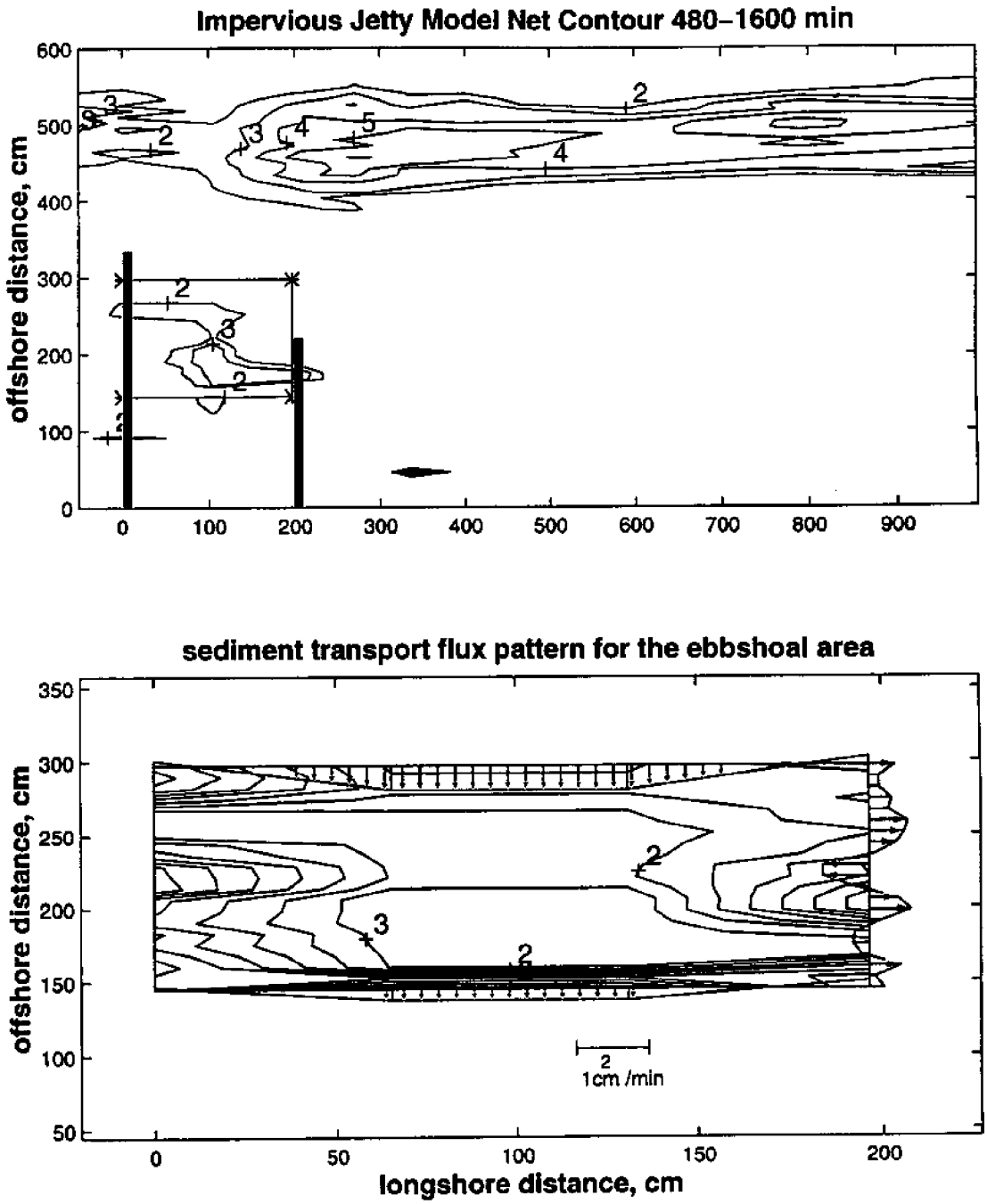

Figure 55: Sediment Flux Pattern in Channel Shoaling Region in Experiment C3 (480-1600 minutes).

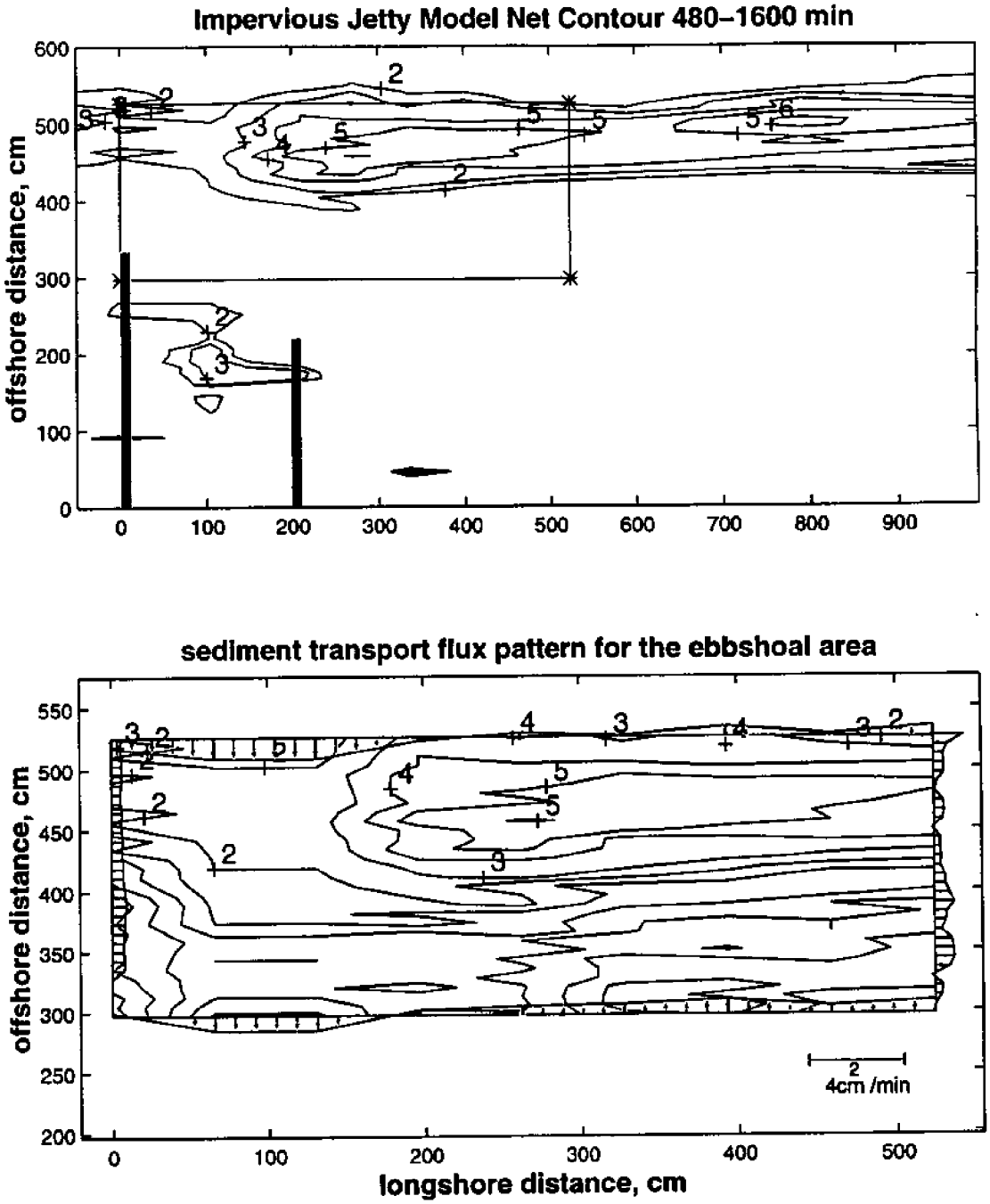

Figure 56: Sediment Flux Pattern in Offshore Shoaling Region in Experiment C3 (480-1600 minutes).

6. SUMMARY AND CONCLUSIONS

Laboratory model experiments were carried out in the present study aimed at improving the fundamental understanding on ebb tidal shoal dynamics. The results from the experiments are also useful for prototype applications through rational scaling laws. The experiments consisted of two parts. The first part was for establishing modeling laws and was conducted with a plane beach. The second part was for studying ebb shoal evolution process and was carried out with three different inlet configurations, a natural inlet, an inlet with porous jetties and an inlet with impervious jetties. All cases were tested under storm wave conditions only.

In the first part, four different modeling laws as proposed by Vellinga (1982), Hughes (1983), Wang, *et al.* (1990), and Wang, *et al.* (1994) were evaluated based on a series of 2-D wave tank and 3-D wave basin tests on beach profile responses at different geometrical scales. The experimental results were compared with data from a prototype scale experiment performed in German Large Wave Tank. The modeling laws were then evaluated based on five different criteria: (1) dune erosion volume, (2) nearshore profile, (3) nearshore bar volume, (4) bar crest location, and (5) bar geometrical location. The results of evaluation indicate that the modeling law proposed by Wang, *et al.* (1994) yields the best performance. This modeling law is adopted for the inlet experiment. Detail of this part is reported separately (Wang, *et al.*, 1994).

The second part of the inlet experiments was all conducted in a 3-D wave basin with an approximate dimension of 28 m x 28 m x 1m. The inlet model consists of a single idealized inlet on a simple beach configuration with straight and parallel bottom contours. The idealized inlet has a rectangular cross section a straight channel normal to shoreline. In all cases, the model was run with alternate ebb and flood tidal conditions. Each ebb and flood tidal phases comprised a duration of 40 minutes in the experiment. Incident waves

were 8 cm in height and 1 second in period for all cases. The wave direction for Cases 1 and 2 was 15^0 but was reduced to 7.5^0 for Case 3.

For the natural inlet case, the inlet was clearly unstable under the test condition as severe inlet shoaling and shoreline erosion occurred and test had to be terminated only after a few tidal cycles. The presence of jetties significantly retarded the growth of shoaling and pushed shoals further offshore as expected. Consequently the experiment can be continued for much longer duration, particularly for the imperious jetty case. The experiment finally had to be stopped when shoals began to move out of the test region.

The ebb shoal evolution processes were documented. A new method based on empirical Eigen function analysis was developed to analyze sediment flux patterns. This enables us to shed light on the dynamics of ebb tidal shoal evolution and the associated nearshore sediment transport process. Specific findings of the present studies are summarized in the followings:

(1) The laboratory model experiments of beach profile responses showed that the results from the 3-D wave basin test are consistent with those from the 2-D wave tank tests in simulating a near-prototype large scale laboratory test conducted in the Big German Tank Experiment (Dette and Uliczka, 1986a,b). This formed the basis for applying the profile scaling laws developed mainly from 2-D experimental results to the 3-D wave basin tests. The modeling law is, however, rather restricted only suitable for erosive conditions under storm waves.

(2) The longshore transport rate measured in the plain beach experiment under the condition with storm waves attacking shoreline in an oblique angle is found to be about 30 percent of the value computed from the SPM formula (U.S. Army Corps of Engineers, 1984). The smaller longshore transport rate obtained in the present model experiment, however, appeared to be more consistent with other existing laboratory experimental results and was also close to the values estimated along the east coast of Florida.

(3) Nature inlet experiment was stopped for only a short test run because of significant shoreline erosion and inlet channel shoaling under the strong storm wave conditions. It is evident that for tidal inlets in strong wave environment, jetty structures are necessary.

(4) The experimental results showed that porous jetty attracts sediment deposition whereas impervious jetty causes more bypassing.

(5) The formation and growth of ebb tidal shoal were observed in all the inlet experiments. The location and rate of growth were different. For the natural inlet case, ebb shoal was very close to the inlet entrance and the rate of growth was the fastest. In the present study, the rate of growth for the natural inlet case was more than twice as much as the cases with jetties. For porous jetty case, the jetty structure behaved like a sink that attracts sand accumulation. Ebb shoal initiated on the down drift side with sand supplied from downdrift beach. The growth of ebb shoal was the slowest. Impervious jetty caused updrift sand to bypass the updrift jetty. Both updrift and downdrift sand sources contributed to the formation and growth of ebb tidal shoal.

(6) A new method of establishing sediment flux patterns based on measured topographic changes was developed. The method is based on Empirical Eigen Function (EEF) analysis. Since there is insufficient information to uniquely determine the flux pattern, the EEF provides the best estimate in the sense of least square error. Upon testings a number of cases, the flux patterns as calculated appeared to be consistent with observation. One must be cautioned, however, that although the solution by EEF under the assumed boundary conditions is unique it is not the only solution to produce the required bottom changes.

(7) The EEF method enables us to determine the sediment transport patterns in ebb tidal shoal development thus aids in the insight on the dynamic process. Generally speaking, ebb current creates ebb shoal whereas flood current destroys it. The cumulative effect, on the other hand, is the continued growth of ebb shoal. The flux contributing to ebb tidal shoal came from three directions: updrift influx, downdrift offshore transport and onshore transport in the zone influenced by the inlet.

In conclusion, the present study represents an exploratory laboratory experiment to apply movable model to examine inlet evolution. The experiment was partially successful in that ebb tidal shoals similar to that observed in nature can be produced in the laboratory. The test wave conditions were by no means realistic. In addition, the modeling law is very restrictive. Based on the experimental results, we gained certain fundamental knowledge on ebb tidal shoal development forms and shapes of growth, the effects of structures and the sand sources and flux patterns. The EEF is a promising technique for sediment flux analysis with incomplete or insufficient information.

The issue of movable bed experiment remains a difficult one and the process of inlet ebb tidal shoal is enormously complex. The present study demonstrated the feasibility and usefulness of such type of experiment as well as provided frame work for future studies of similar kind. Work is continuing with refined scopes.

References

Dette, H.H., and K. Uliczka, 1986a. "Seegangsrzeugte Wechselwirkung Zwischen Vorland und Vorstrand und Kustenschutzbauwerk," Technisher Bericht SFB 205/TPA6, University Hannover, Germany.

Dette, H.H., and K. Uliczka, 1986b. "Prototype and Model Evolution of Beach Profile," Proceedings of Symposium on Scale Effects in Modeling Sediment transport Phanomena, Toronto, Canada.

Hayter, E.J., 1988. "Study of Ebb Tidal Shoal Dynamics," Beach Preservation Technology 88: Problems and Advancements in Beach Nourishment, pp.365-374.

Hughes, S.A., 1983. "Movable-Bed Modeling Law for Coastal dune Erosion," Journal of Waterway, Port, Coastal and Ocean Engineering, New York, Vol. 109, No.2, pp.164-179.

Jonson, I.G., 1966. "Wave Boundary Layer and Friction Factors," Proceedings of the 10th Coastal Engineering Conference, ASCE, New York, New York. pp.127-148.

Led Mehaute, B., 1970. "A Comparison of Fluvial and Coastal similitude," Proceedings of the 12th Coastal Engineering Conference, Washington D.C., pp.1077-1095.

Marino, J. N., and A. J. Mehta, 1986. "Sediment Volumes around Florida's East Coast Tidal Inlets," Coastal and Oceanographic Engineering Department, University of Florida. UFL/COEL-86-009.

Shibayama, T., and K. Horikawa, 1980. "Sediment Suspension due to Breaking Waves," Coastal Engineering in Japan, Vol.25. pp.163-176.

Sill, B.L., J. S. Fisher and S.D. Whiteside, 1981. "Laboratory Investigation of Ebb Tidal Shoals," ASCE Waterways Div. Journal, 107:4, pp.233-244.

Vellinga, P., 1982. "Beach and Dune Erosion During Storm Surges," Journal of Coastal Engineering, Vol.6, pp.361-389.

Walton, T.L., Jr., and W.D. Adams, 1976. "Capacity of Inlet Outer Bars to Store Sand," Proceedings of the 15th Coastal Engineering Conference, ASCE, Vol.II, Honolulu, Hawaii. pp.1919-1937.

Wang, H. , T. Toue, and H.H. Dette, 1990. "Movable Bed Modeling Criteria for Beach Profile Response," Proceedings of the 22nd ICCE, American Society of engineering, Deft, the Netherlands, Chapter 195, pp 2566.

Wang, H., L. Lin, H. Zhong, and G. Miao, 1991. "Sebastian Inlet Physical Model Studies, Part II-- Movable Bed Model," Coastal and Oceanographic Engineering Department, University of Florida. UFL/COEL-91-014.

Wang, H., L. Lin, and G. Miao, 1992. "Sebastian Inlet Physical Model Studies, Final Report-- Movable Bed Model," Coastal and Oceanographic Engineering Department, University of Florida. UFL/COEL-92-006.

Wang, X., L. Lin, and H. Wang, 1994. "Scaling Effects on Beach Response Physical Model," Proceedings of the 24th Coastal Engineering Conference, ASCE, Kobe, Japan.

Wang, X., L. Lin, and H. Wang, 1995. "Laboratory Mobile Bed Model Studies on Inlet, Part I: Modeling Law on Profile Response," Coastal and Oceanographic Engineering Department, University of Florida. UFL/COEL-95-020.

Appendix A:

Bottom Topographic Change at Various Time Intervals for the Natural Inlet Experiment

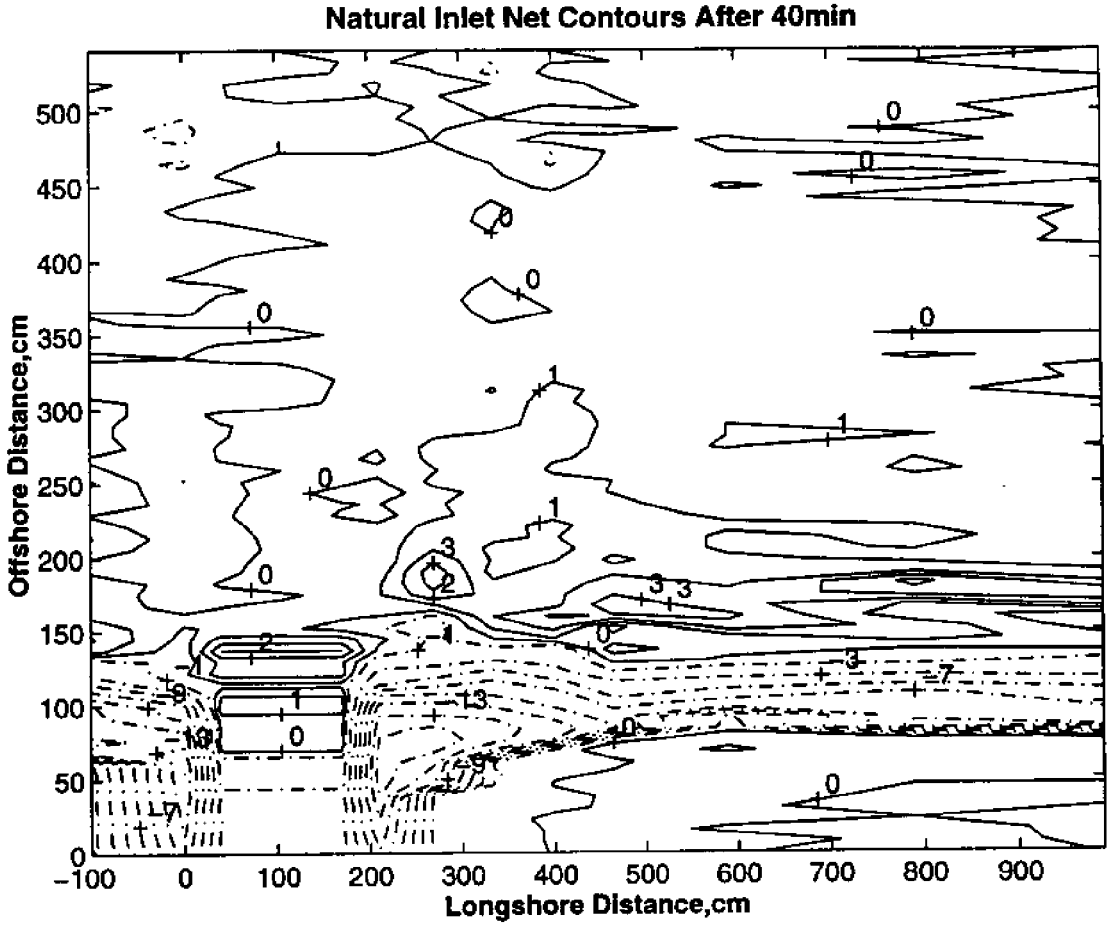

Figure A1: Bottom Topographic Changes after 40 minutes

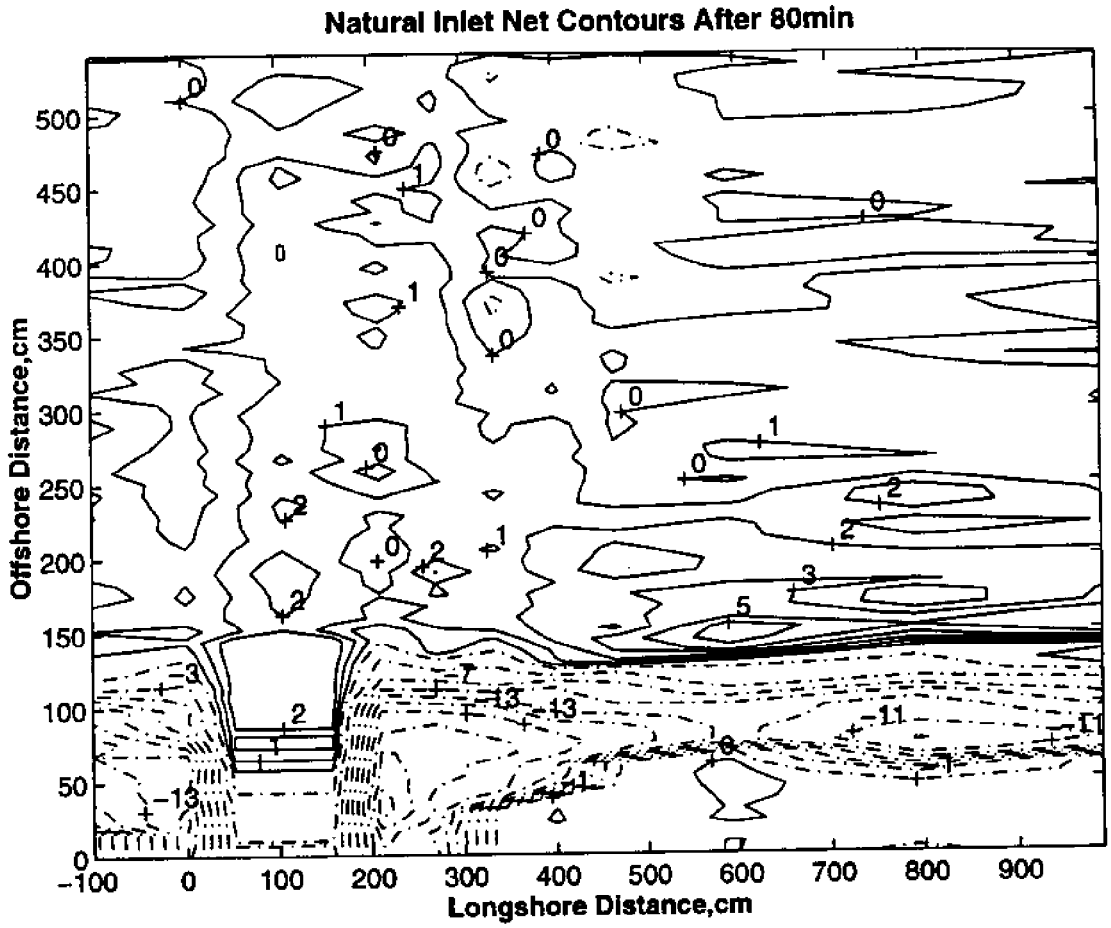

Figure A2: Bottom Topographic Changes after 80 minutes.

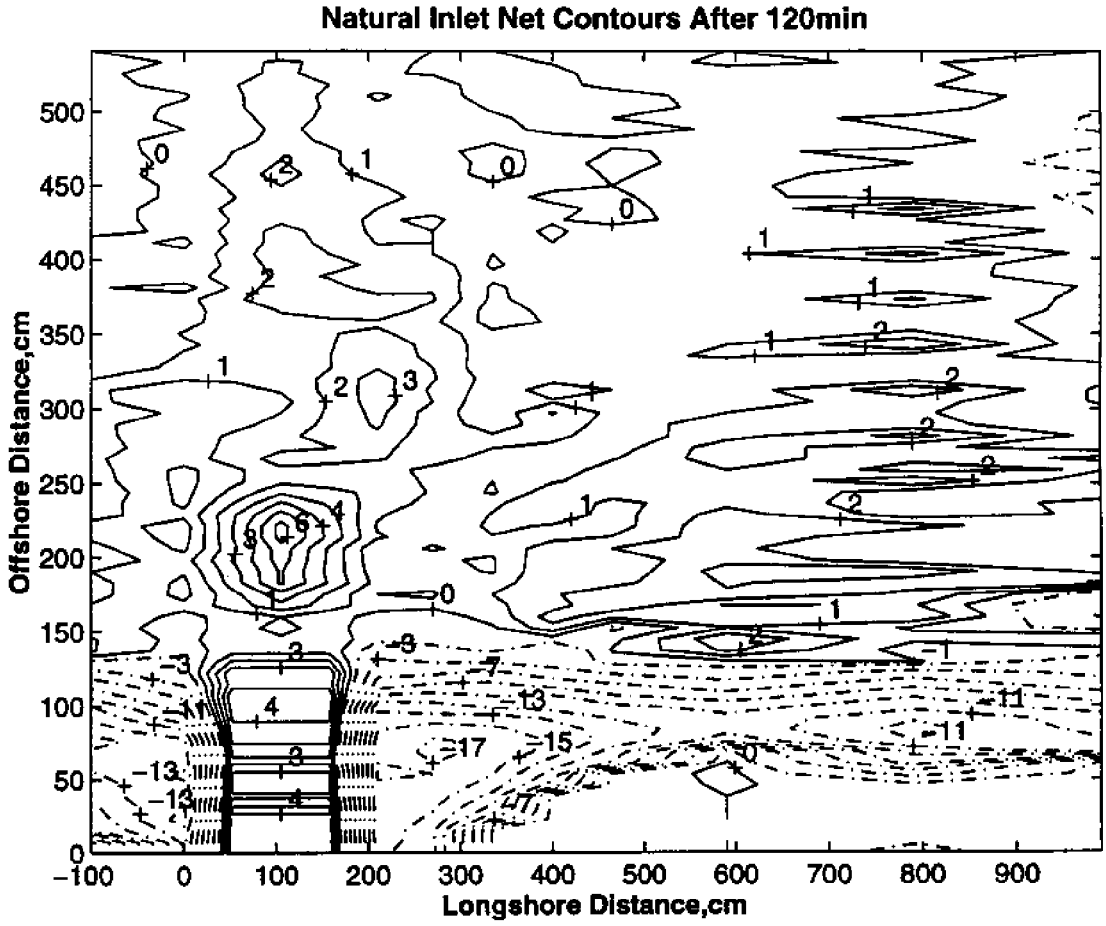

Figure A3: Bottom Topographic Changes after 120 minutes.

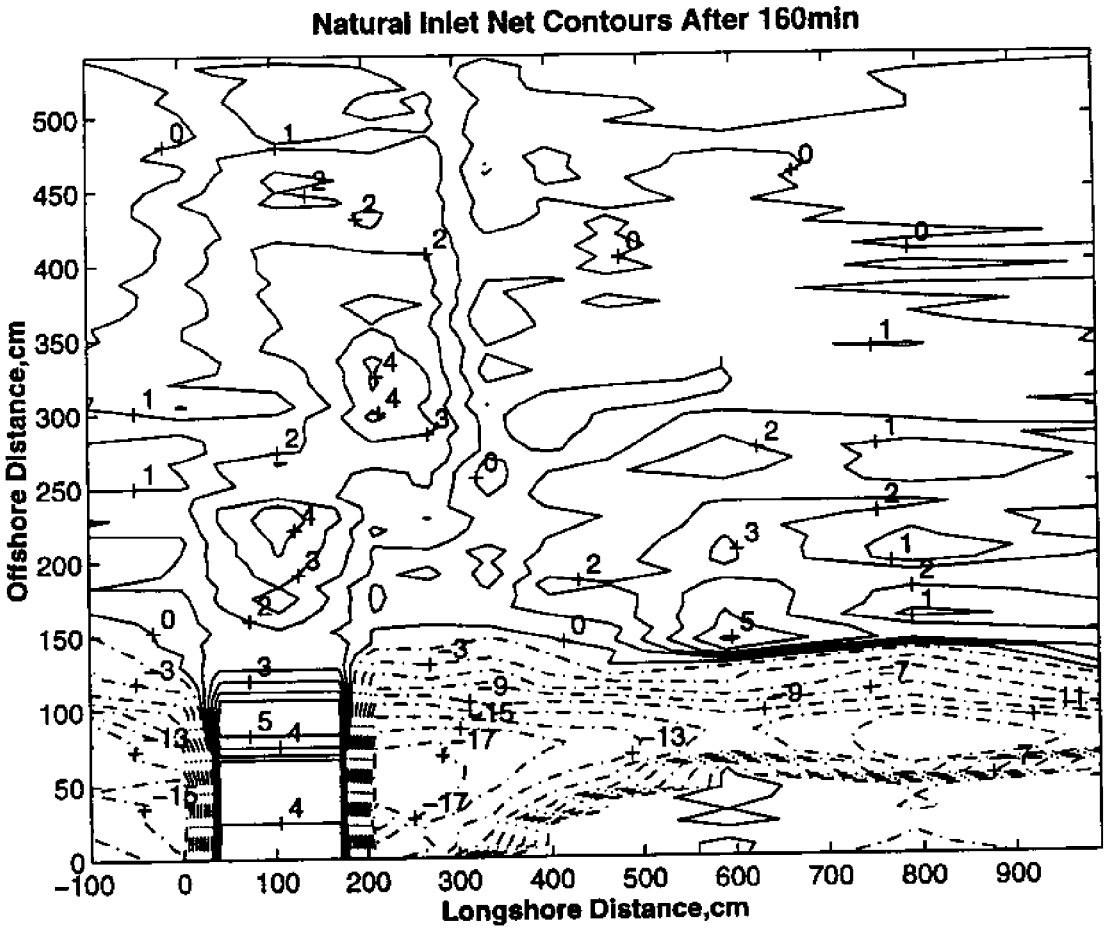

Figure A4: Bottom Topographic Changes after 160 minutes.

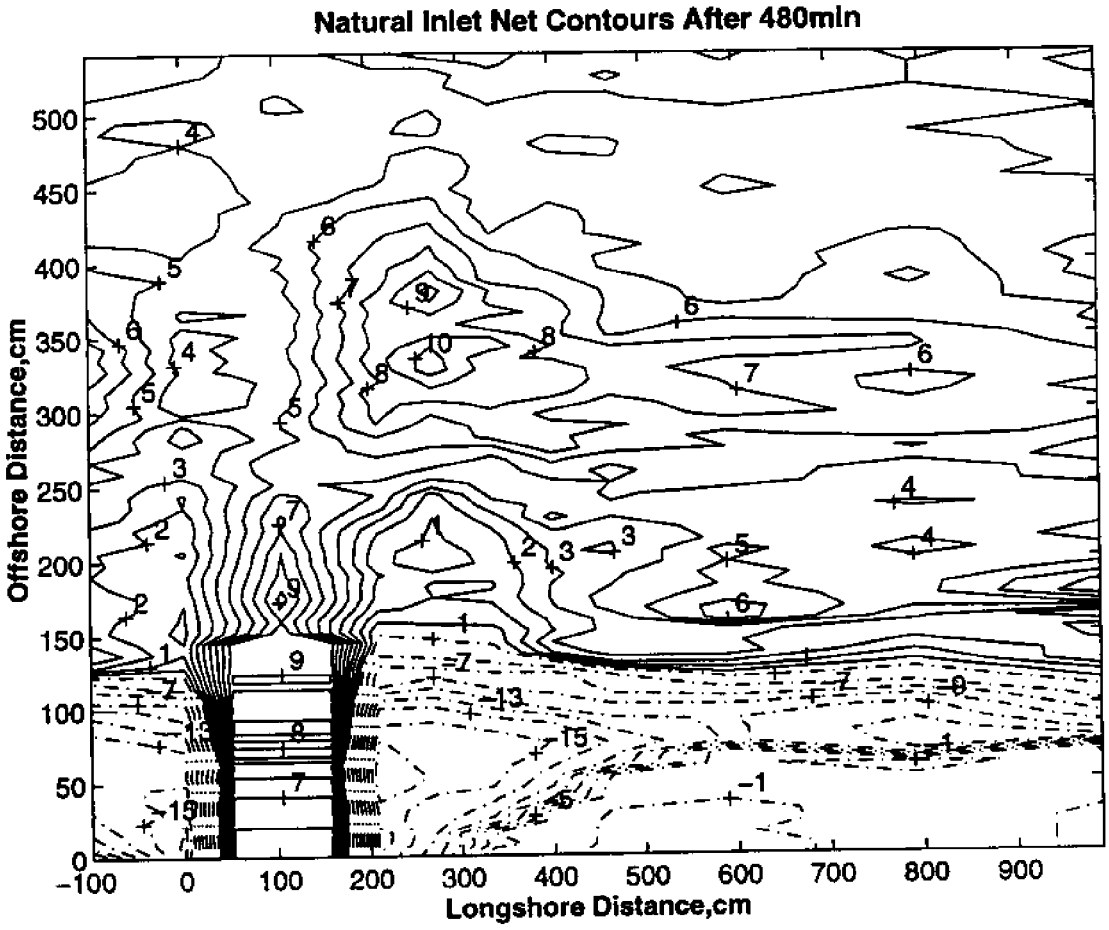

Figure A5: Bottom Topographic Changes after 480 minutes.

Appendix B

Bottom Topographic Change at Various Time Intervals for Porous Jetty Inlet Experiment

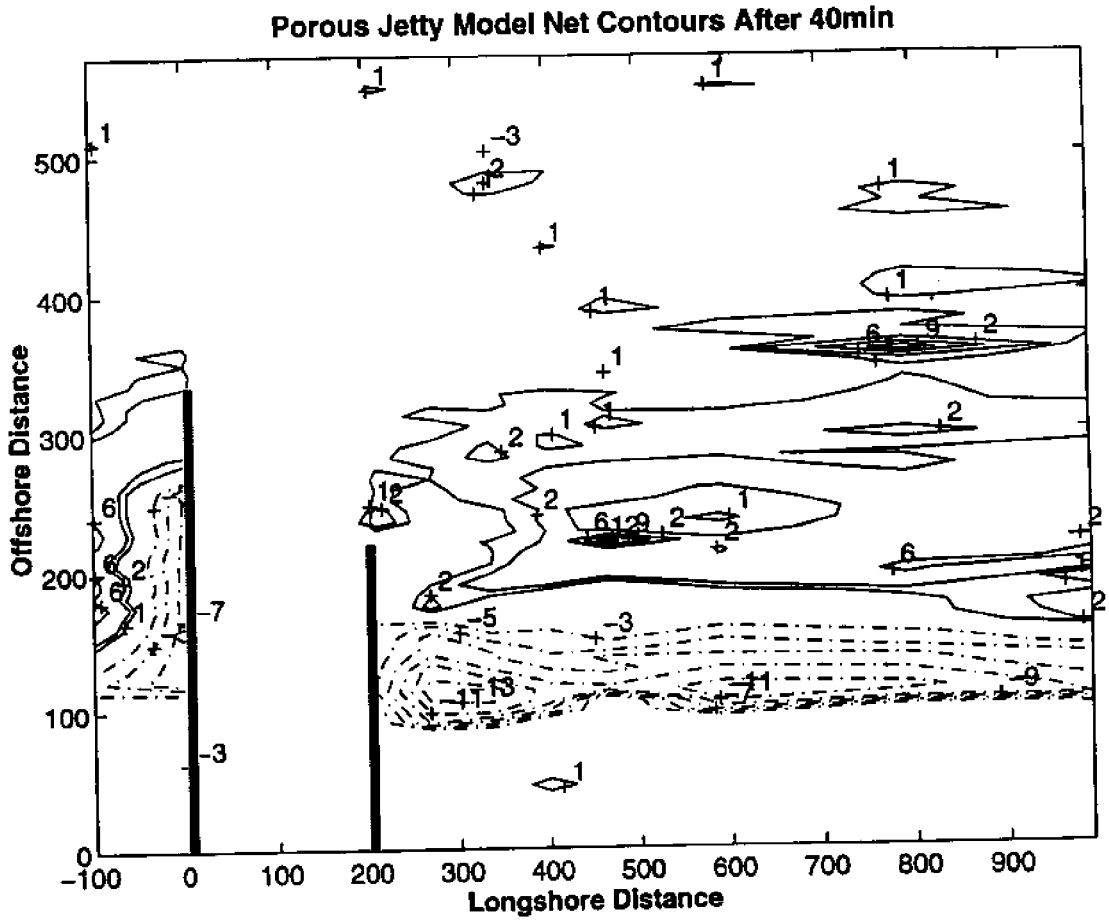

Figure B1: Bottom Topographic Changes after 40 minutes.

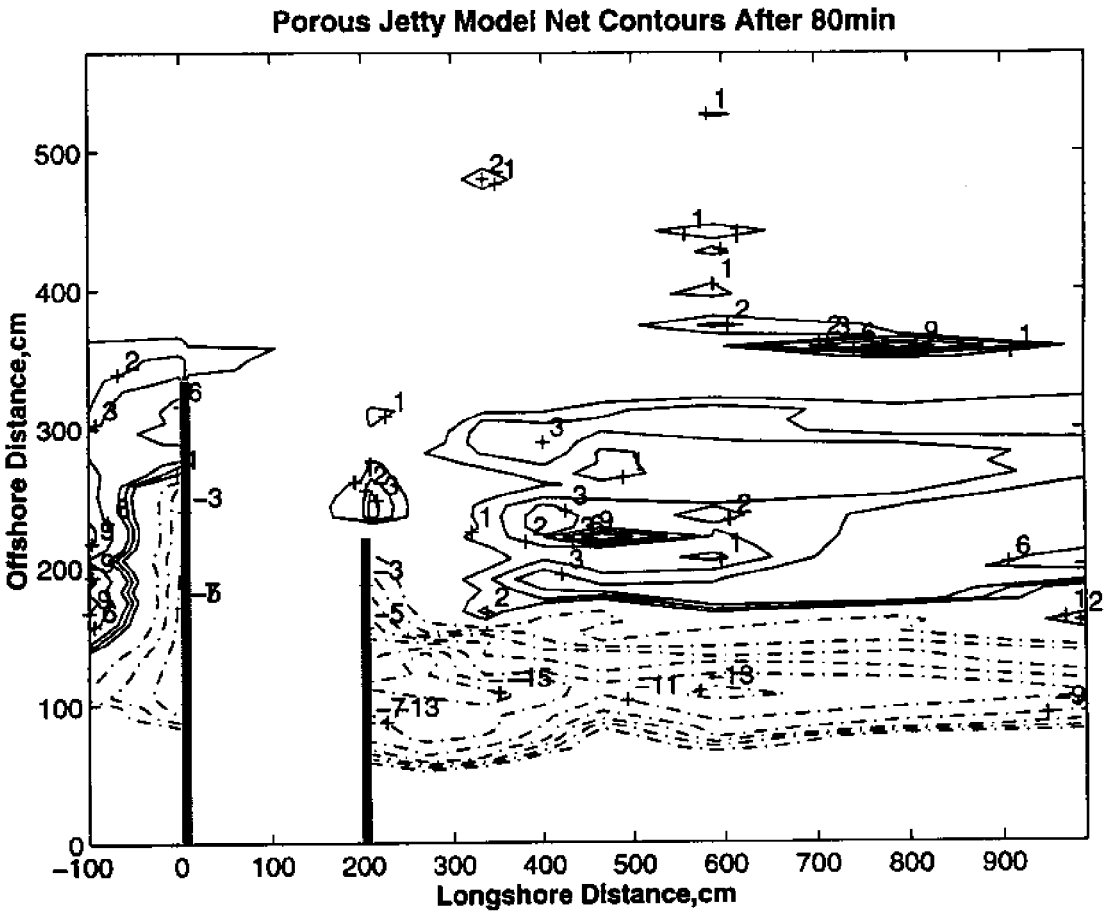

Figure B2: Bottom Topographic Changes after 80 minutes.

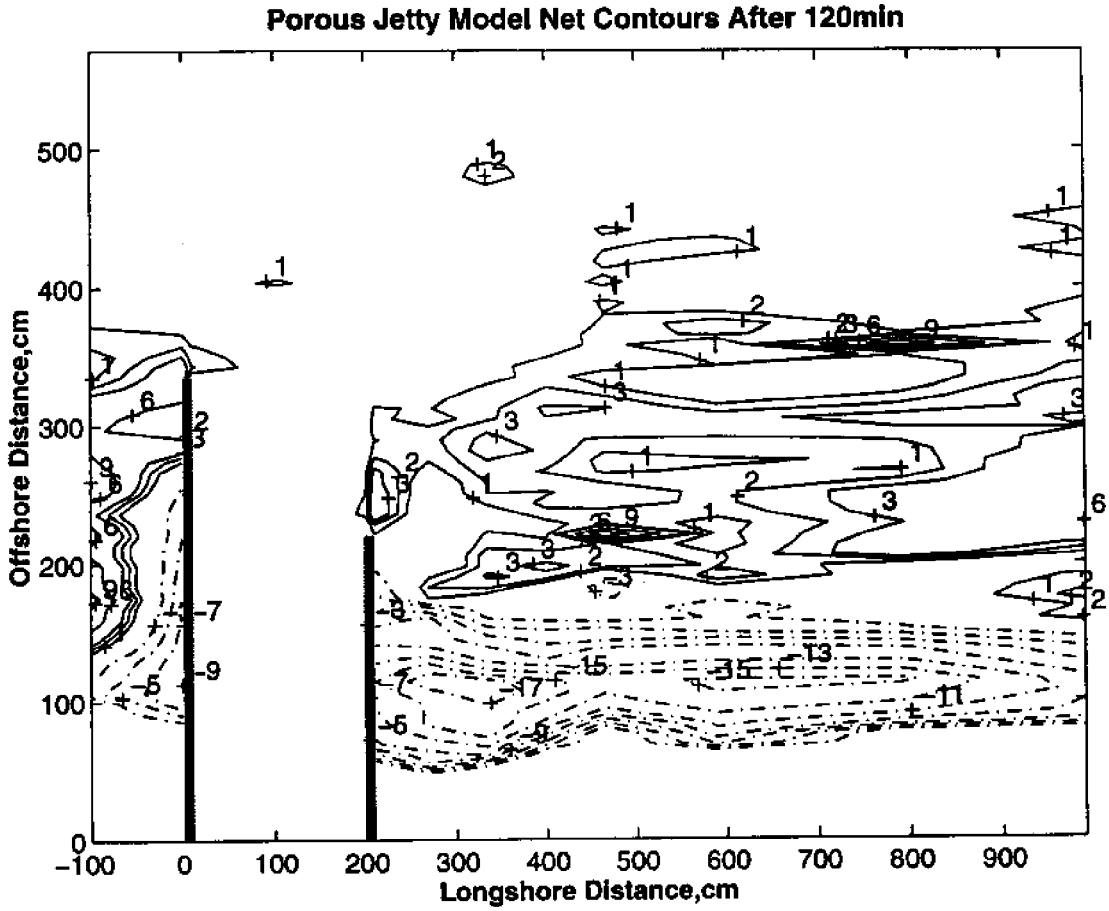

Figure B3: Bottom Topographic Changes after 120 minutes

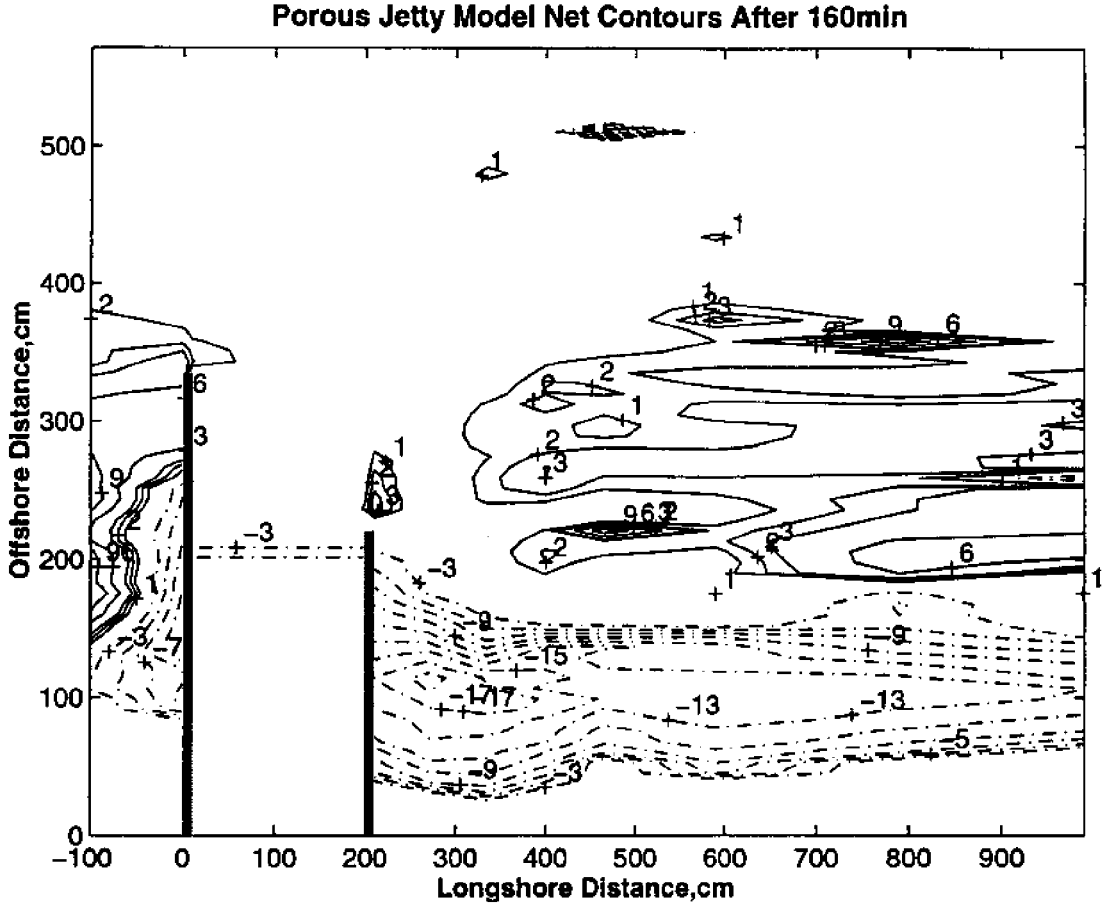

Figure B4: Bottom Topographic Changes after 160 minutes

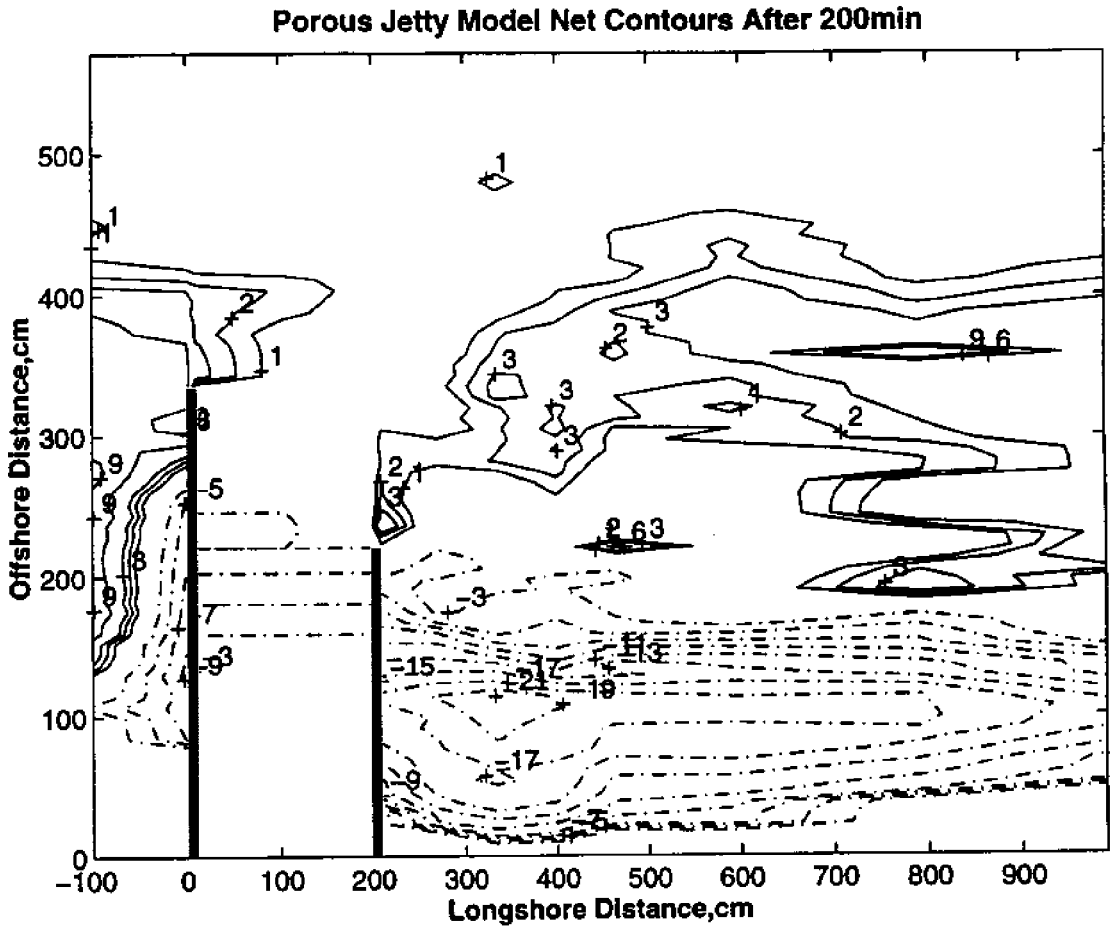

Figure B5: Bottom Topographic Changes after 200 minutes.

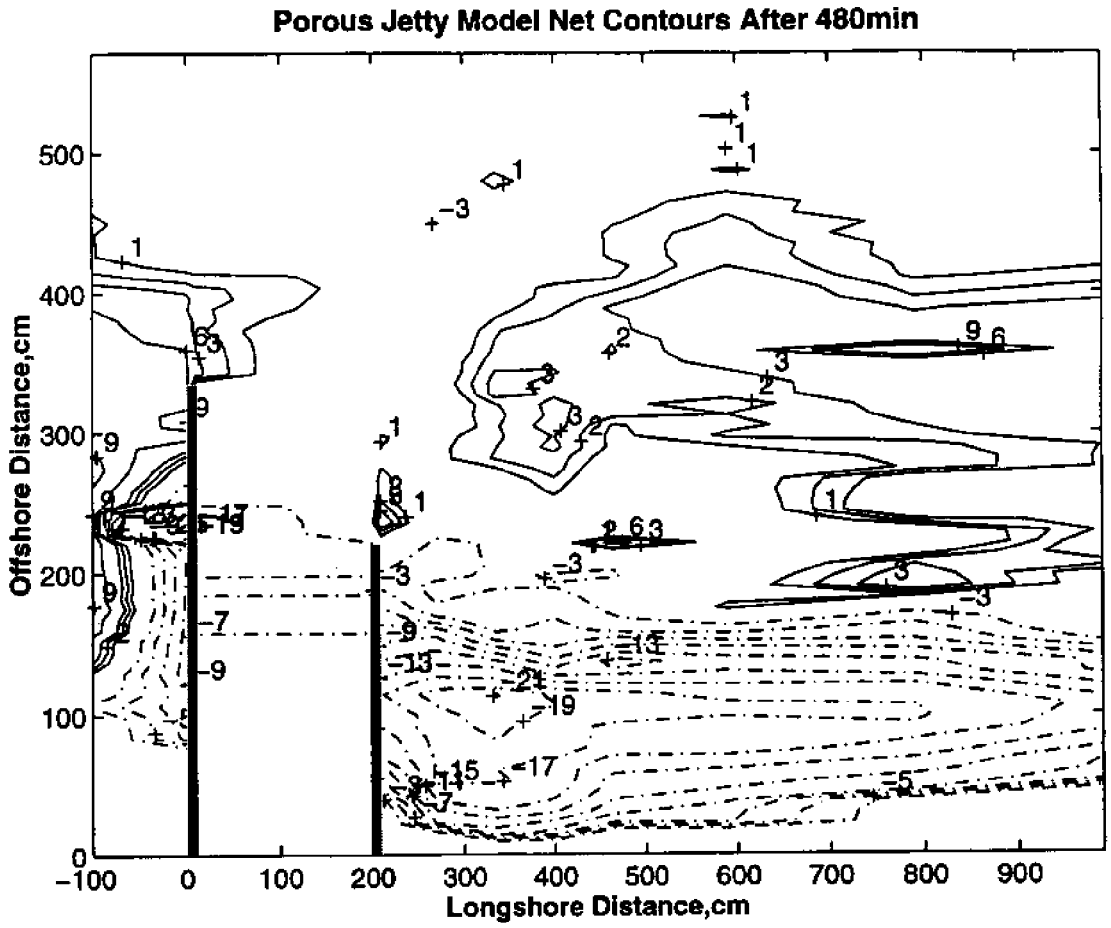

Figure B6: Bottom Topographic Changes after 480 minutes.

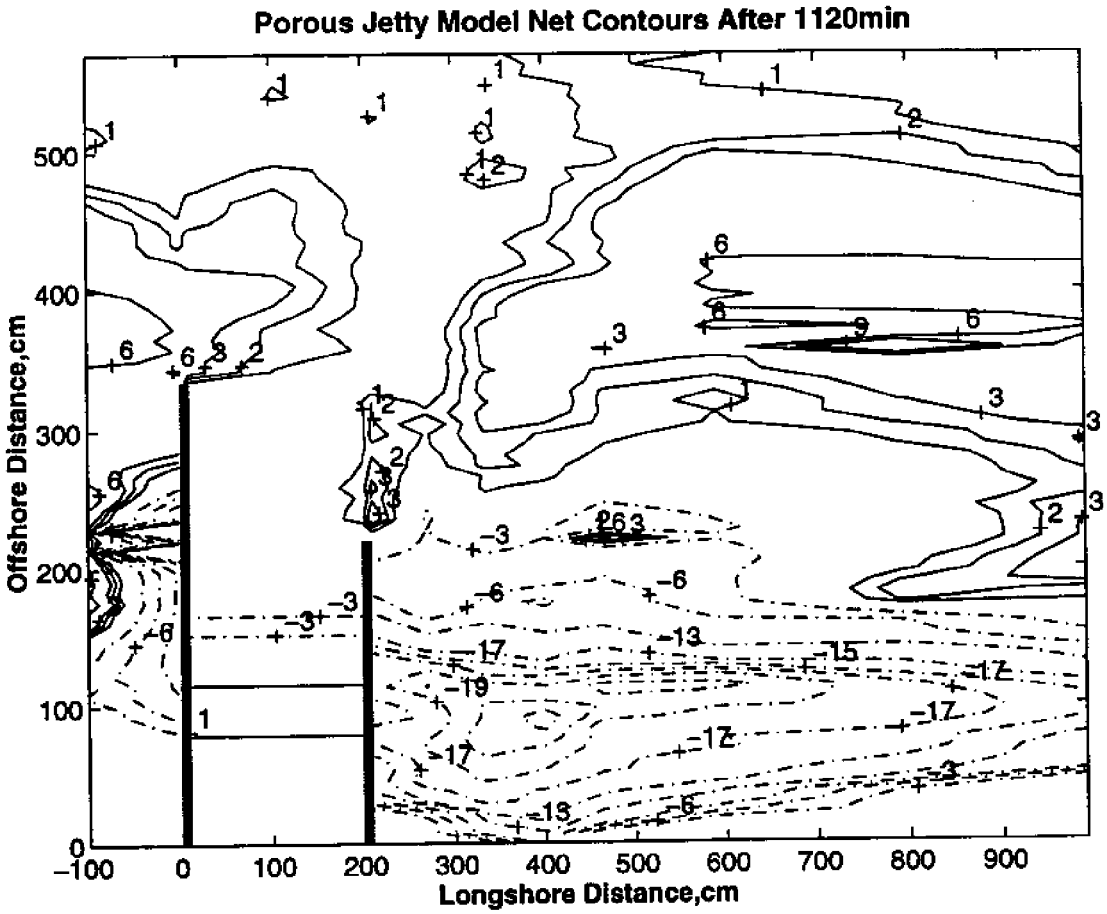

Figure B7: Bottom Topographic Changes after 1120 minutes.

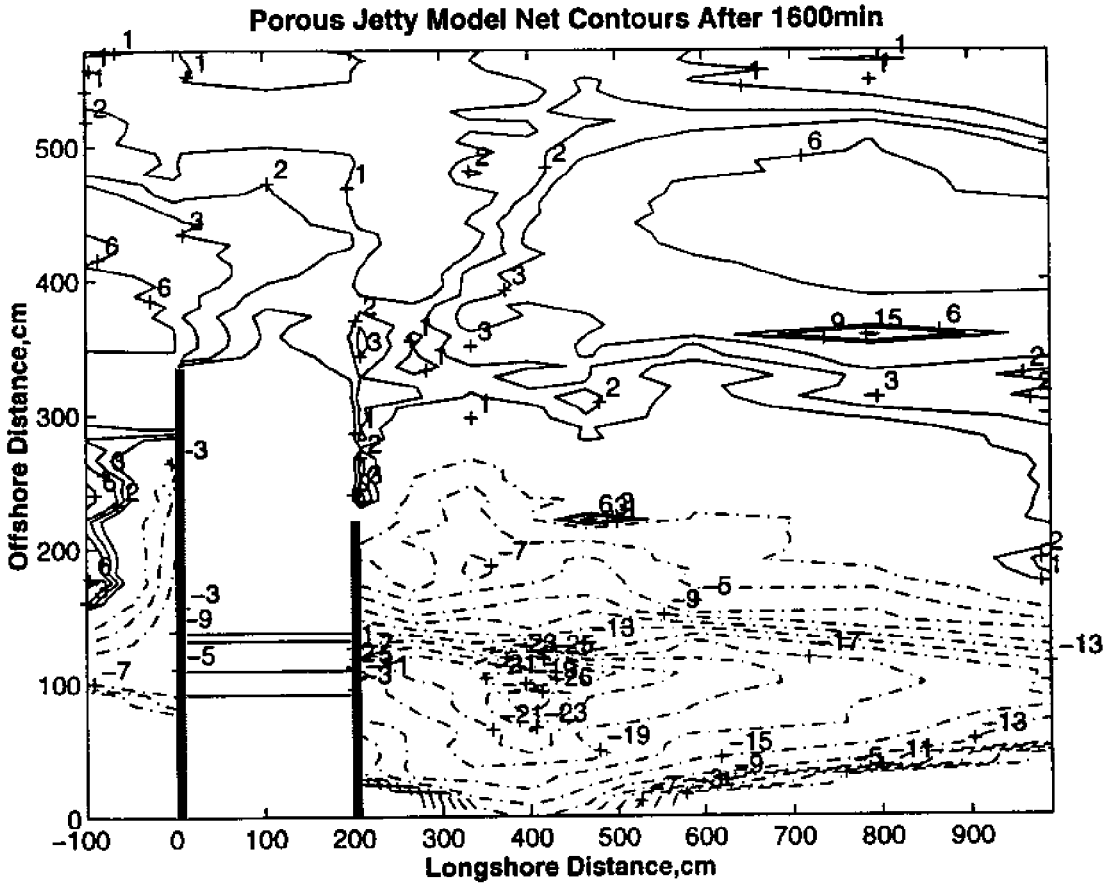

Figure B8: Bottom Topographic Changes after 1600 minutes.

Appendix C

Bottom Topographic Change at Various Time Intervals for Impervious Jetty Inlet Experiment

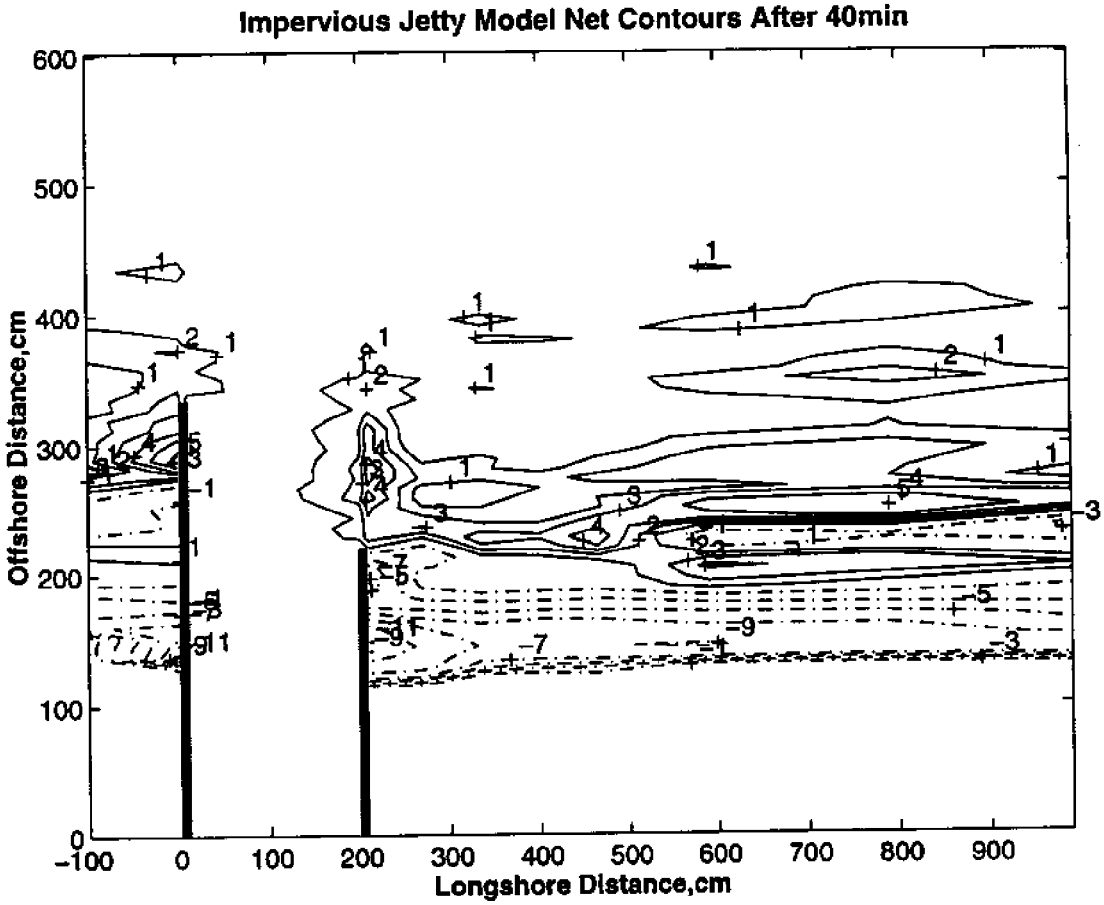

Figure C1: Bottom Topographic Changes after 40 minutes.

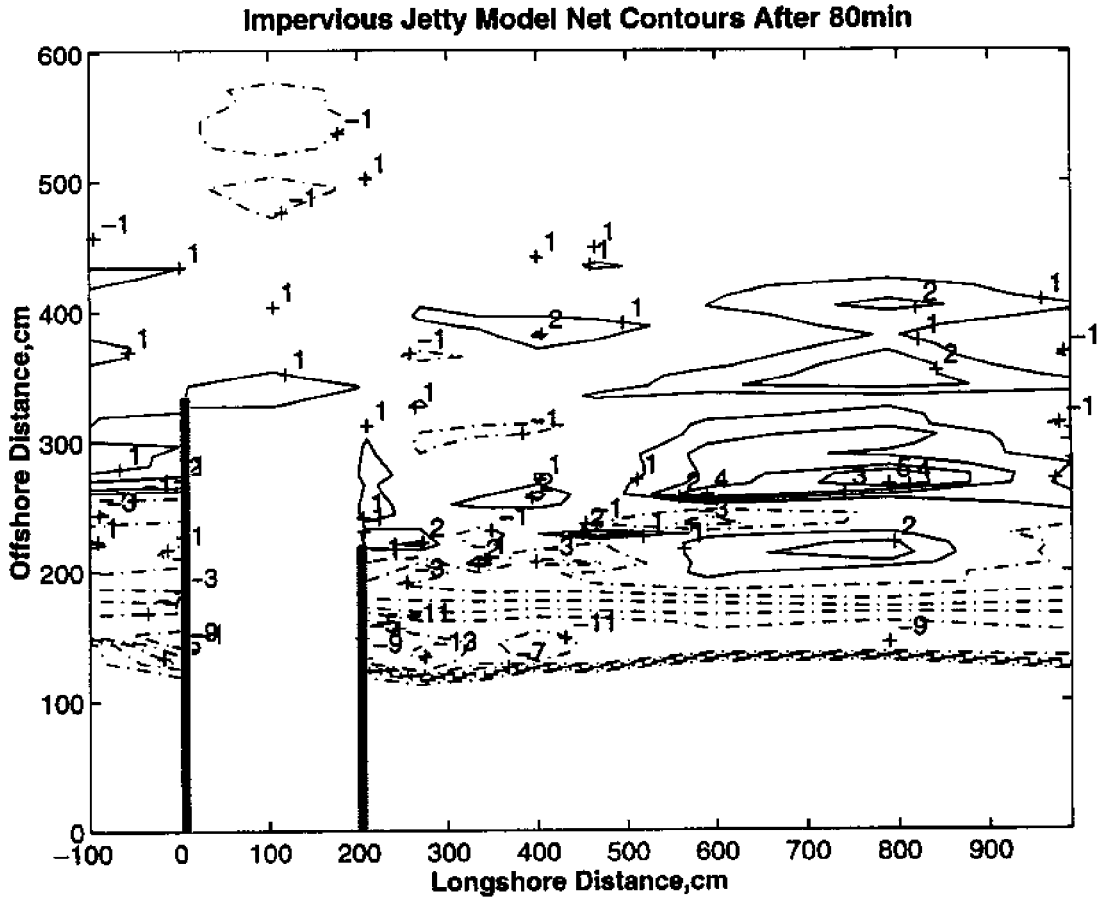

Figure C2: Bottom Topographic Changes after 80 minutes.

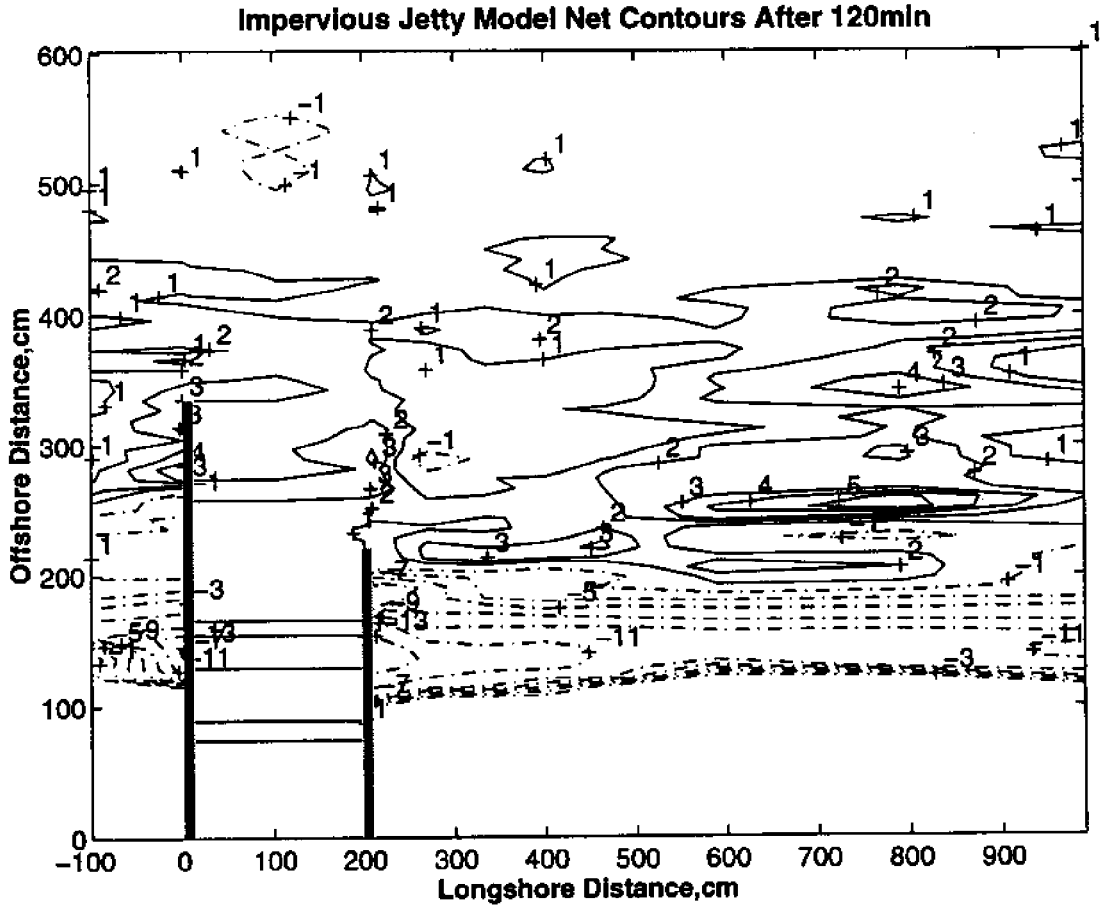

Figure C3: Bottom Topographic Changes after 120 minutes.

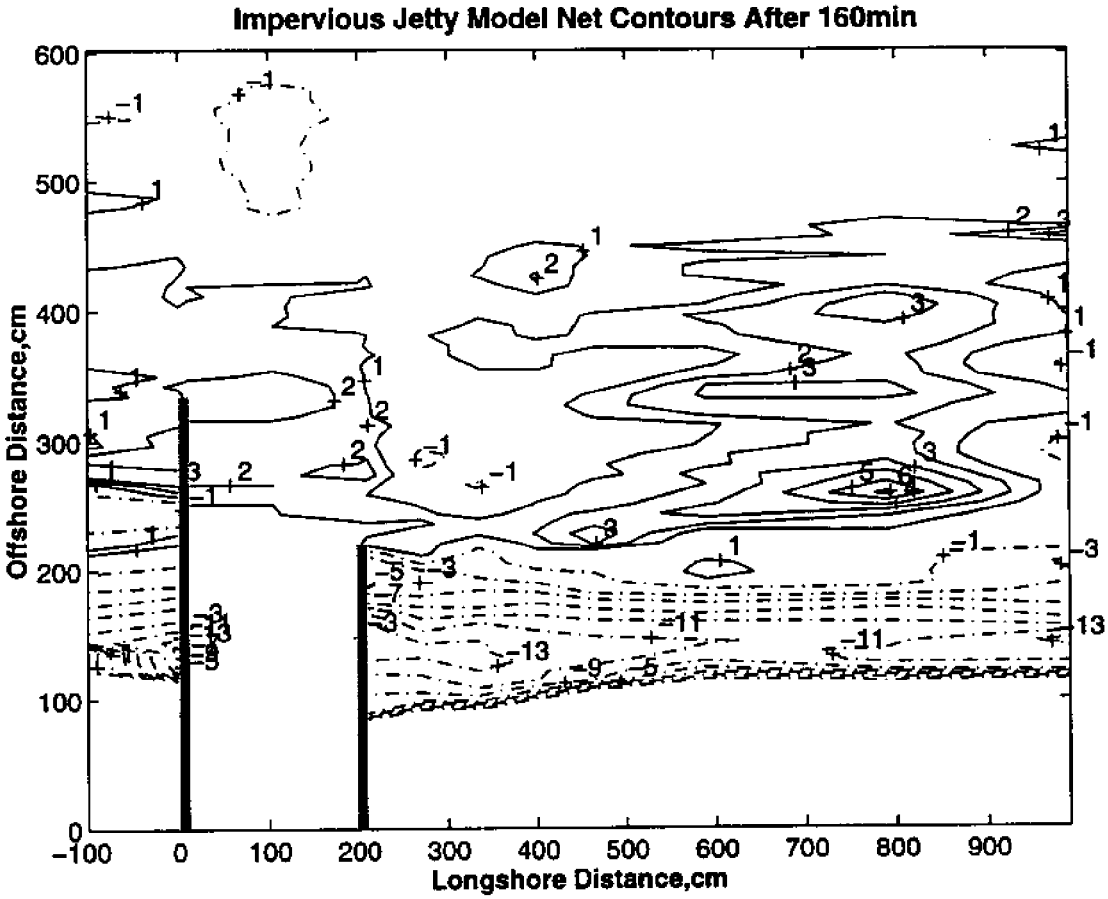

Figure C4: Bottom Topographic Changes after 160 minutes

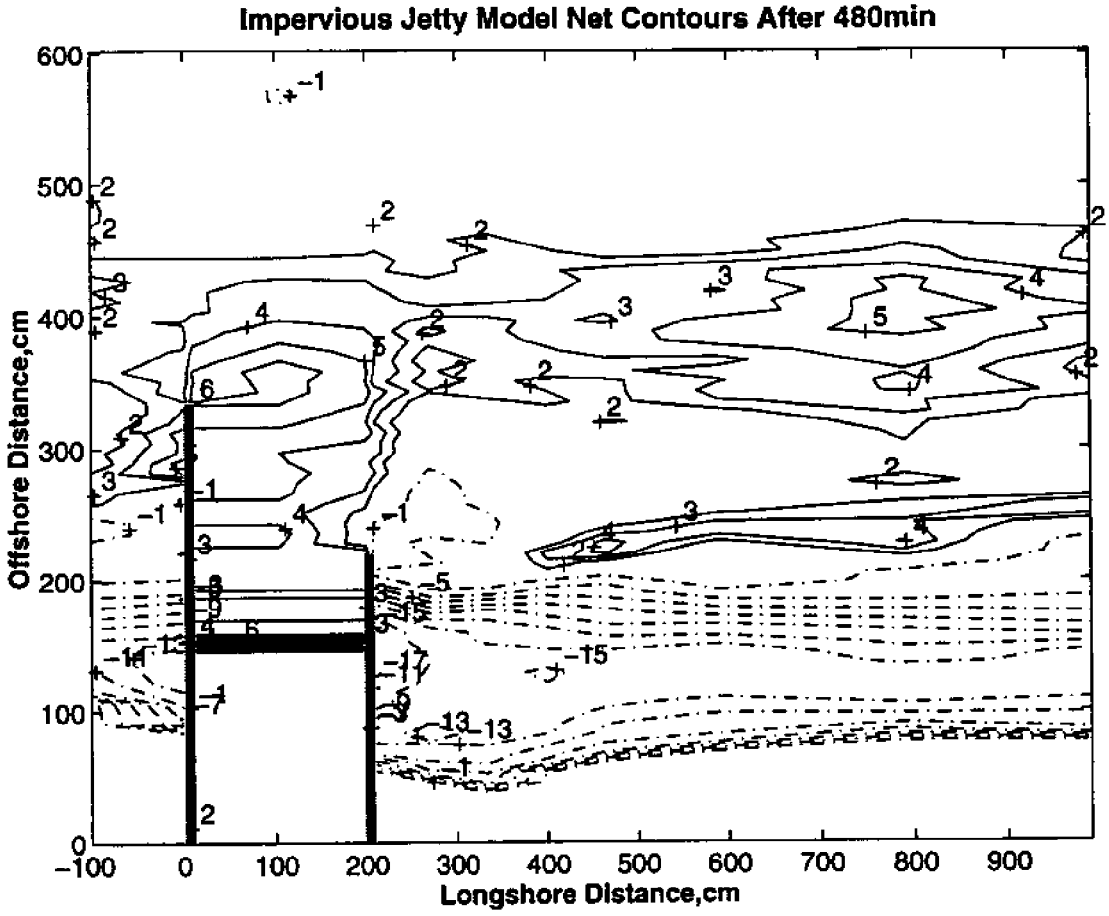

Figure C5: Bottom Topographic Changes after 480 minutes.

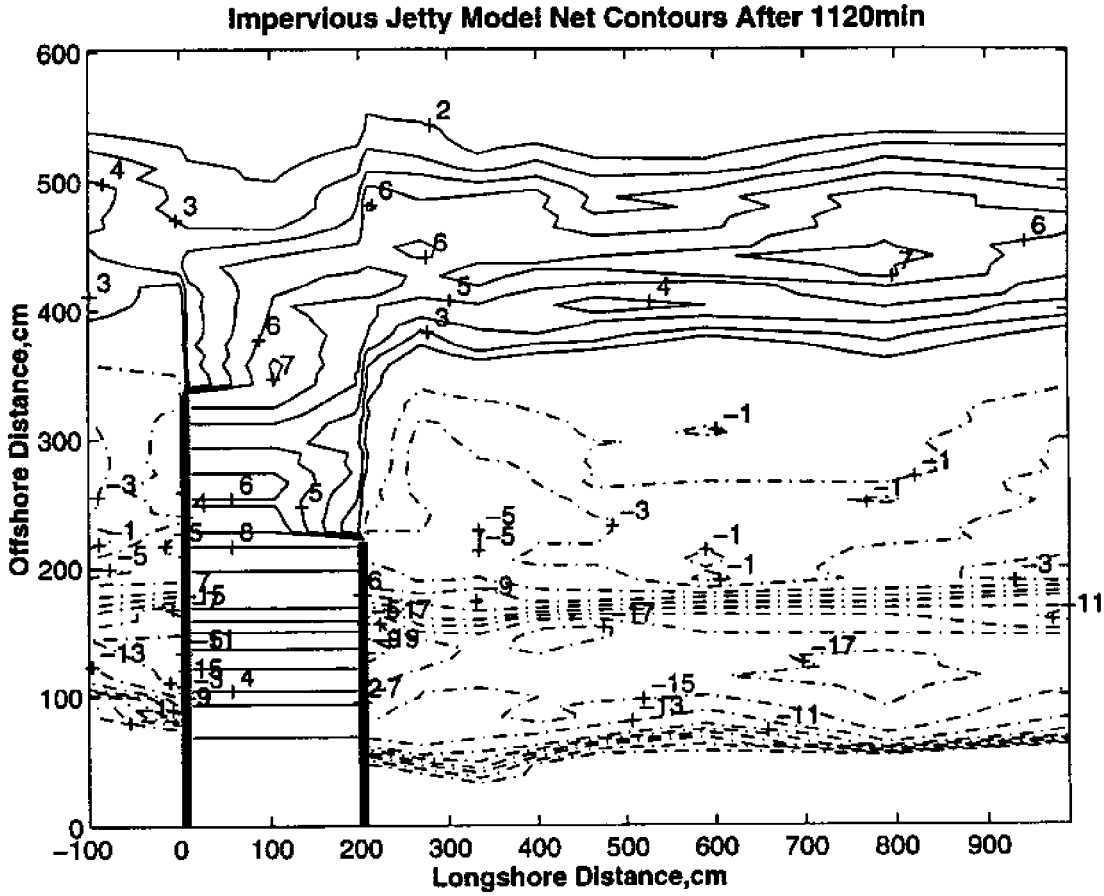

Figure C6: Bottom Topographic Changes after 1120 minutes.

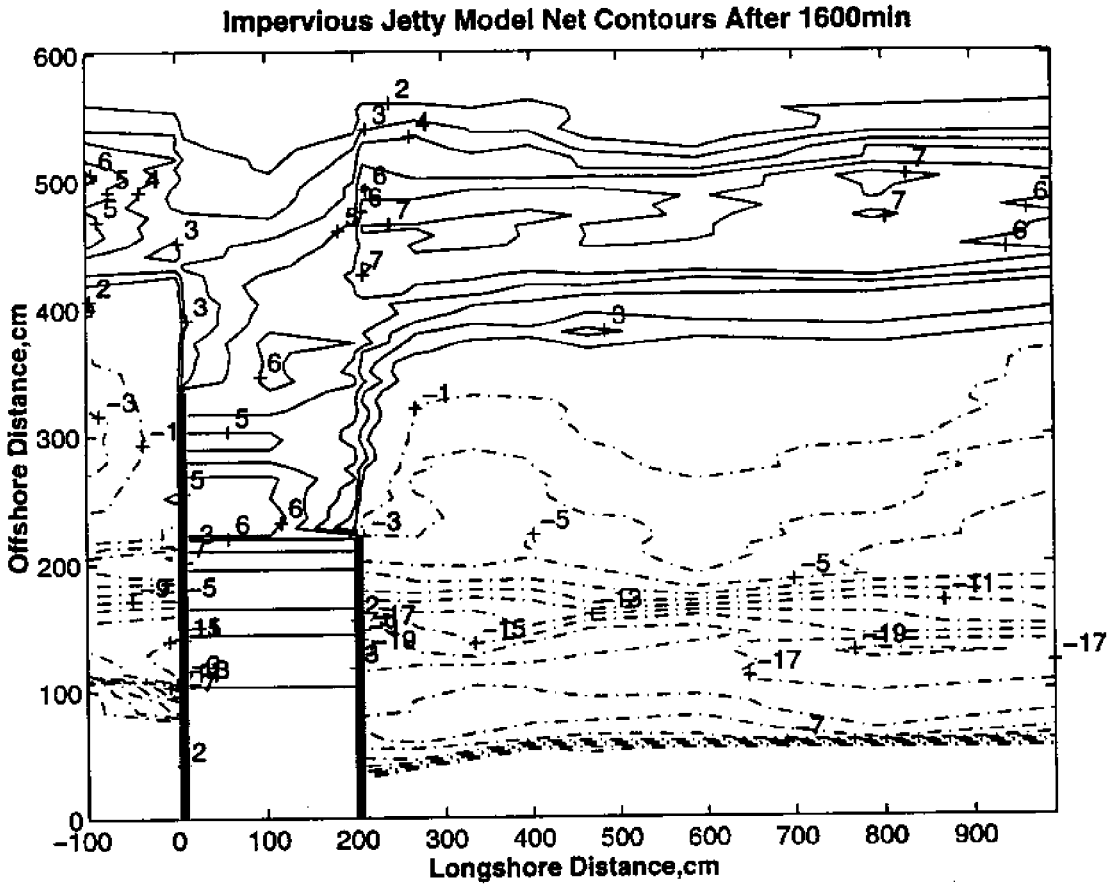

Figure C7: Bottom Topographic Changes after 1600 minutes

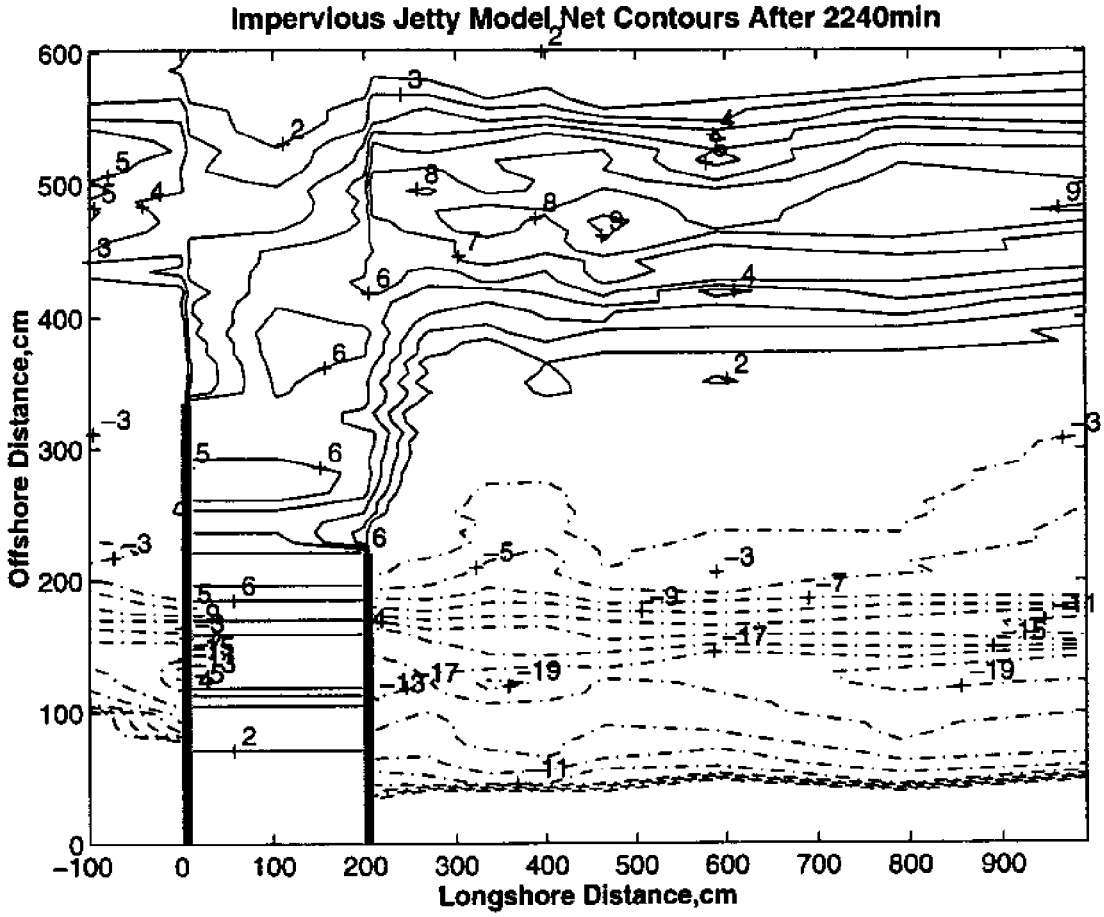

Figure C8: Bottom Topographic Changes after 2240 minutes

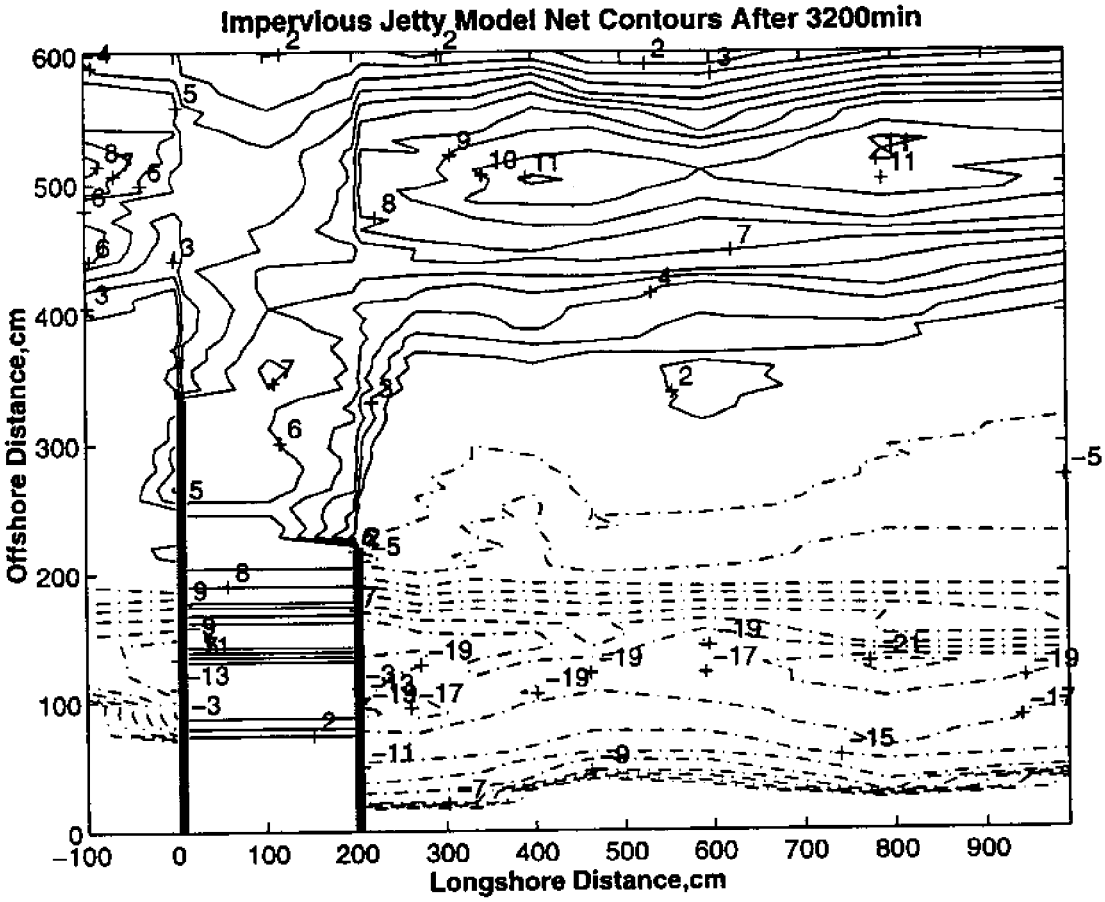

Figure C9: Bottom Topographic Changes after 3200 minutes.

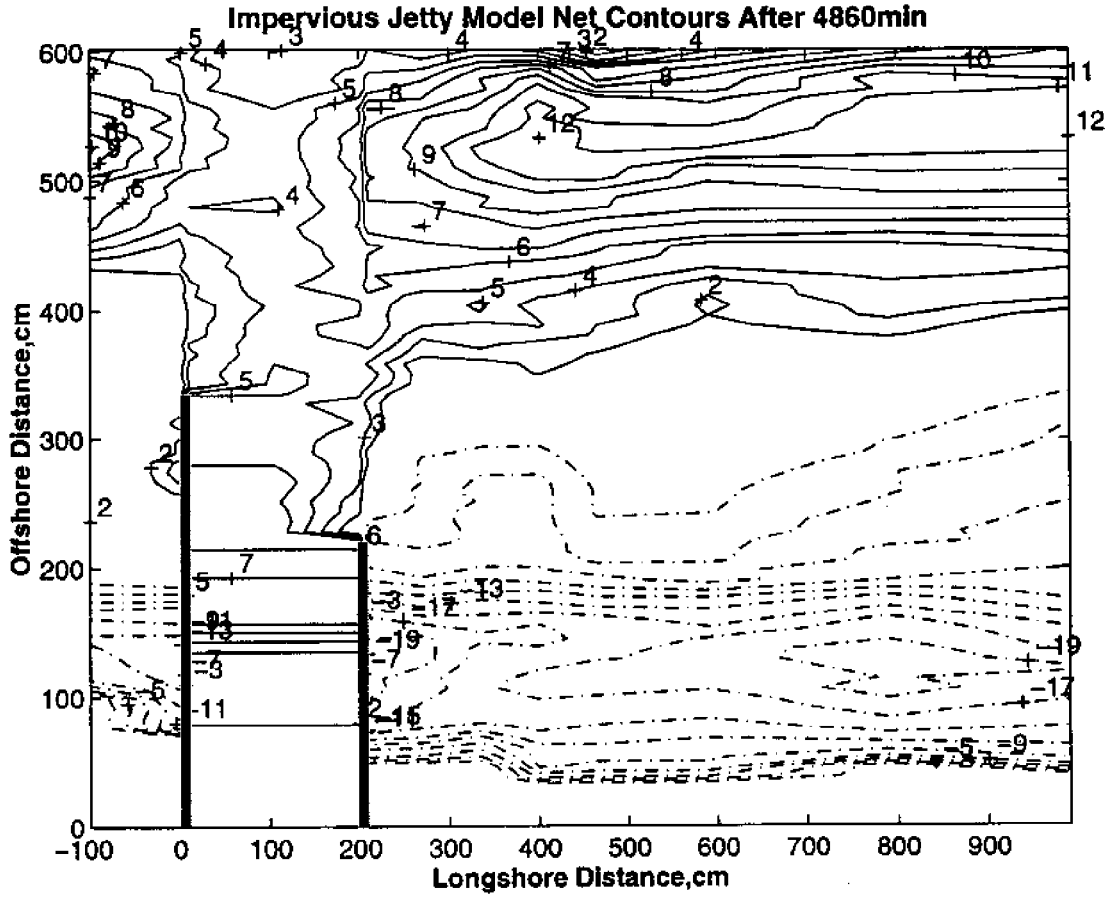

Figure C10: Bottom Topographic Changes after 4860 minutes.